MOVING PHANTOM STUDY OF STEREOTACTIC BODY RADIATION THERAPY FOR LUNG CANCER

APPROVED BY SUPERVISORY COMMITTEE

Lech Papiez, Ph.D., Mentor

Robert Timmerman, M.D.

Mathew Lewis, Ph.D.

Padmakar Kulkarni, Ph.D.

Peter Antich, Ph.D., Chair

DEDICATION

I would like to acknowledge all the people who support me, love me and help me. This has been a wonderful journey. Thanks to the Graduate Program in Radiological Sciences directed by Dr. Peter P. Antich for giving me such an opportunity to taste science, to pursue the dream of becoming a scientist. Thanks to my supervisor, Dr. Lech Papiez, for all the things I learned from you, from how to design and perform a simple experiment, to more importantly, how to think and work as a medical physicist. Thanks to Dr. Robert Timmerman for his serious scientific attitude, patient advice and kind help, all of which will be beneficial my whole life. Thanks to Drs. Padmakar Kulkarni and Mathew Lewis as my committee members.

I also deeply thanks to Dr Kwangyoul Park for his help and ideas for my research. Thanks to Mrs. Ewa Papiez who trained me for clinical practice and clinical support for my research. Thanks to Ms. Kay Emerson for helping with my dissertation preparation. Thanks to Mai Lin for helpful discussions. Thanks to Ms. Dee Hill for helpful editing for my thesis. Without any of these, this mission would have been impossible. This work belongs to each who’ve ever helped me and supported me.

Finally, I wish to dedicate this dissertation to my wife An Ning, my daughter Rebecca Huang and my parents, for the unselfish endless love and support.

MOVING PHANTOM STUDY OF STEREOTACTIC BODY RADIATION THERAPY FOR LUNG CANCER

by

LONG HUANG

DISSERTATION

Presented to the Faculty of the Graduate School of Biomedical Sciences

The University of Texas Southwestern Medical Center at Dallas

In Partial Fulfillment of the Requirements

For the Degree of

DOCTOR OF PHILOSOPHY

The University of Texas Southwestern Medical Center at Dallas

Dallas, Texas

AUGUST, 2010

MOVING PHANTOM STUDY OF STEREOTACTIC BODY RADIATION THERAPY FOR LUNG CANCER

Publication No._____

Long Huang, Ph.D.

The University of Texas Southwestern Medical Center at Dallas

Graduation Year 2010

Supervising Professor: Lech Papiez, Ph.D.

To assess the accuracy of current stereotactic body radiation therapy (SBRT) lung treatment methodologies, we performed a systematic evaluation using phantoms that simulated motions from real patients (irregular motions) as well as sinusoidal motions (regular motions). The irregular patterns investigated in this study were of two types: *small range* irregular breathing motions (≤10mm) and *large range* irregular breathing motions (≥20mm). Four-dimensional computed tomography (4DCT) and cone beam computed tomography (CBCT) are important methodologies for SBRT, but previously have only been used to evaluate regular patterns. For targets moving regularly or irregularly within a small range (7.0 ± 1.8 mm, n = 6), we observed good agreement between the measured and computed dose distributions. However, for targets moving irregularly with a larger range (20.8 ± 2.6 mm, n = 4), the measured isodose lines were found to be shifted relative to the planned distribution, resulting in an underdosing (over 20%) in a portion of the PTV. In this underdosed volume, 1-2% of the PTV is underdosed

by over 18 Gy, causing a 35-40% drop in the local control rate. We further observed that the discrepancy between the planned and measured dose distribution was due to the inaccurate representation of the irregular target motion in the maximum intensity projection (MIP) images generated from 4DCT, which could not be corrected by CBCT. A method of Extended Distance Virtual Isocenter (EDVI) was developed to lower the toxicity of healthy tissues. In all, caution should be used when planning from 4DCT images in the presence of large and irregular target motion. The inaccuracy inherent in 4DCT MIP and CBCT images can be mitigated through the application of methodologies to reduce respiratory motion, such as abdominal compression, and through the use of volumetric image guidance to assure precise targeting with minimal shifts.

TABLE OF CONTENTS

PRIOR PUBLICATIONS

1. K. Park, L. Huang, H. Gagne and L. Papiez "Do Maximum Intensity Projection Images Truly Capture Tumor Motion?" Int. J. Radiat. Oncol., Biol., Phys., V73, 618-625, 2009

2. L. Huang, K, Park, T. Boike, P. Lee, L. Papiez, T. Solberg, C. Ding and R. Timmerman "A study on the dosimetric accuracy of treatment planning for stereotactic body radiation therapy of lung cancer using Average and Maximum Intensity Projection images" Radiother. Oncol., V73, 618-625, 2010.

3. L. Huang, L. Papiez, E. Papiez, R. Albofar, K. Song, T. Solberg and R. Timmerman "Study on extended non-isocentric beams treatment plan in stereotactic body radiation therapy for lung cancer" (manuscript in preparation)

4. L Huang, L Papiez, E Papiez, T Solberg, and R Timmerman "Phantom Study of Cone Beam Computed Tomography Setup Accuracy in Stereotactic Body Radiation Therapy for Lung Cancer Treatment" (manuscript in preparation)

5. L. Huang, L. Papiez, R. Abolfath, E. Papiez, R. Timmerman and T. Solberg "Extend Distance Treatment for Stereotactic Body Radiation Therapy of Lung Cancer" WC 2009, IFMBE Proceedings 25/I, pp. 144-147, 2009

6. C. Ding, L. Huang, L. Papiez, R. Timmerman and T. Solberg "Tumor Alignment between 4DCT and 4D Cone Beam CT for Irregular Respiratory Patient - a Phantom Study" WC 2009, IFMBE Proceedings 25/I, pp. 515-518, 2009

National Professional Meeting Presentations

1. L. Huang, L. Papiez, E papiez, K. Park and R Timmerman "Cone Beam Computed Tomography Setup Accuracy in Stereotactic Body Radiation Therapy for Lung Cancer Treatment- free breathing vs. controlled breathing" ASTRO, 52, San Diego CA **2010**

2. L Huang, L Papiez, E Papiez, T Solberg, and R Timmerman "Phantom Study of Cone Beam Computed Tomography Setup Accuracy in Stereotactic Body Radiation Therapy for Lung Cancer Treatment" AAPM 52, PA **2010**

3. L Huang, L Papiez, E Papiez, T Solberg, W Mao, C Ding, and R Timmerman "Can Four Dimensional Cone Beam Computed Tomography (4DCBCT) Improve the Patient Setup for Stereotactic Body Radiation Therapy?" AAPM 52, PA **2010**

4. L. Huang, L. Papiez, R. Abolfath, E. Papiez, R. Timmerman and T. Solberg "Extend Distance Treatment for Stereotactic Body Radiation Therapy of Lung Cancer" World Congress on Medical Physics and Biomedical Engineering, **2009**

5. C. Ding, L. Huang, L. Papiez, R. Timmerman and T. Solberg "Tumor Alignment between 4DCT and 4D Cone Beam CT for Irregular Respiratory Patient - a Phantom Study" World Congress on Medical Physics and Biomedical Engineering, **2009**

6. L. Huang, K, Park, T. Boike, P. Lee, L. Papiez, R. Timmerman and T. Solberg "Study on the dosimetric accuracy of treatment planning for SBRT lung cancer using Average and Maximum Intensity Projection images" AAPM 51, LA **2009**

7. L. Huang, R. Abolfath, L. Papiez and T. Solberg "Extend Distance Treatment for Stereotactic Body Radiation Therapy of Lung Cancer" 9th ISRS, Seoul, Korea **2009**

8. K, Park and L. Huang "Study on MIP of 4DCT for SBRT lung cancer" AAPM 50, TX **2008**

LIST OF FIGURES

LIST OF TABLES

CHAPTER ONE

INTRODUCTION

1.1 Radiation therapy

Radiation therapy is the medical application of ionizing radiation to treat cancer and control malignant cells. Radiation therapy may be used as a curative or auxiliary treatment. It may be used as a palliative treatment when the aim is local disease control and may provide symptomatic relief for therapeutic treatment when therapy is intended to be curative or prolong survival.

Radiation therapy is used for malignant cancer treatment, and may be used as a primary or adjuvant modality. It is common to combine radiation therapy with surgery, chemotherapy, hormone therapy or some mixture of the three. Most cancer can be treated with radiation therapy. The precise treatment choice will depend on the tumor type, location, cancer stage, and health condition of the patient.

Radiation therapy may also be used for non-malignant conditions, including trigeminal neuralgia [1], pterygium [2], pigmented villonodular synovitis [3], prevention of keloid growth [4], and prevention of heterotopic ossification [5]. The limitation of using radiation therapy for non-malignant conditions is the increased risk of radiation-induced cancers.

1.1.1 History of radiation therapy

Radiation therapy has been used to treat cancer for over a century, since the discovery of x-rays in 1895 by Wilhelm Röntgen [6]. Radiation therapy developed in

the early 1900s largely due to the milestone work of the Nobel Prize-winning Dr. Marie Curie, who discovered radioactive polonium and radium [7]. This began an era of medical treatment and research in radiation therapy. Radium was used in various shapes and forms until the mid-1900s. Then cobalt and cesium units came into use and people stopped using radium. Medical linear accelerators have been popular as sources of radiation since the late 1940s [8]. Orthovoltage x-ray and ^{60}Co units have largely been replaced by megavoltage x-ray linear accelerators because of the latter's penetrating energies and avoidance of a radioisotope source.

Since the invention of computed tomography (CT) in 1971 [9], three-dimensional (3-D) planning became possible and with time became the standard for 3-D radiation delivery. CT-based planning allows physicians to more accurately access the dose distribution inside the patient's anatomy.

The advent of new imaging technologies, such as magnetic resonance imaging (MRI) in the 1970s [10] and positron emission tomography (PET) in the 1980s [10, 11], also contributed to the development of better techniques in radiation therapy. In the late 1990s, radiation therapy moved from 3-D conformal to intensity-modulated radiation therapy (IMRT) and image-guided radiation therapy (IGRT) [12-14]. By using these advanced technologies, radiation oncologists can better shape the treatment dose and deliver it with more precision to targeted tumor volumes, resulting in improved treatment outcome and better preservation of organs at risk.

1.1.2 DNA damage

Radiation therapy treats cancer by damaging the DNA in cancer cells, which prevents their division and uncontrolled growth. The damage is caused either by the direct or indirect ionization of atoms and molecules in the DNA chain. Indirect ionization works through the ionization of water (H_2O). Ionization of water results in the formation of free radicals and hydroxyl radicals (OH^-), which in turn cause damage to the DNA. The main radiation effect is produced through free radicals, i.e. through indirect ionization. As cells have self-repairing mechanisms for DNA damage, the DNA damage caused by ionization is somewhat reversible. However, when DNA has double-strand breaks (DSB)[15] then this damage is irreversible and thus more significant. The DNA damage can be inherited through cell reproduction, accumulating damage from prior cancer cells over several generations, causing them ultimately to die or malfunction.

One of the major limitations of radiation therapy is that cells of solid tumors often become oxygen-deficient. Solid tumors can generate a low-oxygen state known as hypoxia [16], as the tumor outgrows the blood supply providing the oxygen. Oxygen can work as a radiation sensitizer during radiation, increasing the damage of a given radiation dose by forming DNA-damaging free radicals. Tumor cells in a hypoxic state may be more resistant to radiation than those in a normal or rich oxygen state. Several methods have been developed to overcoming this problem, such as high pressure oxygen tanks, blood substitutes that carry more oxygen, hypoxic cell radiation sensitizers such as misonidazole [17] and metronidazole [18], and hypoxic

cytotoxins [19] such as tirapazamine [20]. Carbon ions may have an antitumor effect which is less dependent on tumor oxygenation as these particles act directly to cause DNA damage [21].

1.1.3 Dose of radiation therapy

The amount of energy deposited in a mass by radiation therapy is measured in gray (Gy). For example, the typical total dose range for the irradiation of a solid tumor is from 60 to 80 Gy, while for lymphomas it may be as low as 20 to 40 Gy [22-25]. Physicians need to consider many other factors when they select a dose level for treatment, such as whether the patient is receiving chemotherapy, patient co-morbidities and the degree of success of surgery.

A prescription from a radiation oncologist means that a treatment plan has been determined by imposing a dose distribution over the patient's images. This also means that the delivery parameters of a prescribed dose are decided and approved by a physician. Depending on the optimization algorithm used for a treatment plan, multiple beams set at different angles may be used to complete the delivery of the total prescribed dose [26]. The approval of a treatment plan generally requires an appropriately high dose to the target with a uniform prescription dose to the tumor and a minimal dose to surrounding healthy tissues.

1.14 Fractionation

The total dose is fractionated for patient treatment. There are several reasons to fractionate the total dose. Fractionation provides time for normal cells to repair, while

tumor cells are generally less efficient in repairing themselves during the same time. Fractionation allows tumor cells that happen to be in a relatively radioresistant phase cycle at the time of a given fraction delivery to move into a sensitive phase during the delivery of another fraction. Similarly, chronically or acutely hypoxic tumor cells may re-oxygenate between fractions, which may help to improve the radiation therapy results. Fractionation regimes are individualized. Within the United States, the typical fractionation schedule for a cancer patient is 1.8 to 2.5 Gy per day, five days a week.

1.2 Lung cancer

Lung cancer, which carries the highest cancer mortality rate in humans, is responsible for around 1.3 million deaths worldwide annually [27]. Lung cancer presents either in the form of small cell lung carcinoma (SCLC) or non-small cell lung carcinoma (NSCLC), named by the type of cells. This type distinction is important for treatment, as NSCLC is sometimes treated with surgery, and SCLC usually responds better to chemotherapy and radiation.

Choices of treatment for lung cancer include surgery, radiation therapy and chemotherapy. Radiation therapy is often prescribed together with chemotherapy, and may be used with curative intent in patients with NSCLC who are not eligible for surgery. This form of high intensity, high dose per fraction treatment in radiation therapy is called stereotactic body radiation therapy (SBRT).

1.3 Planned target volume (PTV) and tumor isocenter

The gross tumor volume (GTV) delineates the size and location of the tumor.

Outlining of the GTV is possible if the tumor is visible by imaging as shown in Figure 1.1. The clinical target volume (CTV) consists of the demonstrated variability of tumor tissue relative to any other tissue in the vicinity. The internal target volume (ITV) is defined as the CTV with an internal margin compensating for any internal physiological movements, i.e. a variation in size, shape, and position of the CTV, during therapy. The planning target volume (PTV) is the volume of the ITV with a setup margin compensating for patient movement and setup uncertainties. In SBRT for lung cancer, we use an ITV with a 5mm margin to generate the PTV. However, the accuracy of ITVs using maximum intensity projection (MIP) images acquired from irregular breathing patterns has been questioned by several groups [13,14]. In our studies we have found similar discrepancies between image-based positioning and true localization of the moving target, which seems to suggest an underestimation of the tumor motion in irregular respiratory motion patterns.

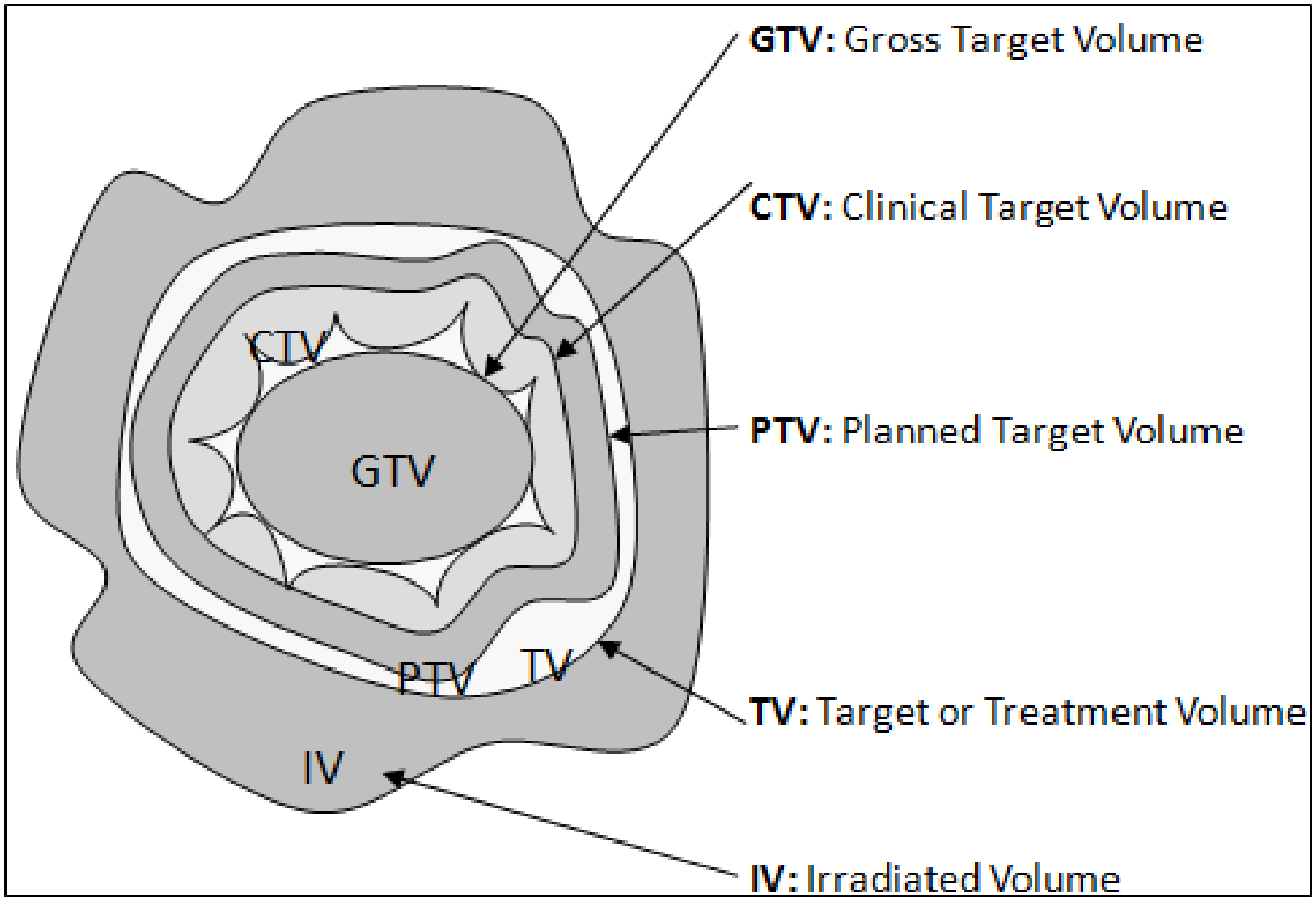

Figure1.1. Schematic illustration of International Commission of Radiation Units and Measurements volumes for radiation therapy

1.4 Stereotactic body radiation therapy (SBRT)

Stereotactic body radiation therapy for primary NSCLC has shown promising results compared to conventional radiation therapy treatment, with tumor control rates exceeding 90% [28, 29]. It improves the inoperable lung cancer patient survival rate and is the first significant change in radiotherapy technique in the last 50 years [30-32].

Compared with conventional external beam radiation therapy, the essential characteristic of SBRT is the precise delivery of a few, high dose fractions (typically 3 to 5) to a total dose reaching 50 to 60 Gy to a small target volume. With image-guided radiation treatment (IGRT) technology, it is possible to safely deliver very large individual doses of radiation to tumors in widely disparate extra-cranial locations. Careful, disciplined analyses of the results of well-designed clinical trials of SBRT have led to new understandings of the nuances of normal tissue response to high-dose ionizing radiation.

SBRT offers a noninvasive treatment choice with a high local control rate. For metastatic disease patients, SBRT can serve as an auxiliary treatment option retarding cancer growth. SBRT offers unique advantages relative to conventional radiation therapy in terms of greater biological potency.

1.4.1 History of SBRT

The dose tolerance of normal tissue for very large dose per fraction treatment is well known. Soon after the discovery of radiation in the 1900s, large dose per fraction

treatments were performed to treat accessible tumors. As the photons used for radiotherapy have low tissue penetration ability due to their energy limit, a large amount of healthy tissue exposure to the high dose was inevitable. The late toxic effects consistently appeared months after treatment and were often severe [33]. The late toxicity appeared to affect mostly normal tissue such as soft tissue, connective tissue and bone. The main toxicity was sclerosing of the normal tissue with signs of reduced vasculature. For this reason, physicians abandoned the use of large dose per fraction treatments and instead used conventionally fractionated radiation therapy (CFRT) that was generally less toxic.

CFRT capitalizes on the inherent differences between normal and cancer tissue repair mechanisms. Cancer tissues for the most part have lost the ability to repair themselves. On the other hand, normal tissues have a good potential for proliferation and repair following radiation injuries. When CFRT is given in small, multiple daily doses of radiation to both normal tissue and tumor, the normal tissue repairs itself better and only modest damage to this tissue occurs relative to the damage to the tumor tissue. Over the course of many days (over 30 treatments), the cumulative damage to the tumor tissue is greater than that to the normal tissue. Hence, there is a therapeutic benefit as explained by Coutard and Baclesse [34, 35]. SBRT, on the other hand, differs considerably in its approach. It relies on high exposure per fraction. In this case it is assumed that normal tissues as well as tumor tissues are both irreversibly affected.

CFRT has been shown to allow the survival of some tumor clonagens, even after large cumulative doses of radiation. The survival of tumor tissue will put the patient at high risk of tumor recurrence. To overcome this inherent radio-resistance in CFRT，radiation oncologists use CFRT as an adjuvant tool for surgery.

The idea to develop SBRT was inspired by stereotactic radiosurgery (SRS). In 1951, the Swedish neurosurgeon Lars Leksell, at Karolinska University hospital, treated brain cancer patients using a stereotactic technique in a single session with ^{60}Co radioisotope sources. Although a single large-dose radiation treatment contradicted the rule of known tissue tolerance, Leksell successfully delivered the treatment. Unlike CFRT, which irradiated a large volume of normal tissue compared to the tumor, Leksell's SRS delivered the high dose to the target only. The first-generation gamma knife was introduced by Leksell in 1968 [36]. The gamma knife was equipped with multiple ^{60}Co sources, which delivered radiation through multiple collimated narrow beams that precisely focused on a tumor. As the dose gradient around the edge of the tumor volume was extremely steep, a high dose could be delivered to a small target volume with much less dose to surrounding normal tissue. The gamma knife provides not only a unique dose distribution but also incorporates a head frame to locate the tumor position relative to the coordinates of the frame.

To mimic the treatment of SRS outside the skull, Hamilton and colleagues reported treating spine tumors with a rigid immobilization frame [37, 38]. The frame for this treatment was designed to screw onto the spine. Despite the help of the frame,

however, the conduct of the treatment was not as good as with the treatment of brain tumors. During the treatment of brain tumors, the immobilized skull assures very little additional movement of the tumor. However, outside of the skull, tumors in the body may be displaced over time with force from muscle contractions, breathing, gastrointestinal peristalsis, cardiac activity, and many other physiological processes. All these movements cannot be eliminated, which make SBRT less accurate than SRS.

To deal with the issue, Ingmar Lax and Henric Blomgren constructed a body frame that provides both comfortable patient immobilization and respiration-related motion control [39]. Subsequently, they treated patients with localized tumors with a dosimetry plan that mimicked SRS. The dosimetry plan was constructed with multiple non-coplanar beams with similar target-dimension apertures. Each beam carried a relatively lower weight than that used in CFRT to help the convergent target dose escalate rapidly. Local tumor control was achieved with this approach and was better than expected. The initiators of the therapy therefore treated more patients than they planned originally [40].

In the 1990s, Shirato and colleagues reported an investigation characterizing and accounting for respiratory motion during radiation treatment. While initially they did not use the same dose schedules as current SBRT regimens, tumor motion control plays an important role in SBRT treatment [41].

With the acquisition of more advanced technology, several groups carried out

extra-cranial treatments and began formalized prospective testing [29, 42-44]. Initially, they performed dose escalation toxicity studies in liver and lung to find the most potent dose schedules for typical primary and metastatic tumors. Those prospective studies helped increase understanding of the use of SBRT.

1.4.2 Immobilization and target motion issues

Precise radiation delivery is an essential component for SBRT. The geometry and dose distribution from the treatment plan should closely match what is actually delivered to the patient. This requires not only that the target is exposed to the minimum prescription dose for tumor control, but also that normal tissue receives no more dose than planned.

In CFRT, target motion is accounted for by enlarging the primary beam's aperture. In contrast, SBRT uses an ablative dose to the target and minimizes normal tissue volume exposure so that the enlargement of margins is very much discouraged. Thus motion control must be applied to restrict the PTV to only slightly larger than the GTV. The entire GTV has to be strictly encompassed by the prescription isodose.

Motion control devices operate in three general categories by: (1) restricting the target movement, (2) gating, and (3) tracking. Restrictive motion devices, such as abdominal compression, aim at decreasing the respiratory motion range. Gating systems coordinate the delivery with the respiratory cycle by activating beams only in specific breathing segments. Tracking systems literally move the radiation beam to follow the path of the moving tumor. Tracking may be applied by moving the entire

accelerator, the multi-leaf collimator, or by moving the patient on the couch counter to the motion of the anatomy. Even with these motion-control devices and processes, some uncertainty still requires that the PTV is larger than the GTV. In general, a typical dose prescription to compensate for the uncertainty of target position due to motion should not be greater than 1.0 cm in the cranial caudal plane and 0.5 cm in the axial plane.

1.4.3 Physics and dosimetry of SBRT

SBRT is an appropriate treatment for well-delimited visible gross disease up to 150 cm^3 in volume. It is not an adjuvant treatment after removal of gross tumor since the intent of the therapy is to ablate targeted tissues. The physics and dosimetry of SBRT must be obeyed with these unique aspects of the therapy. SBRT is characterized by:

1. Secure and comfortable immobilization avoiding or limiting the patient movement for the typical long treatment sessions.

2. Accurate patient repositioning from planning sessions to each treatment session, to ensure proper placement of intended dose deposition.

3. Proper accounting of inherent internal organ motion such as breathing during planning and treatment.

4. Dose distributions must not only cover the tumor within high dose regions but also fall off rapidly to surrounding normal tissues. The dosimetry must be conformal. However, in contrast to CFRT, the dosimetry of SBRT may allow significant heterogeneity of dose distributions inside a target.

5. Registration based on the patient's anatomy, constructed dosimetry, and treatment delivery to 3-D coordinates system defined by markers. The markers positions can be confidently correlated both to the tumor target and the treatment delivery device. A "stereotactic" treatment is one directed by such marker references.

6. The dose prescriptions of SBRT use hypofractions (i.e., 1-5 very high dose fractions of a minimum of 6-8 Gy per fraction but often as high as 20-30 Gy per fraction).

SBRT may use radiotherapeutic innovations such as 3-D conformal therapy, IMRT and IGRT. Most SBRT treatments employ high energy photons (x-rays) as the source of radiation energy. However, any form of ionizing radiation such as protons and electrons can be used within a properly designed delivery system. In the end, it is essential that a very compact dose distribution encompasses the intended target. The effect on tissues within the high dose regions in SBRT is biologically damaging. Therefore, misplaced delivery may lead to often dramatic normal tissue injury.

A conformal dose distribution that falls off very rapidly in all directions generally requires the use of multiple non-coplanar shaped beams. Highly shaped beams are preferred as a high dose is best avoided in normal tissues by sharp collimation of the primary beam attenuation outside of the target at the beam's eye view (BEV). Another approach would be to use Gamma Knife® and Cyberknife® with smaller non-shaped beams and reposition the beam to treat successive regions of the target. A scattered dose is harder to control, even by highly shaped beams, but the scatter contribution is

relatively small comparing to the overall dose deposition for most treatments.

Most modern SBRT treatments for lung and liver targets use at least 8-10 highly collimated beams. To avoid an overlapping dose from opposing beams, the beams' arrangement should not be directly opposite and should have a large angles between them. To assure the dose gradient's rapidly fall-off in all directions outside the edge of the tumor, the beams should be non-coplanar. Coplanar treatments are commonly utilized in CFRT, particularly in IMRT, with low and intermediate doses that surround the tumor in a belt shape. Except for tumors in the vertebral bodies of the spine, there is no reason to build a predominantly axial dose distribution based on anatomy, tissue function, or known patterns of tumor. Not only collisions between the couch and the accelerator head, but also the position of critical organs, limits the ability to generate truly compact decreasing dose gradients around targets; however an effort should be made to construct such an ideal distribution as much as possible.

To judge the quality of the delivered dose distribution for SBRT, we need to appraise the target conformality to prescription dose coverage, accuracy, high dose "spillage", and intermediate dose "spillage". In SBRT, the target is demarcated in space; the dose outside of the target is wasted or harmful and does not serve any specific purpose. It is assumed that the GTV is almost identical to the CTV for conduct of the treatment. IMRT may be utilized to differentiate the dose to the GTV from that to the CTV; however, both targets must still be in the range where tissue ablation occurs for the treatment to constitute SBRT. As target motion and setup

inaccuracies are unavoidable, an additional margin must add to the GTV/CTV targets to avoid missing the intended target during part or all of the treatment session. This expanded target mentioned in section 1.3 as the PTV constitutes the final target for high dose conformal coverage.

In the PTV and in the shell of normal tissue immediately outside of the PTV are the regions of intermediate or high dose coverage where ablation occurs. In this situation, side effects will or will not occur depending on: (1) the thickness of the shell of tissue for normal organ function, and (2) the volume of this shell as it relates to dosimetric quality. This high dose spillage is likely the cause of most toxicity in serially functioning tissues such as the GI tract, and tubular structures in the lung and liver, which may cause obliteration of the lumen and subsequent downstream effects. Furthermore, the quality of the dose distribution also affects the volume and geometry of low and intermediate dose distributions. This low and intermediate dose spillage is evaluated by the maximum dose at a defined distance away from the PTV. Low dose spillage can affect a large volume of critical organs, similar to large fields in CFRT damaging parallel functioning tissues, and can also cause focal organ injury if the prescription dose is too high.

The dose conformality to the PTV is generally assessed by a conformality index. This index is defined as the ratio of the prescription isodose volume to the PTV volume. Generally, this index should be below 1.2 as shown in Table 1.1. Achieving this requirement of conformality is easier for larger targets. Compared with the

homogeneous target dose distributions of CFRT, SBRT may have dramatic heterogeneity of dose. It requires that regions inside the PTV are not underdosed relative to the minimum prescription dose. Overdosage of the target sometimes may be inconsequential and even advantageous for hypoxic tumors. It is critical that the high dose associated with heterogeneity not be physically located outside of the PTV.

Maximum PTV Dimension (cm)	Ratio of Prescription Isodose Volume to the PTV		Ratio of 50% Prescription Isodose Volume to the PTV, $R_{50\%}$		Maximum Dose 2 cm from PTV in Any Direction, D_{2cm} (Gy)		Percentage of Lung Receiving 20 Gy Total or More, V_{20} (%)		PTV Volume (cc)
	Deviation		Deviation		Deviation		Deviation		
	none	minor	none	minor	none	minor	none	minor	
2.0	<1.2	1.2-1.4	<3.9	3.9-4.1	<28.1	28.1-30.1	<10	10-15	1.8
2.5	<1.2	1.2-1.4	<3.9	3.9-4.1	<28.1	28.1-30.1	<10	10-15	3.8
3.0	<1.2	1.2-1.4	<3.9	3.9-4.1	<28.1	28.1-30.1	<10	10-15	7.4
3.5	<1.2	1.2-1.4	<3.9	3.9-4.1	<28.1	28.1-30.1	<10	10-15	13.2
4.0	<1.2	1.2-1.4	<3.8	3.8-4.0	<30.4	30.4-32.4	<10	10-15	21.9
4.5	<1.2	1.2-1.4	<3.7	3.7-3.9	<32.7	32.7-34.7	<10	10-15	33.8
5.0	<1.2	1.2-1.4	<3.6	3.6-3.8	<35.1	35.1-37.1	<10	10-15	49.6
5.5	<1.2	1.2-1.4	<3.5	3.5-3.7	<37.4	37.4-41.7	<10	10-15	69.9
6.0	<1.2	1.2-1.4	<3.3	3.3-3.5	<39.7	39.7-41.7	<10	10-15	95.1
6.5	<1.2	1.2-1.4	<3.1	3.1-3.3	<42.0	42.0-44.0	<10	10-15	125.8
7.0	<1.2	1.2-1.4	<2.9	2.9-3.1	<44.3	44.3-46.3	<10	10-15	162.6

Table 1.1 Dose limit for various PTV of SBRT lung cancer in RTOG 0236 [45].

Minimum low and high dose spillage criteria for SBRT treatments were established in the RTOG 0236 protocol for treating medically inoperable patients with lung cancer. These dose requirements were based on dose distributions from patients treated with SBRT for lung cancer in prospective trials at Indiana University.

Basically, as these criteria were met and patients were treated with the prescription of 60 Gy total in 3 fractions (20 Gy per fraction) to tumor targets, the treatments were

reasonably well-tolerated. While meeting these requirements, there were still side effects but with acceptable toxicity. The target conformality index criteria shown in Table 1.1 include: the $R_{50\%}$ which is the ratio of the 50% of prescription dose volume to the PTV volume (used to measure low dose spillage); the D_{2cm} is the maximum dose 2 cm from the PTV in any direction (used to measure the isotropic dose falloff); and the V_{20} which is the volume of total lung that receives a dose of 20 Gy or more (a parameter found to be important for CFRT toxicity).

Although most quoted tolerances are generally quantified as major dose limits, it is clearly inadequate for SBRT where toxicity is related to exceeding a specified volume of tissue receiving the dose rather than the absolute dose level. Experimental data collected in active protocols justify changing dose-volume tolerances for specific organs in SBRT. At the present time, however, not enough data have been accumulated to provide final values for tolerances. Instead, most researchers are using limits converted from linear quadratic modeling from CFRT or applying limits based on limited data in treated patients. As volume effects are not fully understood, absolute point limits were used for critical organs such as the spinal cord, esophagus, and major bronchial airways in RTOG 0236. These limits may be subject to modification in further evaluation and are listed in Table 1.2.

Organ	Volume	Dose (cGy)
Spinal Cord	Any point	18 Gy (6 Gy per fraction)
Esophagus	Any point	27 Gy (9 Gy per fraction)
Ipsilateral Brachial Plexus	Any point	24 Gy (8 Gy per fraction)
Heart	Any point	30 Gy (10 Gy per fraction)
Trachea and Ipsilateral Bronchus	Any point	30 Gy (10 Gy per fraction)
Whole Lung (Right & Left)	(See Table 1)	(See Table 1)

TABLE 1.2 Normal tissue dose tolerance limits in RTOG 0236 for SBRT for primary lung cancer with 60 Gy in 3 fractions [45].

The dose quality also depends on the complexity of the treatment planning system. It is essential for SBRT to use 3-D conformal therapy with multi-plane representation of dose and ability to obtain accurate dose volume histograms (DVH) for assessment. Many SBRT cases will require beams to travel through heterogeneous tissues to the target. In these cases, the planning system should provide algorithms for accurate accounting of tissue heterogeneity effects on dose deposition from both attenuation and scattering events. However, some published reports show that using a heterogeneity correction algorithm may cause greater inaccuracies of dose representation at the edge of the PTV than using no correction at all [46]. The pilot study from Indiana University that formed the basis for RTOG 0236 was carried out without heterogeneity corrections in the treatment planning process as lung and all other tissues were set to water density [29, 47]. Researchers at Indiana University used Monte Carlo treatment planning to compare with the heterogeneity uncorrected actual treatment plans. They found significant absolute errors in the plans without accounting for heterogeneity particularly at the center of the target and within the lungs. However, the doses to the PTV and beam monitor units were reasonably close.

In all, it seems most reasonable to either use sophisticated heterogeneity corrections such as collapsed cone or no heterogeneity corrections at all for SBRT treatments in or near the lungs.

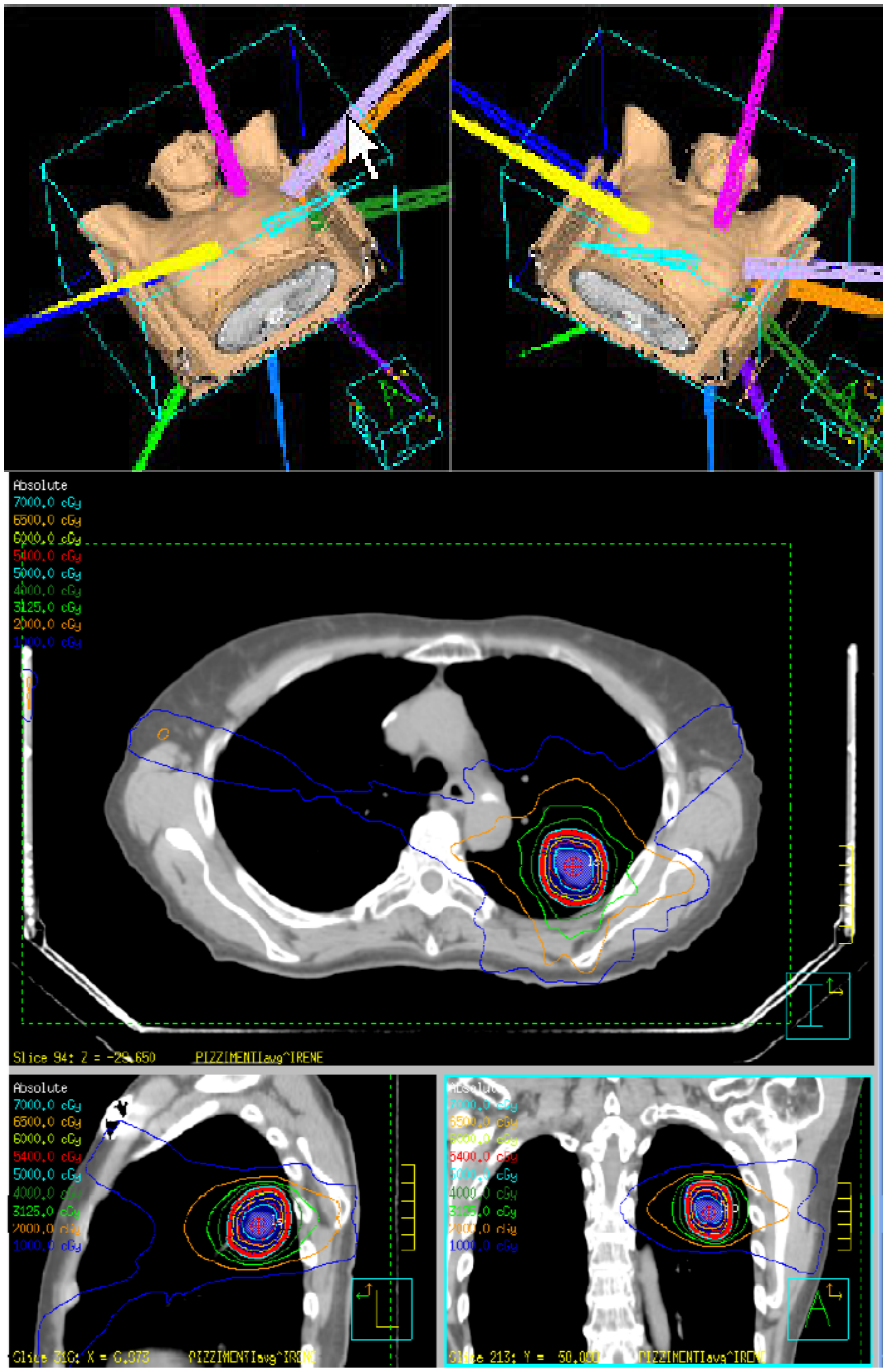

Figure 1.2. Typical SBRT dosimetry for treating a primary lung cancer patient

An example of typical SBRT dosimetry for treating a primary lung cancer is shown in Figure 1.2. The patient was immobilized in the Elekta Body Frame with abdominal compression to decrease respiratory motion. The GTV was outlined using lung windows on a CT simulator. Based on RTOG 0236, the PTV was expanded from the GTV by 0.5 cm in the axial plane and 1.0 cm in the superior-inferior plane. Fluoroscopy was recommended to confirm tumor movement. Dosimetry was constructed after targeting the PTV with an 8-12 static field beam arrangement. The choice of beam angles took into consideration not only the realm of attainable beam angles for a tumor in this location but also the need to avoid collisions with the accelerator head. With a set of attainable beam angles, beam weight optimization was used to obtain these angles, using the RTOG tolerances to construct avoidance structures. After optimization, these beams are non-coplanar, non-opposing, and are separated by fairly large angles. Beam weights are fairly equal for all beams for the purpose of spreading out the entrance dose. The patient was treated with 60 Gy total in 3 fractions (20 Gy per fraction) without heterogeneous correction.

1.4.4 SBRT procedure for lung cancer treatment

The SBRT procedure for lung cancer patients involves teamwork and new imaging technologies. Well-trained physicians, physicists, dosimetrists and therapists work together to assure the correct procedure for patients. The whole SBRT procedure is outlined in Figure 1.3. Both 4DCT and CBCT planning play important roles during

the process to assure accuracy in treatment.

In order to minimize mobility of the tumor in lung cancer, a body frame is used for patient setup. The laser on the body frame aligns with body markers (tattoos) on the patient. After setup, patients are monitored with fluoroscope for their tumor movement. Abdominal compression is used at UT Southwestern Medical Center if the tumor movement is over 10mm. Patient's 4DCT scan is finished in 2 minutes, after which, following 4DCT reconstruction, the average and MIP images are sent to the Pinnacle treatment plan system. Based on these images, the physician will contour the tumor size (ITV) on MIP images. The ITV is expanded with a 5mm margin in all direction to create the PTV for treatment. The dose calculation and critical organ contouring are based on average images.

A typical SBRT plan for lung cancer contains 9-12 non-coplanar beams. A sample listing of related couch and gantry angles is presented in table 1.3. Four of them are non-coplanar beams, which helps to build a more compact dose distribution around the target. However, due to the limits of the linear accelerator, the non-coplanar beams' angle relationship between gantry and couch will vary based on the brand of machine. The data presented in Table 1.3 are from an Elekta Synergy S machine.

Beam	Plans	
	Gantry	Couch
1	180	0
2	220	345
3	270	25
4	270	335
5	315	0
6	30	270
7	330	270
8	45	25
9	90	0
10	150	0

Table 1.3. Typical gantry and couch angles of beam setup for SBRT in lung cancer

After completion and approval of a treatment plan, quality assurance for the plan is performed to ensure the correct treatment. Part of the quality assurance is verification that the gantry and couch angles can be achieved without collision. Before initiating patient treatment on the accelerator, we need to reproduce the same patient position as utilized in the 4DCT simulator and represented in the treatment planning software. The body frame provides accurate patient reference to within 1mm if the body is rigid, fixed and immobile and if no human error interferes with the data collection and transfer. We use CBCT as final verification of patient setup for treatment. Thus each patient receives a full CBCT scan after they are repositioned to simulation geometry setup in the body frame. Based on registration of the CBCT images relative to the 4DCT images, we shift the couch so that the target isocenter is moved to the isocenter of the accelerator. The whole procedure of SBRT treatment is shown in Figure 1.3.

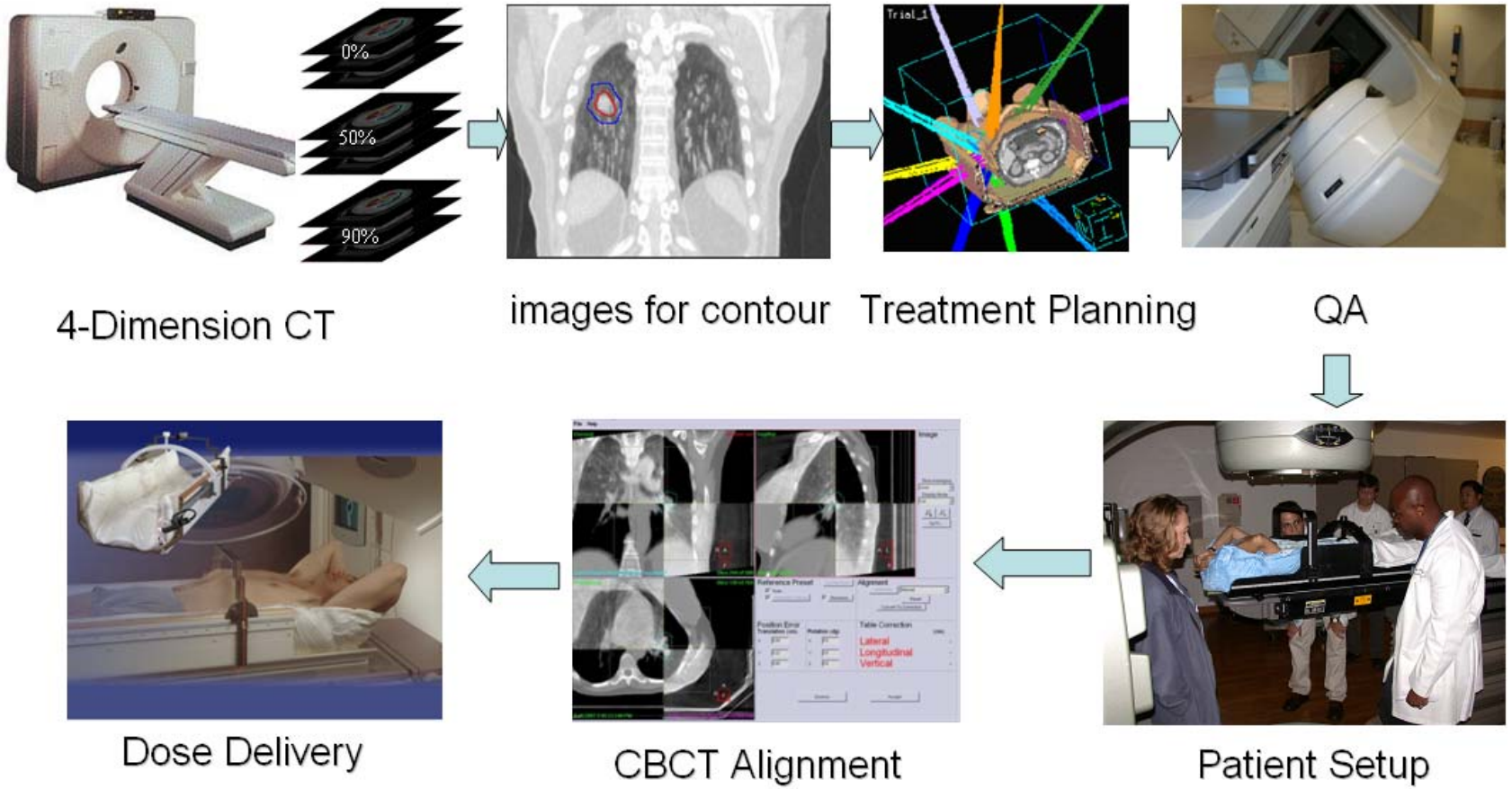

Figure 1.3. The SBRT procedure for lung cancer in UT Southwestern Medical Center

1.5 Four-dimensional computed tomography (4DCT)

Respiratory-induced motion of the tumor and normal tissues may cause significant artifacts in images acquired by CT scan. 4DCT was invented to account for respiratory motion during imaging, and to produce accurate images of tumors at different phases of the breathing cycle. 4DCT is an integral step used in 4D radiotherapy and has been used as part of treatment planning in clinical settings.

For sinusoidal respiratory motion, 4DCT is able to produce images that are more accurate than ones produced by regular CT scan. The accuracy of these 4DCT images may increase the accuracy of tumor delineation for radiation therapy.

Another advantage of 4DCT is that it provides tumor location information over a period of around 100 seconds. Each image reconstructed from data was acquired through a span of 100 seconds. Since 4DCT produces images at ten phases in the patient's breathing cycle, the images provide information on the tumor location for an "average" breathing cycle.

1.5.1 4DCT algorithm

4DCT obtains information from the real-time monitoring of a patient's breathing cycle during the scan. The monitoring can be performed by a number of different devices; however, all of them provide a waveform that approximates the superior-inferior position of patient's abdominal surface as a function of time. The assumption is made that the waveform is directly correlated to the cranial-caudal motion of the patient's internal organs as a function of time. During scanning, the

acquisition time of each image slice is assigned to a corresponding respiratory phase at each point of the waveform. Phases are specified as a percentage of the whole breath cycle, such as 0%, 10%, 20%… 90%.

4DCT uses a conventional 3DCT simulator coupled with a breathing monitoring device. In cine mode, the CT couch stops at one of multiple pre-defined couch positions while the simulator continuously acquires data. The duration of these positions are set for at least one period of the patient's breathing cycle, around 4 to 5 seconds. Then the x-ray beam is turned off while the couch moves to the next position and the scanning is repeated. Couch translation limits are set to cover the entire cranial-caudal imaging region of interest (ROI); couch positions do not overlap at each image area.

In the helical mode, the couch positions are not stationary. The couch moves very slowly as the CT simulator continuously acquires projection data and the x-ray image beam is never turned off. Figure 1.4 demonstrates how sorting of the images works in 4DCT based on the respiratory signal. The external device such as an air bellows belt or respiratory position monitor (RPM) provides the respiratory signal while 4DCT scanning proceeds. After scanning is complete, the raw data is used to reconstruct 4DCT images in multiple breathing cycle phases. There are two main approaches to data sorting: one is sorting data before reconstruction (GE), and the other is sorting after reconstruction (Philips). Since we only used the Philips system in our study, all the 4DCT images were sorted after reconstruction. Comparisons of the accuracy of

these two approaches in representing the geometry of moving structures of the body are not investigated in our studies.

MIP images are generated from ten-phase image sets from 4DCT as shown in Figure 1.4. It is more convenient and more efficient for physicians to contour the tumor in MIP instead of contouring the target in the ten-phase image sets.

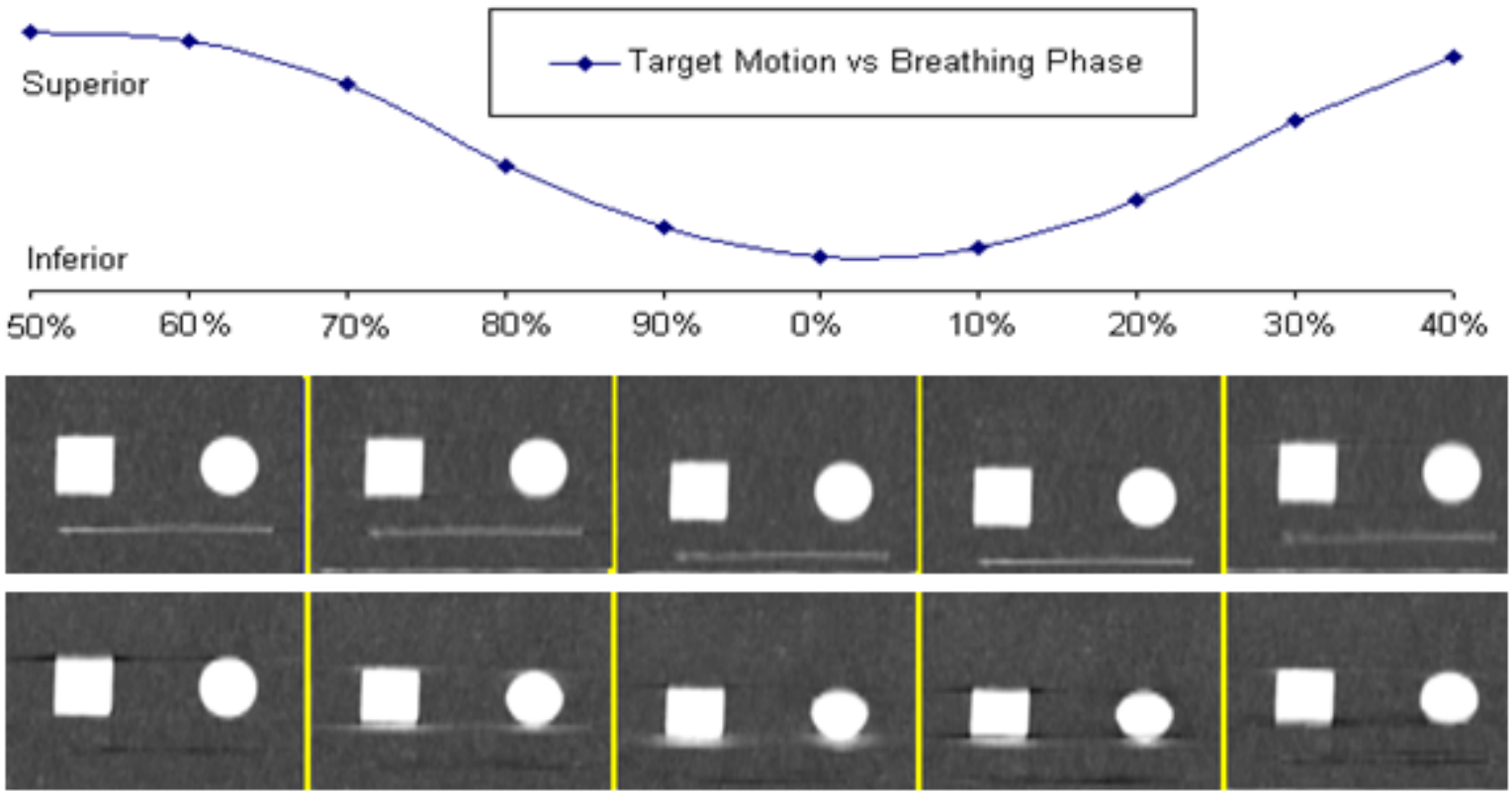

Figure 1.4. 4DCT sorts the phase images based on the position of breathing pattern.

1.5.2 Problem of 4DCT

One critical source of errors in GTV delineation is tumor motion due to the patient's breathing. In order to obtain more accurate temporal and spatial information on a moving target, 4DCT is widely used. This technology enables clinicians to individualize the ITV [48], which includes organ motion and an additional margin for setup errors, more precisely. Utilizing a modified cardiac phase binning technique used in imaging respiratory-related target motion, 4DCT combines and sorts raw data into phase-binned images [49, 50].

In principle, 4DCT allows the generation of an ITV from the set of binned CT images containing temporal and spatial information related to the patient's breathing. However, irregular breathing motion intrinsically affects the consistency of the 4DCT images due to the use of a binning algorithm to process the raw data. Incomplete or mismatched data may result in geometric irregularities. Various approaches to cope with the artifacts due to irregular breathing patterns have been investigated [51-53]. For example, breath-holding and breath-coaching techniques as well as amplitude sorting reconstruction algorithms are being actively studied by many researchers [50].

1.6 Cone-beam computed tomography

Image-guided radiation therapy (IGRT) may be defined as a radiation therapy procedure that uses image guidance at various stages of its process: patient data acquisition, treatment planning, treatment simulation, patient setup, and target localization before and during treatment. One of the techniques for patient setup is

cone-beam computed tomography (CBCT). Based on the x-ray source, CBCT can be defined as either KVCBCT or MVCBCT. The KVCBCT for radiation therapy is introduced by Jaffray et.al. [54, 55] and is discussed in this work.

The idea of CBCT is based on a KV x-ray source and detector mounting on a medical linear accelerator for radiography, fluoroscopy, and volumetric images. CBCT depicts the bone and soft tissue positions using three-dimensional volumetric image data acquired from projections during a single rotation. CBCT uses a cone shaped beam and acquires projections by means of a 2D detector. The 2D projected images from the detectors are reconstructed into a 3D volumetric image data set using a filtered back-projection technique. It is widely used for patient setup in IGRT.

However, due to the typical linear accelerator imaging equipment limitations, CBCT provides only 360 degree scan images and allows only a limited number of scanning speeds in clinical applications, as shown in Figure 1.5. The advantage of CBCT is that this tool has the ability to visualize the patient's anatomy for every treatment fraction and is suitable for adaptive corrections of treatment position. As SBRT delivers a very potent dose per fraction, the imaging of the patient's body before final alignment for treatment seems necessary for accurate dose delivery conforming to the treatment plan approved for therapy.

Thus CBCT seems to play an essential role for patient setup accuracy and precision of tumor position alignment. Wang *et al* reported a phantom study for CBCT as applied to regular respiratory motions and found that CBCT in this case provides very

accurate verification of the target position for treatment [56]. However, the accuracy of setups based on CBCT in the case of irregular breathing motions has not been thoroughly investigated so far.

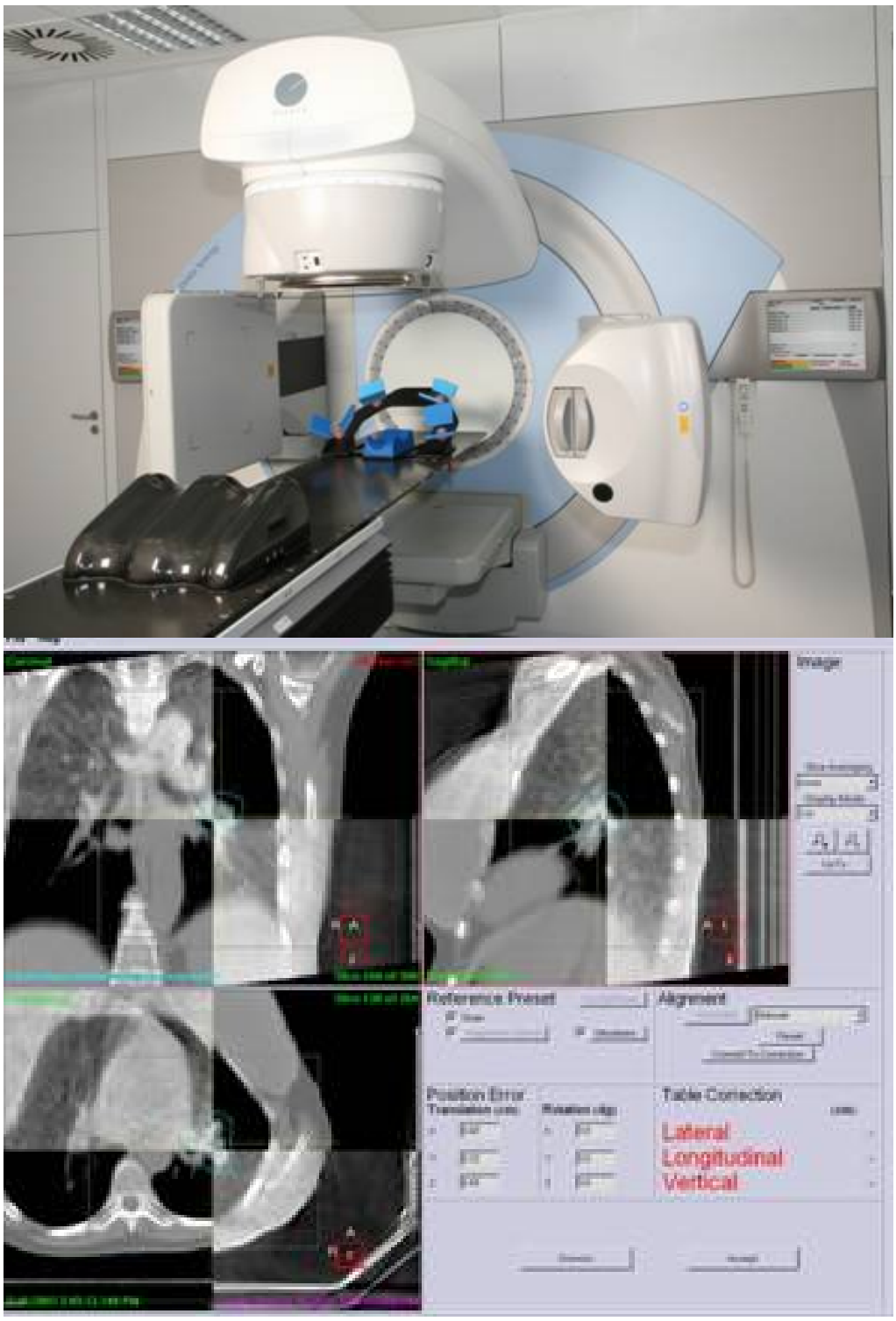

Figure 1.5. Elekta x-ray volume image (XVI) system with imaging registration software.

1.6.1 X-ray volumetric imaging (XVI)

The Elekta Synergy S treatment unit (Figure 1.5) at UT Southwestern Medical Center is equipped with an x-ray tube and an amorphous silicon (a-Si)/cesium iodide (CsI) radiation image detector panel [57] placed orthogonally to the treatment head and its electronic portal imaging device (EPID). This kV imaging system is X-ray volumetric imaging (XVI) system. The XVI unit shares the same axis of rotation with the MV treatment source.

In a single 360-degree rotation, or even in a 180-degree rotation, the XVI system can obtain a whole volume scan with lower image quality compared to a diagnostic CT scan. In a full 360-degree scanning, the XVI will acquire approximately 640 planar images which are used to make a full three-dimensional image. The rotation takes approximately two minutes with motion artifacts.

The KV photons are generated in a circular cone from the x-ray tube. Images can be acquired with three different field of views (FOVs): small, medium and large. The difference between the three FOVs is the offset from the kV central axis, which is 138.4 mm for the small FOV, 213.2 mm for the medium FOV and 262.0 mm for the large FOV. When a FOV is chosen, the detector panel is shifted to match the beam setup via a translation in the up-down direction. For the SBRT lung cancer treatment protocol, a medium FOV was chosen for CBCT scanning.

1.7 Significant studies

As SBRT requires a significantly high dose per fraction for lung cancer, the accuracy of delivery plays an important role in achieving a high tumor local control rate. To evaluate the dose delivery accuracy, 4DCT, CBCT and 4DCBCT techniques were involved in this study. These imaging techniques definitely improve the quality of SBRT treatment. However, most of these technologies operate on the assumption of static or regular target movement, which is not the case during actual patient treatment. To investigate the accuracy of these imaging techniques using simulated patient irregular movement, we may use a phantom study to assess these imaging techniques' accuracy and treatment quality for various types of breathing motions from real patients.

In this thesis, I will focus on these techniques to fully investigate the effect of irregular breathing motions. It not only helps us to prove the importance of breathing control for current lung cancer treatment, but also provides better margin choice for each individual patient.

CHAPTER TWO

4DCT IMAGES STUDY

2.1 Introduction

Stereotactic body radiation therapy (SBRT) has shown a promising result with tumor control rates superior to treatment with current conventional treatments [28, 58]. The essential characteristics of SBRT are precise delivery of a few high dose fractions to a small target volume. Thus PTV, which is derived from the delineated GTV, is a critical component in treatment planning where set up variations, as well as inter−fractional and intra−fractional target motion must be accounted for. Errors in PTV may lead to under-dosing the tumor or over-dosing the normal tissue causing increased toxicity. For hypo−fractionated dose escalation techniques, the PTV must be as small as reasonably possible in order to respect normal tissue tolerances when delivering higher total doses of radiation.

One critical source of errors in GTV delineation is the tumor motion due to patient's breathing. In order to obtain more accurate temporal and spatial information on a moving target, 4DCT is widely used. This technology enables clinicians to individualize ITV[48], which includes organ motion and an additional margin for setup errors, more precisely. Modifying cardiac phase binning techniques for use in imaging respiratory related target motion, 4DCT combines and sorts raw data into phase-binned images [49, 50]. In principle, 4DCT allows the generation of an ITV from the set of binned CT images containing temporal and spatial information related

to patient's breathing. However, irregular breathing motion affects inherently the consistency of the 4DCT images due to the use of regularly in time spaced binning algorithm to process the raw data that is naturally of random nature. Incomplete or mismatched data may result in geometric irregularities. Various approaches to cope with the artifacts due to irregular breathing pattern have been investigated [51-53]. For example, breath holding, regularizing breathing pattern through coaching techniques as well as improving amplitude sorting reconstruction algorithms have all been suggested as and actively studied by many researchers as means of removing the geometry definition inaccuracies in 4DCT[50].

As a trial to develop a more accurate ITV delineation method of moving tumor in clinical setting using 4DCT, we focused on the use of composite images such as MIP, MinIP and AVG CT images. MIP images reflect the highest data value encountered for each pixel along the set of phase images and so, they should defined complete volume inside body that contains any part of the target volume during its breathing motion pattern. On the other hand MinIP and AVG image reflect the lowest and average data value encountered respectively. It has been reported that the composite images, especially MIP, utilizing these standard volume–rendering post-processing images, are effective for the assessment of tumor mobility [59-62]. It provides accurate representation of the spatial domain that needs to be irradiated to cover fully the target with prescribed dose irrespective of motion that the target will exhibit during irradiation. There were preceding studies investigating the accuracy of ITV

determined using MIP images. Using MRI for real patients [61], MIP based internal target areas (ITAs) were shown to be comparatively smaller than the ITAs generated by MRI. Using a phantom moving along the anterior–posterior direction, evaluation of the 4DCT imaging was performed[63]. In this study, we investigated the correlation of the MIP images with breathing irregularity and scan parameter like gantry speed by using a lung phantom placed on a programmable motion platform. Taking advantage of the accuracy and reproducibility of our phantom, we implemented various target motions to determine the accuracy of 4DCT generated MIP images.

2.2 Material and methods

2.2.1 Phantom

A programmable motion platform was built using two stepper motors (Optimal Engineering Systems Inc, Los Angels, CA) and a driver / indexer unit with three degrees of freedom. A personal computer equipped with control software was used for coding and controlling platform motion. Despite the 2-D motion capability of the platform, only one dimensional motion along the superior-inferior direction was utilized in the current study. A cubic lung phantom made of an acrylic frame (dimension of 24(L) x 17(W) x 12 (H) cm^3, density of 1.20 g/cm^3) was built and placed at the top of the platform. Three cork plates (density 0.26 g/cm^3) were inserted into the frame to model aerated lung tissue known to have average density of 0.23 g/cm^3 [14]. Two different acrylic targets, a 25mm (D) × 20mm (H) cylinder and

a 25mm (L) × 20mm (W) × 20mm (H) block, were embedded in the middle of a cork plate as shown in figure 2.1-B.

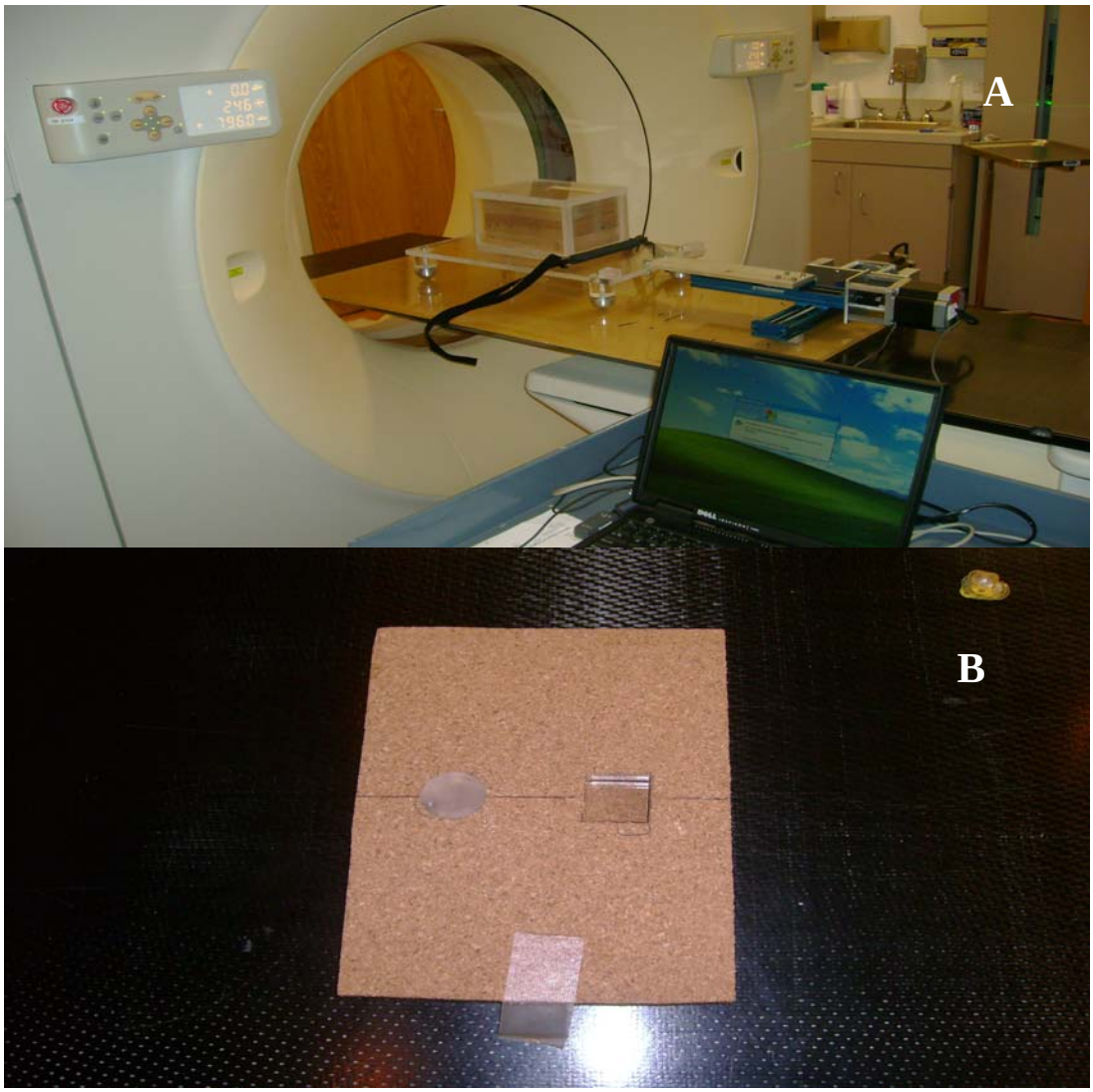

Figure2.1 A Dynamic Phantom setting for the measurement. **B** Two targets inserted in cork.

2.2.2 Target motion

In clinical settings with 4DCT capability, MIP is frequently used for the determination of ITV for lung tumors. Thus, to check its spatial accuracy, several sinusoidal motions and real patient tumor motions were implemented into our

programmable lung phantom. Simulated tumor motions are only along the superior-inferior direction. This is direction where most significant for clinical outcome motions of target occur. Moreover the choice of one dimensional motion simplifies our analysis and makes results apparent and easily interpretable for their clinical significance. Moreover, we notice that for one dimensional type of motion along the superior-inferior axis data acquisition parameters for 4DCT such as Pitch and Fan Angle are directly related to the motion.

Before 4DCT scan has been performed, phantom motions were monitored by linear position transducer with accuracy of 0.5mm and repeatability of ±0.05% for full stoke of 10cm (Unimeasure, INC., Corvallis, Oregon). As a result, the spatial accuracy was less than 0.5 mm about reference position, and the temporal target motion was within 0.2 sec about reference time.

The breathing pattern of a patient is irregular in both rate and amplitude and these irregularities are known to cause artifacts when reconstructed images are created. Our aim was to evaluate how these irregularities affect the final images in a measurable model. For that purpose, we designed several sinusoidal motion patterns first. For mono sequence, the amplitude and period of target motion were kept constant. Dual and triple sequences referred to target motions were designed by combining two or three different amplitudes as shown in figure 2.2. An example of dual sequence in figure 2.2, named as 2S2L, and was made by combining two small peaks (amplitude of 5mm) and period of 4sec with two large peaks (amplitude of

10mm and period of 4sec). The triple sequence was made by combining four small peaks (5mm, 4sec), four middle peaks (7.5mm, 4sec) and two large peaks (10mm, 4sec) and named accordingly as 4S4M2L. Most of target motions' periods were set to 4 seconds to simulate average breathing cycle of 15 breathing per minute (BPM). However, to study the influence of faster breathing on MIP image, some target motion was designed with shorter periods of 3.3 sec corresponding to 18 BPM.

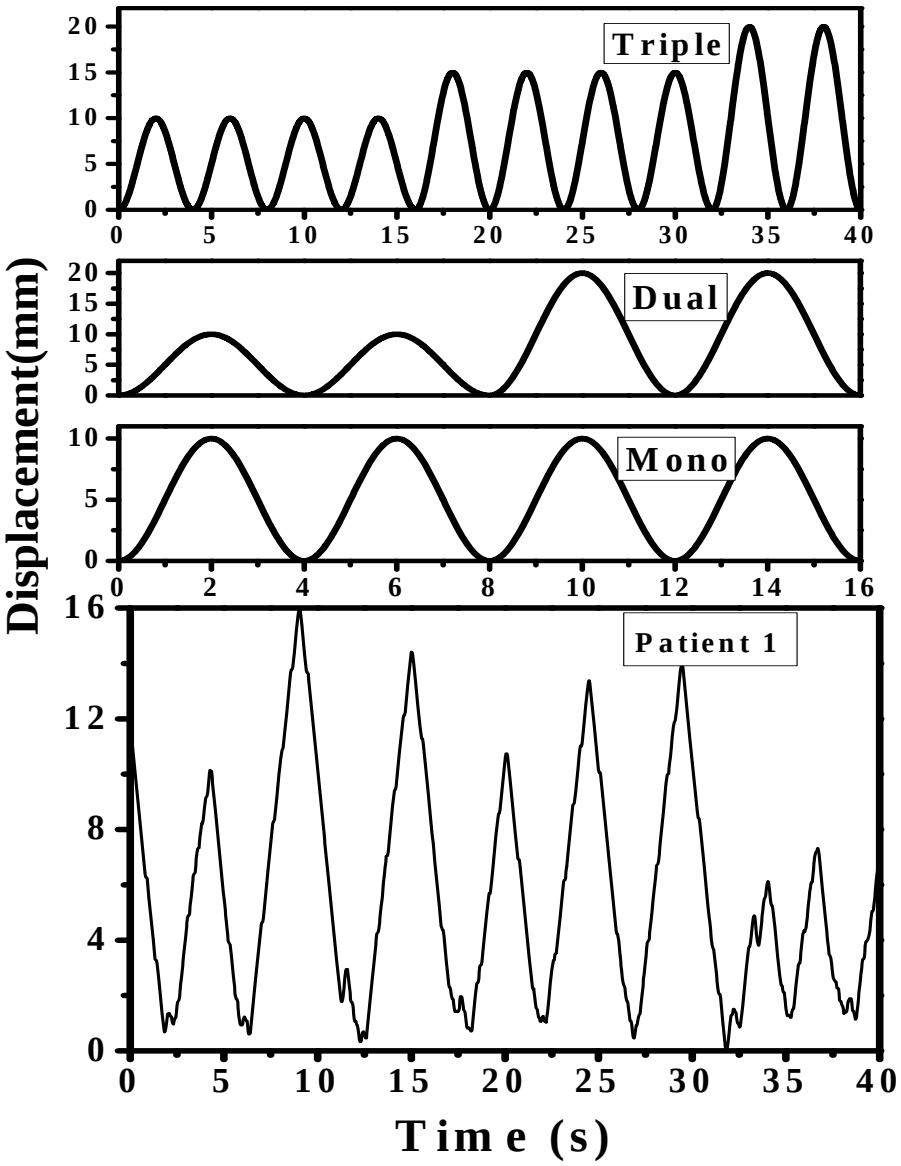

Figure2.2 Motion sequences: mono sequence in 15 BPM breathing, dual sequence in 15 BPM breathing, triple sequence in 15 BPM breathing, and patient motion

Clinically observed free breathing patterns and corresponding tumor motions of patients show spatial and temporal irregularities. We studied real patient tumor motion by implementing tumor motion data (originally from H. Shirato group[64]) into our dynamic phantom as shown in the figure2.2. Like the sinusoidal target motions, we simulated patient data only along the superior-inferior direction. In total, we have studied 40 different motion patterns of mono, dual and triple target motions with various combinations of amplitudes and periods and 10 patient cases.

2.2.3 4DCT data acquisition and analysis

All data acquisitions were made in helical mode on Philips Big Bore CT scanner, equipped with 16×1.2 mm^2 detector array. The CT current and voltage was set to 100 mA 120 kV respectively in all scans. Phantom motion was monitored by Philips Bellow System. The scanner software enables users to predefine protocols to optimize scan parameters for various anatomical parts. In the protocol for 4D lung imaging, the relationship of pitch and gantry rotation time is crucial for acquisition of accurate images. As shown in previous studies, the pitch factor and the gantry rotation time need to satisfy the following inequality (1):[65]

$$\text{Gantry rotation time} \times (1/\text{Pitch} + \text{Fan angle}/360) \geq \text{Breathing period} \quad (1)$$

Our lung protocol was set as recommended by the vendor to satisfy the above inequality. Default setting parameters were a pitch of 0.082, field of view of 440mm

and gantry rotation time of 0.5 sec/rotation. Typical scan time took up to 100 seconds in our measurements with these settings.

After scanning, the raw CT data were sorted and reconstructed by phase binning reconstruction algorithm using the respiration profile from the bellow system. Inhalation and exhalation positions on each breath cycle were defined automatically by the bellow system and simple statistical summary of respiration cycles were provided. After reconstruction, 10 phase images were generated from raw data and the composite MIP images were created using these phase images. The MIP images were exported from 4DCT server into Pinnacle^3 8.0h (Phillips Medical Systems, Cleveland, OH) treatment planning system for further analysis.

Utilizing Pinnacle^3 8.0h, we contoured the coronal view of MIP images by using both automatic and manual contour tools. To keep consistency in contouring, we used a pre-fixed window levels. Auto contour tools may be less prone to subjective errors in measurement, while manual contouring was more accurate in identifying distorted target regions. For cases with seriously distorted images as shown in Figure 3, we used manual contouring. However, for most cases without conspicuous image distortion, we used auto contouring since the maximum difference in the two contour methods was less than 1mm. In case manual contouring was used, to minimize human error, averages were taken after repetition on cylindrical and block targets. By measuring the maximum span of contoured image along the superior-inferior direction, MIP range was determined.

2.3Results

2.3.1 MIP from sinusoidal target motions

4DCT is known to produce truthful MIP images for regular periodic breathing[61] Therefore, we measured the MIP span for mono sequence first. The measured spans were compared with the expected values calculated from the size of target and the maximum amplitude. For motion with amplitude of 5mm and 7.5mm, the measured MIP span was close to the expected value of 35.0mm and 40mm as shown in Table 2.1. The difference between the measured and expected span was less than 3mm for 15 BPM and 4mm for 18BPM. The scan thickness, set to be 2mm, contributed to these differences, as did image artifact due to the interface of the high density acrylic targets and surrounding low density cork. The square target tended to have more artifact than the circular target due to a greater amount of acrylic at the leading edge of the square target.

Sequence(amplitude) BPM	Expected Value (mm)	Square (mm)		Circle (mm)	
		Measured /	Difference	Measured /	Difference
S (5mm), 15 BPM	35.0	37.6	+2.6	36.8	+1.8
M (7.5mm), 15 BPM	40.0	43.2	+3.2	43.2	+3.2
S (5mm), 18 BPM	35.0	38.5	+3.5	38.8	+3.8

Table2.1 Measurements MIP span along superior–inferior direction for mono component target motion.

Component waves(amplitude) ,BPM	Sequence	Expected Value (mm)	Square (mm) Measured /Difference		Circle (mm) Measured / Difference	
S (5mm), L (10mm) 15 BPM	1S1L	45.0	40.1	- 4.9	41.9	-3.1
	2S1L	45.0	42.2	- 2.8	41.8	-3.2
	2S2L	45.0	36.9	- 8.1	36.5	-8.5
	3S1L	45.0	33.8	- 11.2	34.6	-10.4
S (5mm), L (15mm) 15 BPM	1S1L	55.0	40.6	- 14.4	39.5	-15.5
	2S1L	55.0	35.3	- 19.7	37.0	-18.0
	2S2L	55.0	35.8	- 19.2	37.0	-18.0
S (5mm), L (10mm) 18 BPM	1S1L	45.0	46.4	+1.4	46.7	+1.7
	2S1L	45.0	46.3	+1.3	47.1	+2.1
	2S2L	45.0	47.0	+2.0	47.4	+2.4
	3S1L	45.0	45.6	+0.6	47.1	+2.1

Table2.2 Measurements of MIP span for irregular dual component target motion. nSmL represents a dual component motion sequence made by combining n small and m large amplitudes.

For the dual sequence, the measured MIP span showed a much larger discrepancy from the expected value, as shown in Table 2.2. For 1S1L, we obtained span of 41.9mm and 40.1mm for circular and square target respectively. Both of them are shorter than expected value of 45mm, by 3.1mm for the circular and 4.9 mm for the square target. These results are not dramatically different from the regular motion considering 2mm scan thickness and high contrast between target and surroundings had to be illustrious. We note that the span of 1S1L measured from images was underrepresented while the corresponding values of mono sequence were overrepresented. We obtained span of 33.8mm and 34.6mm for square target and circular target respectively in motion sequence of 3S1L, on the order of 10 mm shorter than the expected value of 45 mm. The MIP span results for 1S1L and 2S2L in table 2.2 are something worthwhile to compare and pay attention. Even if the ratio of

small peak and large peak was 1:1 for both motion sequences, span difference of 5.4 mm for the circular target and 3.2 mm for the square target were measured. This suggests reconstruction of phase images and MIP depends on the details of target motion sequence.

We extended the amplitude of the large peak from 10mm to 15mm to investigate whether MIP span is influenced by the amplitude of large peak. For this adjustment we kept periods and the amplitude of small peak unchanged. For all motions, the measured span is smaller than the expected by 15mm ~ 20mm as shown in Table 2.2. This model suggests that the large peak is drastically underrepresented in MIP.

Since MIP span of 2S2L and 3S1L with 15BPM underrepresented the size of the actual motion range, other dual sequences were designed to investigate further. We designed 18 BPM motions and implemented into phantom to test the correlation between breathing frequency and MIP span, as listed in Table 2.2. For these faster motion sequences, the difference between expected and measured span are less than 2mm for square target and 2.4mm for circular target. Compared with 15BPM results, these results are much more accurate. However, each phase and MIP image showed more distortion for these faster targets as shown in figure 2.3. This could be explained by the fact that in this case the inequality (1) was not satisfied. Breathing period of 3.3 sec was too short to produce an undistorted image for the given gantry rotation time of 0.5 sec/rotation and pitch (0.082).

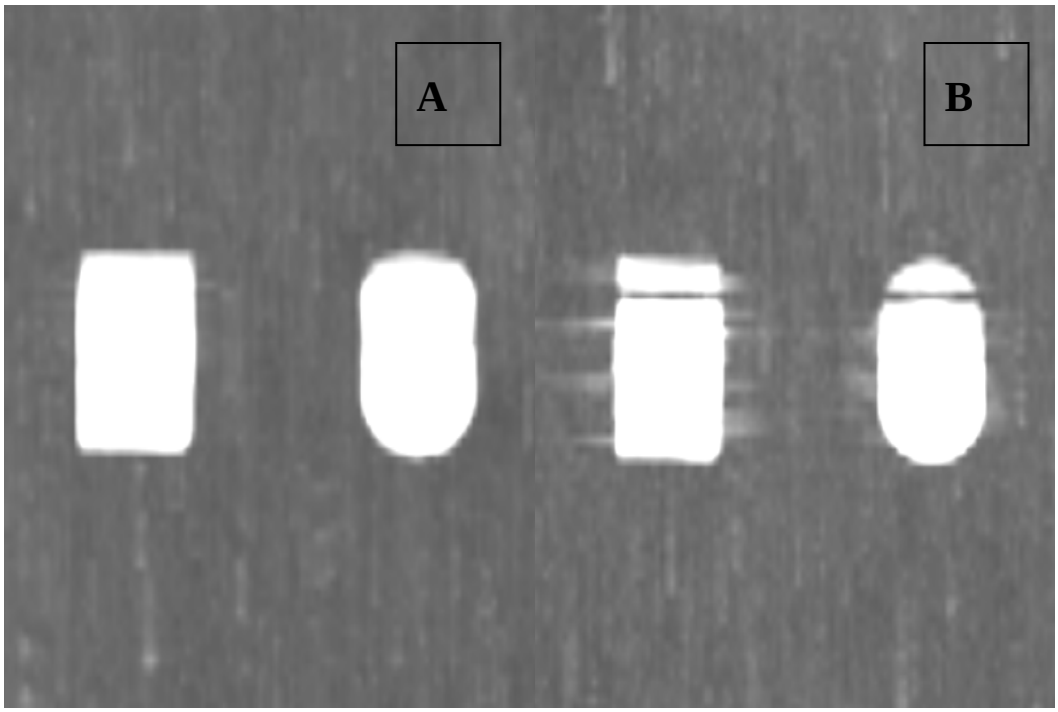

Figure2.3 A MIP image of 15BPM 1S1L (5mm, 10mm) target motion. **B** MIP image of 18BPM 1S1L (5mm, 10mm) target motion.

For triple sequence made by combining small (5mm), middle (7.5mm) and large (10mm) amplitudes, the MIP results are shown in Table 2.3. We obtained MIP span of 41.8mm for both targets moved in sequence 4S4M2L. The measured values were 43.6mm for circular and 44.0mm for square target in sequence 2S2M1L. Similar to the comparison of 1S1L and 2S2L, the MIP span difference suggested that each phase image and size of MIP depends on the detail of motion sequence: even if the ratio of peak numbers were 2:2:1 for both motions, amplitudes in 2S2M1L varied more frequently. 6S2M2L and 3S1M1L sequence had more small peaks than other triple motions. And we noticed that the MIP span become shorter as the number of small peak increased. For 6S2M2L, MIP span is 7.8mm shorter than the expected value of 45.0mm.

Component waves(amplitude) ,BPM	Sequence	Expected Value (mm)	Square (mm) Measured / Difference		Circle (mm) Measured / Difference	
S(5mm) M(7.5mm) L(10mm) 15 BPM	4S4M2L	45.0	41.8	-3.2	41.8	-3.2
	2S2M1L	45.0	44.0	-1.0	43.6	-1.4
	6S2M2L	45.0	37.2	-7.8	37.2	-7.8
	3S1M1L	45.0	37.4	-7.6	37.4	-7.6

Table2.3 Measurements of MIP span for triple component target motion.

2.3.2 MIP of simulated patient tumor motion

	Average BPM	Expected Value (mm)	Square (mm) Measured /Difference		Circle (mm) Measured / Difference	
Patient 1	14	41.0	33.3	- 7.7	33.1	-7.9
Patient 2	18	33.0	32.6	- 0.4	32.1	-0.9
Patient 3	12	48.0	37.3	- 10.7	37.5	-10.5
	14	48.0	40.2	- 7.8	40.0	-8.0
	18	48.0	47.3	-0.3	47.3	-0.3

Table2.4 Measurements of MIP span for simulated patient tumor motion.

For simulated patient tumor motions with spatial and temporal irregularities, the measured MIP spans, are shown in Table 4. The measured MIP span is smaller than the expected value by about 8mm for Patient 1 and 11 mm for Patient 3 with average breathing rate of 12BPM. On the other hand, MIP span showed accurate results (less than 1mm span difference for both targets) for the faster moving sequence of Patient 2. In order to measure the correlation between target speed and MIP accuracy, the dynamic phantom was set to simulate the motion sequence for Patient 3 in three different motor speeds. Thus for Patient 3, we simulated three different average breathing rate, 12, 14 and 18 BPM, but with an identical spatial trajectory. As shown in Table 4, the measured MIP spans became more accurate as the target moved faster. The difference between the expected and measured span decreased from about -11

mm to less than -1 mm, similarly to the observation made in sinusoidal motions. The MIP images for the cylindrical target for the sequence of Patient 3, shown in the figure 2.4, became more elongated and distorted as target moved faster.

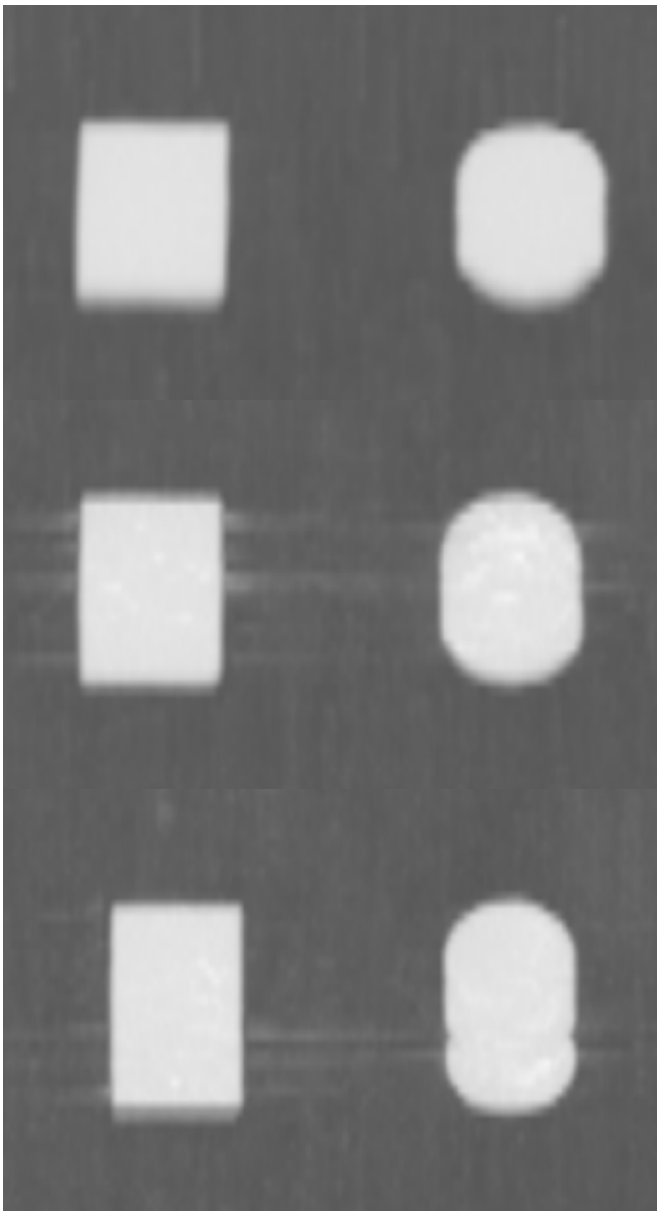

Figure2.4 MIP images for Patient 3 for average breathing rate of 12, 14, 18 BPM.

2.3.3 Study of image distortion

Our MIP data revealed imaging distortions and truncation of the span of the target for dual and triple sequence. This prompted us to characterize distortions by investigating each phase image. Three radio opaque markers (BBs, CT-spots®) were placed at the reference points as shown in figure 2.5A. One BB was placed on the leading edge and one BB was placed on each side at the center of target. By measuring the distance between edge and center points marked by BBs for 10 % phase increments, we evaluated the degree of image distortion.

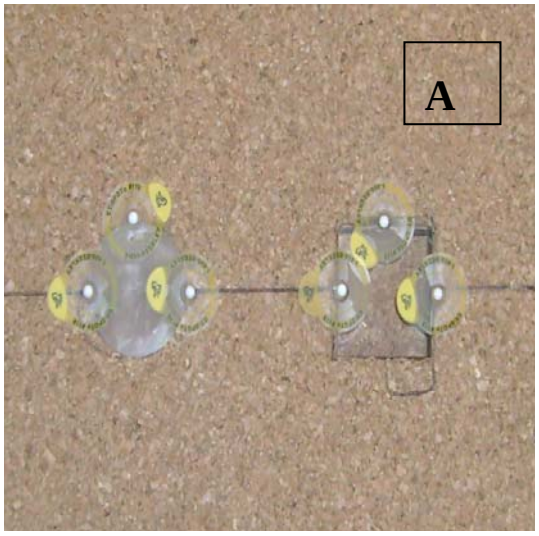

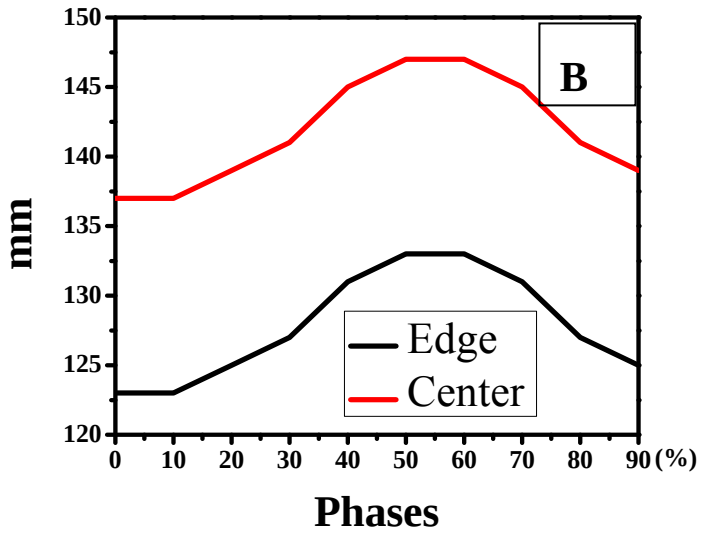

Figure2.5 A Radio opaque markers (BBs) on the leading edge and center of each target. **B** Edge and center position (measured with respect to CT zero position) on each phase is equally distributed throughout all phases as we expect from the real target.

First we scanned the 15BPM mono sequence with amplitude of 5mm, and obtained edge and center position on each phase as in figure 2.5B. The exhale and inhale phases are designated by 0% and 50% respectively, and the distance between them is 14mm. This is close to the real half distance of target 12.5mm considering the scan thickness of 2mm.

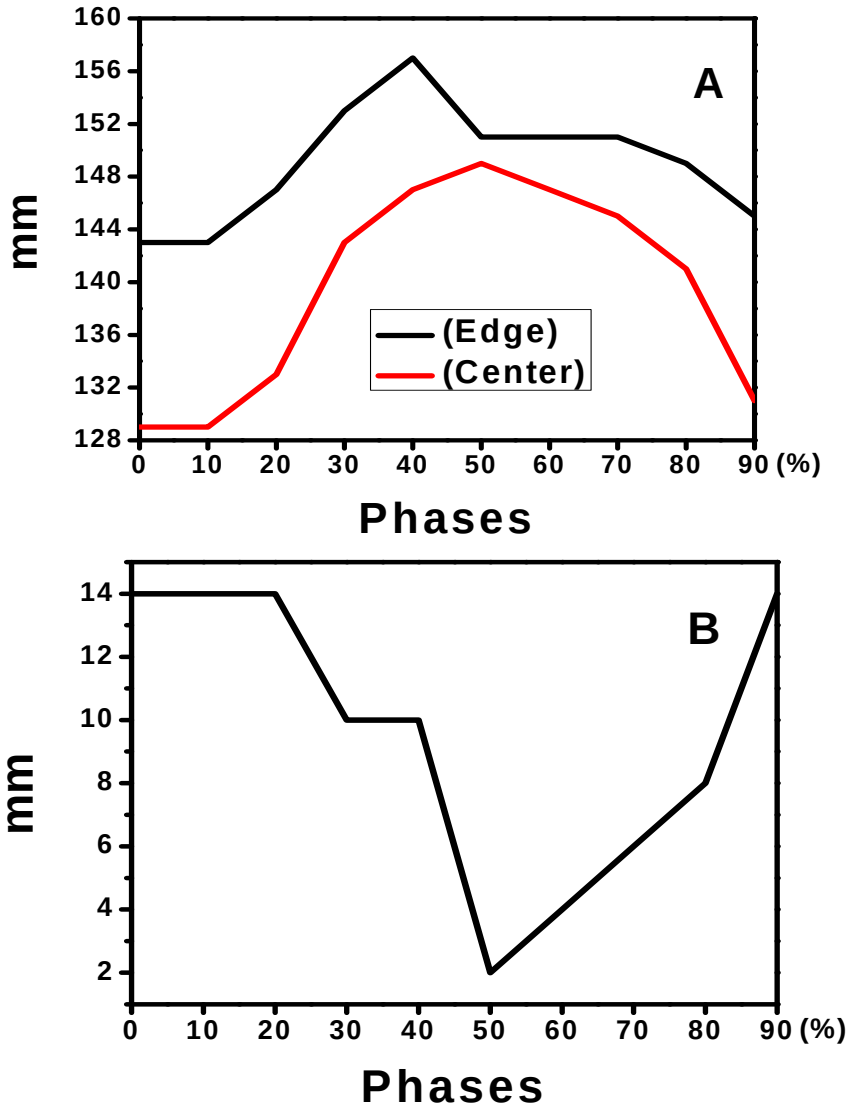

Figure2.6 A Results of edge and center analysis of dual sequence 15BPM 2S1L (5mm, 10mm). Black line presents edge position; red line presents center position. Square and circular targets show the same results. **B** Distance difference of edge and center of 15BPM 2S1L (5mm, 10mm) in different phases. The actual distance between edge and center of the target is 12.5mm.

For 15BPM dual sequence of 2S1L (5mm and 10mm amplitude), we graphed reference points as a function of phase as in figure 2.6A. The center point moved 19mm between inhale and exhale phase, which is comparable to the target motion span of 20mm. However, the edge point moved only 14mm, far less than the expected value of 20mm. These results suggest that target edges are more distorted in phase images for amplitude varying motion like dual sequence. For ideal scan image without any distortion, the distance between the edge and the center points should be 12.5mm throughout all phases. Thus comparing our results with this true value, we can assess the degree of distortion in each phase images. In figure 2.6B, we found the most serious distortion appeared in 50% and 60% phases. There exists only 2mm distance (instead of expected 12.5 mm distance) between edge and center points suggesting serious distortion.

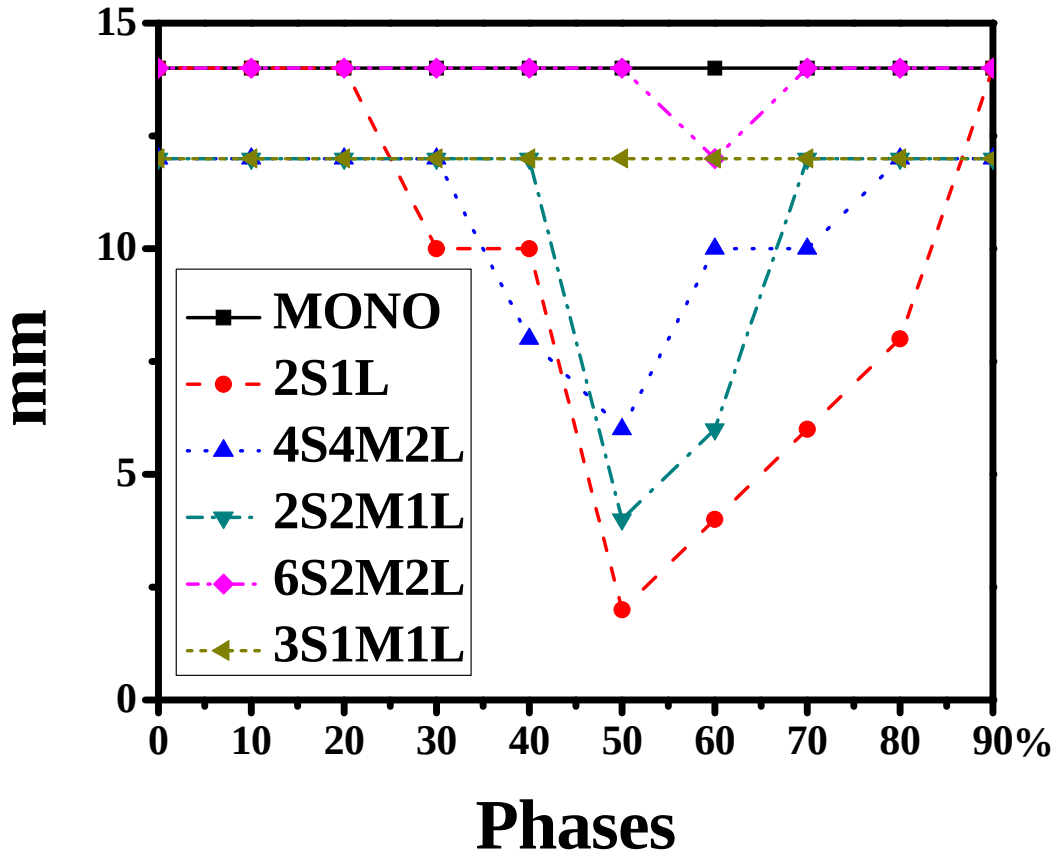

Figure2.7 Edge and center distance for mono (5mm), 2S1L (5mm, 10mm), 4S4M2L, 2S2M1L, 6S2M2L and 3S1M1L (5mm, 7.5mm and 10mm) on each phase. All of them are 15BPM

In figure 2.7, we graphed distance of edge-to-center on each phases for mono, dual and triple sequences in15BPM. For mono and 6S2M2L, the distance was 14mm at 50% phase, and image qualities were good without much distortion. By comparing 2S2M1L and 4S4M2L, we found 2S2M1L showed more distortion. However the MIP span of 2S2M1L was more accurate, even if both sequences have the same ratio of small, middle and large amplitude components. Thus the degree of distortion and MIP

span depends on the detail of motion sequence. This result is consistent with what we have found on the fast breathing target where more distorted phase images produce more accurate MIP span. For motion sequence 6S2M2L and 3S1M1L, both showed no distortion at almost all phases except 60% maintaining the edge-center distance constant. However, as shown already measured MIP span were much shorter than the expected one.

2.4 Discussion

In our study, all target motion and data acquisition parameters were designed and executed with clinical settings and applications in mind. Scanning parameters and procedures to generate composite images were exactly the same as those recommended by the 4DCT vendor and used in clinics. The target motion sequences we created were designed to simulate specific physiologically-relevant characteristics of lung tumors. The dynamic lung phantom was programmed to move only along superior-inferior direction to reduce the related parameters. For 4DCT helical scanning used in our measurements, each section of target volume needs to be imaged throughout the entire breathing cycle in order to prevent distortions such as apparent gaps or missing slices in the reconstructed images. This can be ensured if the gantry rotation time multiplied by the inverse of the pitch plus the fractional fan angle is greater than or equal to the breathing period as expressed in inequality (1). The gantry rotation time directly affects the z-axis resolution due to the correlation between the temporal resolution and the amount of image data per reconstructed volume. A longer

rotation time allows more target motion per phase bin resulting in the blurring and poor z-axis resolution. Our measurements, performed in a fixed rotation time, also showed that faster target speed resulted in blurred or distorted phase and MIP images.

However in the measurements of motion span for irregularly moving targets, MIPs obtained by faster targets are more accurate. This result is somewhat contradictory to the existing literature. For example Luc Simon et al. recommended the gantry rotation time to be as small as possible[63]. Wink et al. reported that slower gantry speed resulted in increased blurring of image, but the calculated volume did not increase[65]. Their explanation was that the averaging of the edge pixels with the background resulted in densities below the threshold set for the segmentation process. On the other hand, the slower scanning produces accurate volume estimations as has been documented for MVCT and cone beam CT. The study by Smeenk et al. on the MVCT reported that an ultra slow scan leads to better averaging of the density in the CT images and hence better correspondence of iso-contours with the true occupancy of the target[66]. Also the study by Sonke et al. showed that the slower gantry rotation speed of a linear accelerator resulted in the ultra-slow scanning in cone beam CT but accurately reproduce the target motion envelope[67]. These preceding observations using different imaging modalities were made by varying gantry speeds for a fixed rate of target motion, while our results using 4DCT were obtained for targets moving in different breathing rates with a fixed gantry rotation. However all these results

show a tendency that faster target motion with respect to gantry speed results in better estimation of target motion span.

This issue of MIP accuracy in 4DCT may have something to do with phase based reconstruction algorithms available with commercial 4DCTs. Shortcomings of phase binned reconstruction, such as the difference of actual end inspiration and tag delivery of phase monitoring systems or irregularities of patient's breathing, are well-known and various techniques to improve the resultant composite images have been actively researched and published. One area of active research is displacement based binning reconstructions algorithm. Some vendors are already preparing beta version of this software. We are planning to use displacement based binning to check MIP accuracy and its implication in the planning and delivery of lung tumors.

2.5 Conclusion

We investigated the accuracy of 4DCT generated MIP images by using a programmable phantom. Various sinusoidal target motion sequences and tumor motions of real patients were implemented into the programmable phantom and motion span was measured. According to our measurements, irregular target motion tends to be underrepresented by MIP, sometimes by 1 cm or more. Clinical ITV determination utilizing MIP requires caution especially when there is breathing irregularity. We found that slow gantry speed may generate a more accurate target span and volume representation even if most phase and MIP images are distorted. With current phase based binning algorithms, irregular target motion may not be

accurately incorporated into the final reconstruction. A viable alternative could be a slow gantry speed helical scanning for the acquisition of MIP and determination of ITV.

CHAPTER THREE

DOSIMETRY STUDY

3.1 Introduction

One major source of uncertainty in GTV delineation is the tumor motion. In order to obtain more accurate temporal and spatial information on moving anatomy, four dimensional CT (4DCT) is widely used [68]. This technology enables clinicians to individualize the internal target volume (ITV)[49], explicitly accounting for organ motion through the use of appropriate margins. In principle, 4DCT allows the generation of an ITV from the set of binned CT images containing temporal and spatial information related to a patient's breathing. In many clinical settings using 4DCT, ITV delineation is based on maximum intensity projection (MIP) images, while the dose calculation is performed on average (AVG) CT images[59, 69]. MIP and AVG images reflect the highest and average value for each voxel within the set of phase images respectively. It has been reported that these composite images, utilizing standard volume–rendering post-processing techniques, are effective for the assessment of tumor mobility [59, 60].

Several prior studies have investigated the accuracy of ITVs deduced from MIP images. Cai et al. showed that MIP-based internal target areas (ITAs) were comparatively smaller (10-40%) than the ITAs generated from MRI using dynamic magnetic resonance imaging (MRI) [61]. They concluded that the variability in breathing patterns was the dominant factor that affected the 4DCT quality and that of

the resulting MIP-based ITA. Studies by our group employing a dynamic phantom have shown that the range of target motion is underestimated when the motion is irregular in amplitude and periodicity [62]. For most non-gated delivery methods currently used, treatment planning is performed on AVG images, while the ITV is determined from MIP images [59, 70]. This approach makes it possible to generate a 3D plan that incorporates approximate information on the target motion. During delivery, however, the target continues to move in relation to the ITV (PTV), which as shown by earlier studies, may not be accurately delineated for irregular motions [70]. Thus it is necessary to investigate whether this clinical scheme for dose calculation and delivery is dosimetrically reliable and accurate. Several investigations have been performed to compare calculations based on static 3D dose and 4D image sets [70, 71]. Guckenberger et al. found that the dose to the GTV was not compromised in the 4D plan compared with the 3D plan [69]. They further observed that while the 3D doses calculated for the GTV, ITV, and isocenter were good approximations for the 4D calculation, the 3D dose at the PTV margin underestimated the 4D dose significantly.

In this study, we investigated the dosimetric accuracy of a standard, static 3D approach to SBRT planning (when dose is prescribed to outline of the target rather than its center) by employing a programmable lung phantom. Tumor motions representing free breathing patients were programmed into the phantom, which was subsequently scanned by 4DCT to generate AVG and MIP images. Treatment plans

were constructed, and the resulting dose delivered to the phantom was measured using radiochromic film. By comparing the measured dose and planned (computed) dose, we are able to assess the validity and accuracy of the 3D SBRT treatment planning approach utilizing AVG and MIP images.

3.2 Materials and methods

3.2.1 Lung phantom

The programmable motion platform used in this study, shown in Figure 3.1A, has been presented in our previous work [70]. A cubic lung phantom made of an acrylic frame (dimensions of 24(L) x 17(W) x 12 (H) cm^3, density of 1.20 g/cm^3) was placed on the motion platform. Three 1cm thickness cork plates with a of density 0.26 g/cm^3 were inserted into the frame to model aerated lung tissue (known to have average density of approximately 0.23 g/cm^3). Two pairs of cylindrical acrylic targets, with dimensions of 25mm (D) × 10mm (H) and 13mm (D) × 10mm (H), were embedded in the middle cork plates as shown in Figure 1B. Two 5cm thickness cork plates were inserted at the side of three cork plates. These targets were designed to mimic lung tumors such as those treated with SBRT, while facilitating dosimetric measurement in 3 planes (top, middle and bottom of cylindrical targets) using Gafchromic EBT films (International Specialty Products, Wayne, NJ). In addition, a fiducial marker was affixed to the platform base to provide a reference for consistent localization at CT and on the treatment machine.

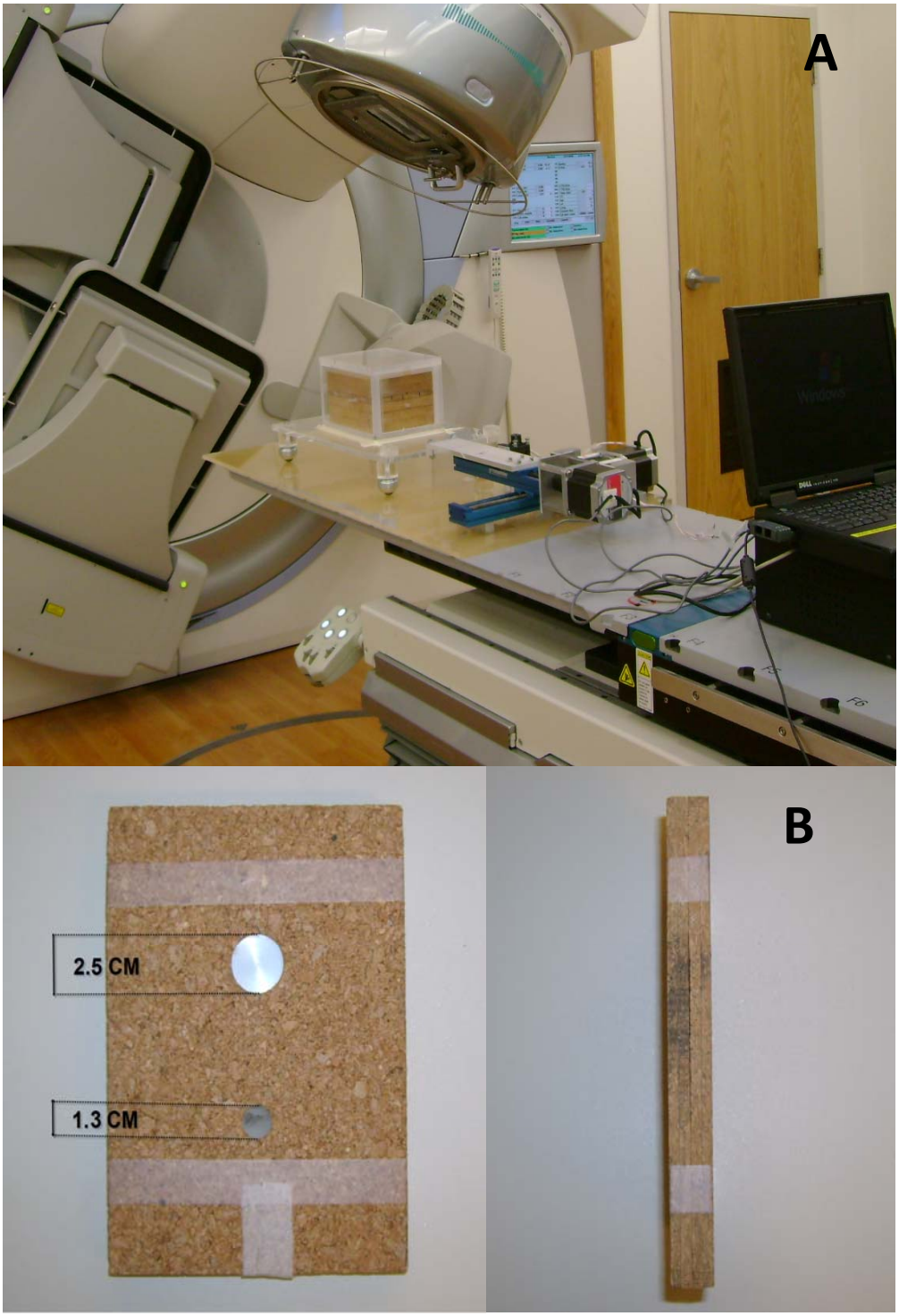

Figure 3.1 A: A programmable platform capable of two-dimensional motion; **B**: Two cylindrical acrylic targets, one large (25mm (D) × 20mm (H)) and one small (13mm (D) × 20mm (H)) inserted in a cork phantom. The phantom and targets were cut symmetrically at the midline to facilitate three film measurement planes.

3.2.2 Target motion

To investigate the dose distribution delivered to a moving target, the motion platform was programmed for thirteen separate motion profiles: one sinusoidal and twelve irregular motion patterns obtained from patient data (originally registered during treatment irradiation by H. Shirato[64]). Four of these profiles are shown in Figure 3.2. We limited target motion to along the superior-inferior direction, since this is the most significant in patients with lung tumors.

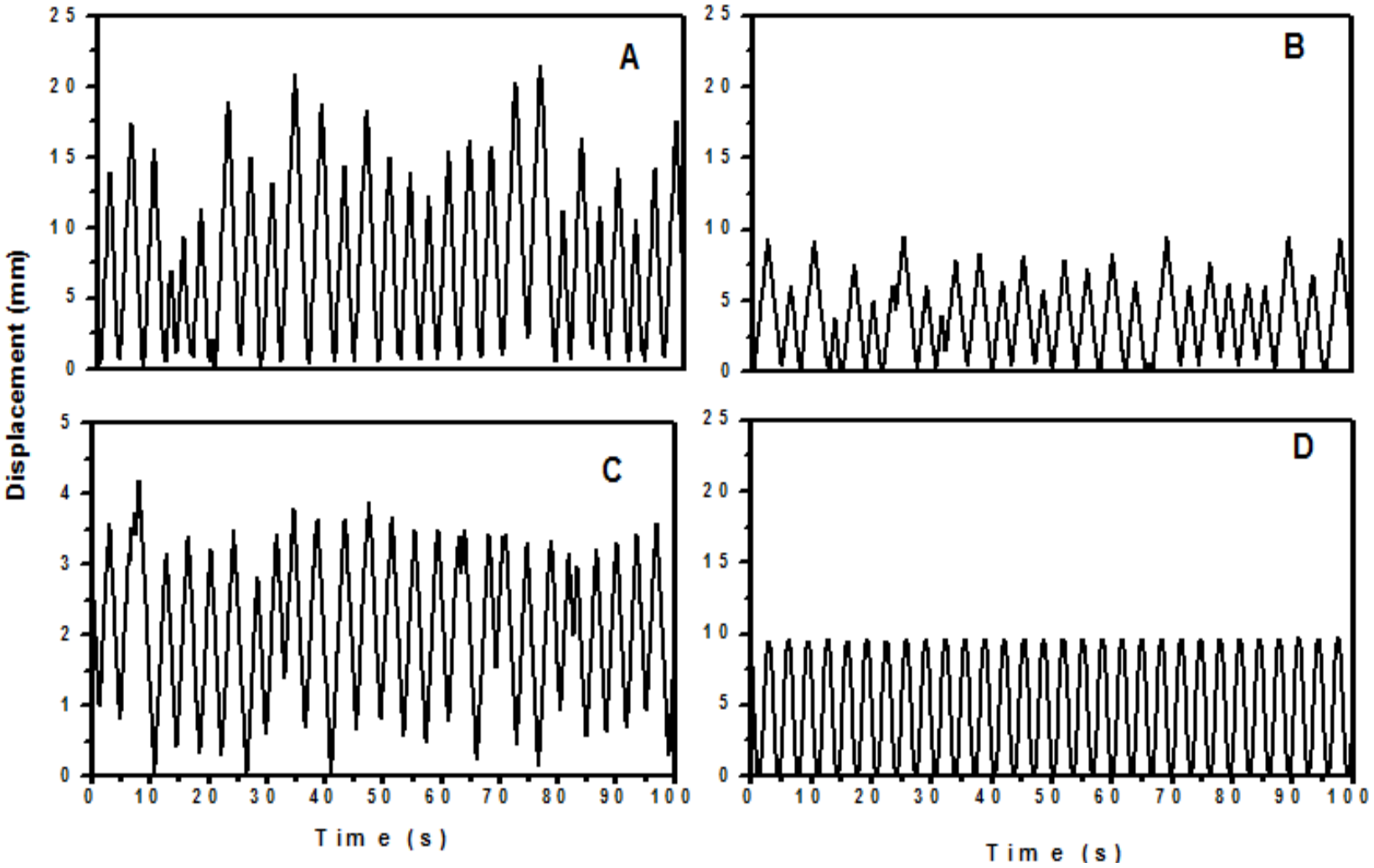

Figure 3.2 The four motion profiles used in this study: A: Patient_Large; B: Patient_Median; C: Patient_Small; and D: Regular Breathing Pattern

Irregular motion patterns were carefully selected from 20 motion patterns. Four motion patterns among thirteen are characterized in Table 3.1: Patient_Large represents the case of a free breathing patient with an average and maximum target motion range of 15.2mm and 21.5mm respectively; Patient_Median represents the case of a free breathing patient with an average and maximum target motion range of 7.3mm and 9.5mm respectively; Patient_Small represents the case of a free breathing patient, under abdominal compression, where the average and maximum target motion range are 3.4mm and 4.4mm respectively. Lastly, regular sinusoidal motion is represented by a perfectly periodic profile with range of 10mm. The average breathing periods of these profiles range from 16 to 18 breaths per minutes (BPM). To characterize irregularity of target motion, we adapted the respiratory variability (v) used by Cai et al. [61]. This is the mean of the standard deviation (SD) within the maximum (peaks) and minimum (valleys) amplitude displacements:

$$v = \frac{SD(Peak) + SD(Valley)}{2} \qquad (1)$$

To characterize variability in period of these profiles, we also used the standard deviation of the first 25 breathing periods. All target motions were monitored by an independent linear position transducer with an accuracy of 0.5mm and repeatability of ±0.05% over a full stoke of 10cm (Unimeasure INC., Corvallis, Oregon).

Motions	Average BPM	Maximum Range (mm)	Average Range (mm)	Respiratory Variability	Period Variability
Regular	18	10.0	10.0	0.01	0.01
Small	16	4.4	3.4	0.33	0.56
Middle	17	9.5	7.3	0.93	0.63
Large	17	21.5	15.2	2.02	0.72

Table 3.1 Characteristics of the target motion patterns implemented into the dynamic lung phantom

3.2.3 4DCT data acquisition and treatment planning

All CT data acquisition was performed in helical mode on a Philips Big Bore CT scanner (Philips Medical Systems, Cleveland, OH, USA), equipped with 16×1.2 mm^2 detector array. The phantom motion was monitored using the Philips Bellows System. The CT current and voltage were set to 100 mA and 120 kV respectively in all scans. The following scanning parameters were used: pitch of 0.082, field of view (FOV) of 440mm and gantry rotation time of 0.5 sec/rotation. The scan thickness used was 2mm, resulting in a scan time of approximately 100 seconds. After scanning, the raw CT data were sorted and reconstructed using a phase binning reconstruction algorithm based on the respiration profile provided by the bellows system. Following reconstruction, the 10 phase image sets were used to generate the composite AVG and MIP images. The AVG and MIP images were exported from CT console to the Pinnacle^3 8.0h (Phillips Medical Systems, Cleveland, OH) treatment planning system for SBRT planning.

From the imported images, the ITV and PTV were contoured according to a clinical protocol used for lung SBRT patients at our institution. First, we manually contoured the targets on the MIP images to determine an ITV. The MIP-derived ITV

was expanded with a 5mm margin in all directions to generate the PTV. Dose calculations were performed on AVG images for plans based on PTVs defined from MIP images. At our center, the typical prescription for lung SBRT is 60 Gy delivered to target outline in three fractions. A similar prescription was used for our phantom plans. Ten non-coplanar beams per target were used to achieve dose coverage following the recommendation of Radiation Therapy Oncology Group (RTOG) 0236. After setting up the treatment fields, we manually adjusted the beams' shape by fine tuning MLC leaves to satisfy the requirement of at least 95% of the PTV volume is exposed to the prescribed dose.

3.2.4 Delivery and analysis

After exporting treatment plan from Pinnacle to MOSAIQ 1.5 (IMPAC Medical Systems, Inc., Sunnyvale, CA) and to the linear accelerator, all gantry and couch angles were verified to ensure there were no gantry-couch collisions. Since the radiochromic film used in our measurements has sensitivity range up to 10 Gy, the planned MU of each beam was reduced by a factor of two for delivery. Three pieces of radiochromic film were inserted for dose measurements, one at the top, one in the middle and one at bottom of targets, as shown in Figure 1B. To keep the delivery time approximately similar to the original plan, the dose rate was decreased from 500 MU/min to 300 MU/min. An Elekta Synergy*S* (Elekta group, Stockholm, Sweden) linear accelerator was used for the delivery.

For the delivery to the moving lung phantom, the center of the target identified on the plan was placed at the machine isocenter. To facilitate this, the reference fiducial marker at the phantom base was first established, and couch shifts derived from the treatment plan were applied. This assures precision in target center localization at the isocenter of the machine to within 1 mm; this minimizes any potential uncertainties due to setup variation. Following the setup, radiation was delivered to the moving lung phantom. The typical delivery time for each phantom irradiation was approximately 30 minutes.

We used an Epson 10000XL (Epson America Inc., Long Beach, CA USA) flatbed scanner to scan the exposed films. The FilmQA software (3cognition LLC, Wayne, NJ, USA) was used for analysis. The film dosimetry system has been cross-calibrated with ion chamber measurement, and the gafchromic film dosimetry results in our experiments are accurate to within ±3% at any point within the target film plane. Scanned films were compared with the computed planar dose images generated by Pinnacle planning system. Prior to irradiation, the beam isocenter was marked at the edge of each film using permanent marker. This allowed accurate alignment of the beam isocenter from exposed film with the planned isocenter from the computed planar dose. After the alignment of the isocenters, we compared various aspects of computed and measured planar dose such as isoline matching and absolute maximum dose.

3.3 Results

3.3.1. MIP Results

The 10 image sets were used to generate MIP and AVG images. The extents of targets on the MIP images were measured along the superior-inferior direction. These were compared with the expected range, based on the target extent and input motion amplitude; the target spans deduced from these trajectories are listed in Table 2. For irregular motion, MIP images under-estimate the true span of moving target, as we demonstrated in a previous study [70]. The measured target MIP span for Patient_Large was smaller than the expected target span by 8mm. For Patient_Median, the difference between was approximately 4mm. The span of the target MIP image for Patient_Small was accurate, largely because the maximum motion range is only 4.4mm. For the regular motion, in contrast to irregular target motion set as a reference, accurate target MIP spans have been observed. We have seen previously that regular motion results in MIP image targets are approximately 1-2 mm larger than the true target size and motion extent [70].

The average range of target motion, listed in fourth column of Table 3.1, is closely related to measured MIP span listed in the third column of Table 3.2. Adding the target diameter (2.5cm in case of the large target) to the average range of target motion, we obtain values very close to the measured target MIP span. This observation implies that, at least four cases investigated, irregular target motions characterized by some-amplitude variation, MIP images represent rather the average

range of motion and not the maximum span of varying amplitudes. This property is very likely related to the sorting methods for 4DCT involved in generating MIP images. While we have observed this phenomenon is a small number of patient samples available to us, further investigation with more samples is needed to support this observation in a statistical manner. Better understanding of this property may be gained if timing of image binning is correlated with temporal properties of amplitude statistically significant distribution of irregular target motion.

Motions	Target	Measured MIP span (mm)	Expected MIP span (mm)	Difference (mm)	80 % Isolines shift(mm)	PTV Dose Coverage (%)
Regular	Large	36.9	35.0	1.6	<0.5	≈0
	Small	24.3	23.0	1.3	<0.5	≈0
Small	Large	28.6	29.4	-0.8	<1	≈0
	Small	16.7	17.4	-0.7	<1	≈0
Middle	Large	30.2	34.6	-4.4	3.0	-7.4
	Small	21.9	22.6	-0.7	4.5	-8.4
Large	Large	38.5	46.5	-8	5.5	-13.8
	Small	28.7	34.5	-6.8	8.0	-19.0

Table 3.2 Comparison between measured MIP spans and expected MIP; span 80% isodose line shift and percentage of PTV underdose coverage

3.3.2. Isodose line analysis

For static targets, a comparison of dosimetric results (computed vs. measured) is provided and analysis of the process used later for measurements performed on moving targets is given. [72] For static case over 99% of pixels on film is passing criteria of 3% in dose and 3mm in distance-to–agreement on Gamma analysis.

Dosimetry results for Patient_Large, showing the greatest difference between the measured and expected target MIP span, are consistent for films inserted at the top,

middle and bottom of the small target. There is a clear shift in the measured isodose lines, showing the discrepancy between plan and actual delivery. For the 80 % isodose lines, which were prescribed to cover 95% of PTV volume, the maximum shift is approximately 1cm. Accordingly, the edge of the PTV closest to the diaphragm is under-dosed while the opposite edge of the PTV is overdosed. Additionally, the shift and corresponding delivery error are more prominent superiorly, where the CTV would be located during end-inhalation. The asymmetry in the isodose lines is due to the irregular target motion that is not encompassed by the ITV (PTV). During deep inhalation with a large amplitude, a portion of ITV travels beyond the field covering the entire PTV, defined by the MIP, while the opposite portion of ITV moves further into the field.

Figure 3.3 shows the isoline analysis of films at the middle of large target for all four target motions. For target motions of Regular and Patient_Small, the computed and measured isodose lines match well. Due to the small range of motion involved in Patient_Small, the measured MIP span is close to that expected, as shown in Table 2. Thus the ITV determined by the MIP accurately encompasses the entire target motion span, resulting in an accurate matching between measured and computed isodose lines (Figure 3.3B). Isodose lines for Regular motion also exhibit good agreement (Figure 3.3A), despite the fact that the motion range (1cm) is larger than that of Patient_Small. These results clearly demonstrate that the dosimetric mismatch is due to the irregularity of target motion and corresponding inaccuracy of target MIP

image rather than the amplitude of motion itself. In other words the discrepancy results in random mismatch of regular binning of 4DCT images and irregular appearance of motion amplitudes along the time axis. The 1-2mm discrepancy in MIP span for regular motion is within the uncertainty of the 4DCT scan thickness of 2mm. Thus summing up, we see for Patient_Large and Patient_Median, poor agreement between the measured and calculated isodose lines (shift of isoline of 5mm or more). For Patient_Large, with the largest difference between measured and expected target MIP span, the superior portion of the measured 80% isoline, corresponding to end inhalation, shifts approximately 5mm with respect to the computed distribution (Figure 3D). For Patient_Median, the measured 80% isoline shifted 3 to 4mm with respect to the computed isoline. These shifts imply that the inhalation-end of the PTV is under-dosed, while the exhalation-end of normal tissue is over-dosed. All the shifts measured on 80% isodose lines for large and small targets are listed in Table 2.2.

In order to identify a solution for the isoline shift observed for Patient_Large and Patient_Median, four revised plans were generated with an alternate definition of the ITV. Since the target MIPs generated by 4DCT were not encompassing the full motion of targets, the resulting ITVs (PTVs) were not sufficiently large. Thus we calculated new extended ITVs (PTVs) by using the known tumor motion span instead of the MIP span determined by 4DCT. For Patient_Large, for example, we extended the original PTV by 8mm towards inhalation, and for Patient_Median, we extended

the PTV by 4mm towards inhalation, to compensate for the difference between the measured and expected MIP span. The revised plans were executed in a manner identical to the original plans to measure the dose delivered to the target. As shown in Figure 3E and 3F, the computed and measured isodose lines from the revised plans match more accurately. The shifts between the measured and computed 80% isodose lines are less than 2mm for the large and small targets. These results clearly show that the ITV (PTV) determined using 4DCT generated target MIP is not large enough to encompass the whole target motion for irregular breathing pattern. Clearly an ITV (PTV) defined by the true tumor motion span results in better agreement of the planned and measured isodose lines.

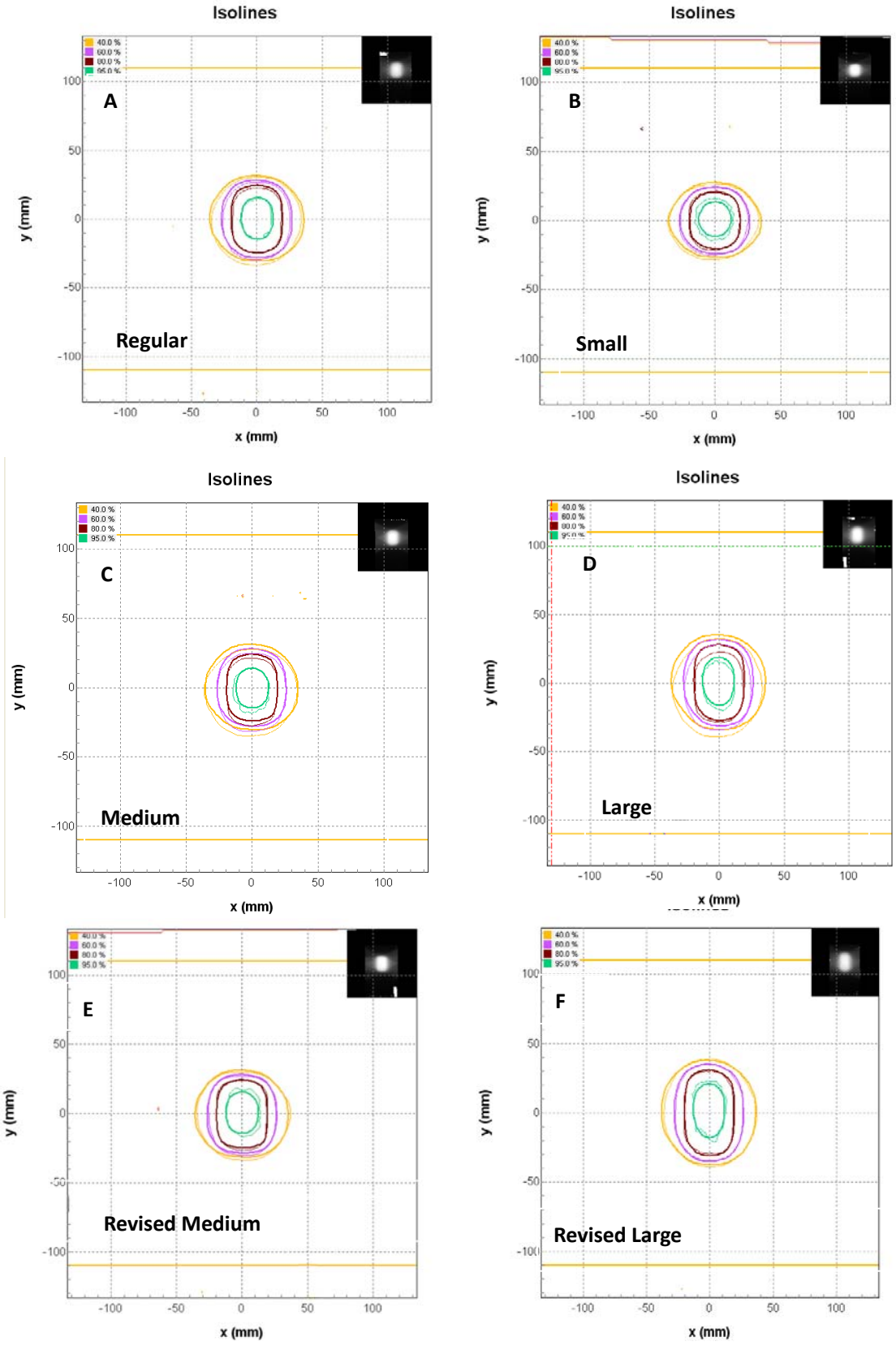
Isolines
A
Regular
Isolines
B
Small
Isolines
C
Medium
Isolines
D
Large
E
Revised Medium
F
Revised Large
y (mm)
x (mm)

Figure 3.3 Isodose lines matching for original plans **A**: Regular **B**: Patient_Small **C**: Patient_Median **D**: Patient_Large revised plans **E**: Patient_Median **F**: Patient_Large

3.3.3. PTV dose coverage analysis

We evaluated dose distributions for each motion pattern within the superior-inferior direction. However, it is also useful to know the three dimensional dose distributions and the percent of PTV underdosed clinically. A typical prescription for lung SBRT has 95% of the PTV receiving prescribed dose, thus we selected the prescribed dose region to estimate the ratio of underdosed volume to the whole volume in the original plans. As shown in Table 2.2, for Patient_Large, this underdose represents 13.8% of PTV volume for the large target, and 19.0% of PTV volume for the small target. In Patient_Median, 7.4% of the PTV volume was underdosed for the large target, while 8.4% of the PTV volume was underdose for the small target. In the revised plans with expanded PTV, we found that the volume of the PTV underdosed was insignificant for both Patient_Large and Patient_Median.

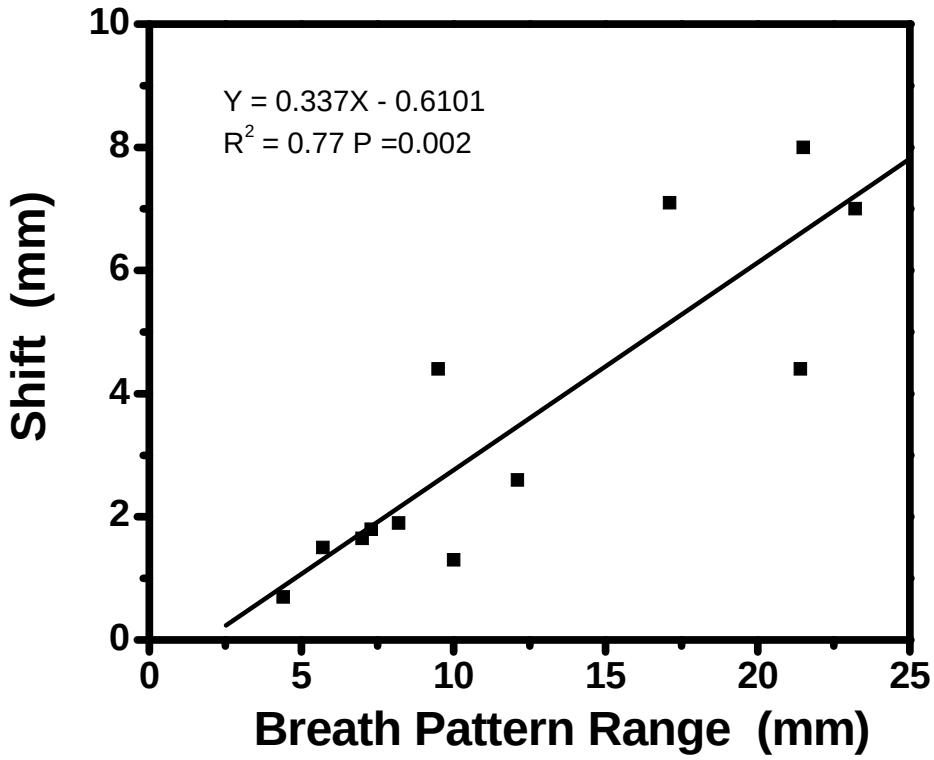

Figure 3.4. Shift of 80% isodose line versus range of irregular breath motion.

To verify our measurements for more representative sample of patients, we selected more irregular breathing patterns (n=12) to perform a sample comparisons. The number of motion patterns that can be classified as Patient_Large is four. The average range of these patterns is 20.8 ± 2.6mm, while the average shift of isodose lines is 6.6 ± 1.6mm. The number of motion patterns that can be classified as Patient_Small is six. The average range for these samples is 7.0 ± 1.8mm, while the shift of isodose lines is 2.0 ± 1.3mm. We investigated the correlation between the shifts for prescribed isodose line with respect to motion range for irregular breath patterns. Figure 3.4 shows the shift versus the motion range (n=12) and a linear fit to these data. As correlation coefficient is over 0.8 (R =0.87, P=0.002), we find the trend of increasing

shift between prescribed isodose lines and increasing range in irregular motion breath pattern. Moreover, we see in Figure 3.4 that investigated irregular breathing patterns with largest ranges may cause shift of 80% isodose line reaching up to 8 mm. This may result in clinically significant underdose of PTV.

3.4 Discussion

In our study, the phantom material, target motion, image acquisition method, treatment planning and delivery were designed and executed to simulate clinical SBRT lung treatments. We chose lung phantom materials to simulate the physiologically-relevant characteristics of lung tumors (unit density targets surrounded by a low density medium). The target motion sequences, three irregular motion patterns implemented on the motion stage, were derived from actual patient data. Scanning parameters and procedures used to generate target MIP and target AVG images were identical to those used in our clinic. Treatments were planned based on ITV (PTV) determined using MIP images in a manner identical to our clinical SBRT lung treatment planning protocols.

The phantom motion procedures assume that a patient has the same breathing pattern during scanning and delivery. While this may or may not actually be the case, it is the same assumption used in the clinical application at our institution and many others. Additionally, it is useful in quantifying the dosimetric effect of irregular motions during delivery.

The dosimetric accuracy of current SBRT treatment procedures was evaluated[73]. For targets moving periodically, represented by the regular pattern, motion planned and measured isodose lines demonstrated excellent agreement. Patient_Small, representing targets moving with a small range (< 5mm), also exhibited relatively accurate isoline matching (this motion pattern is characteristic for target moving when abdominal compression is apllied at simulation and delivery). Conversely, Patient_Median and Patient_Large, representing targets moving irregularly with median and large motion ranges respectively, (these motion patterns are characteristic for targets located in the vicinity of diaphragm when free breathing is allowed) showed measured isodose lines shifted by 3 to 8mm from the planned ones. The origin of this discrepancy is due to the inaccurate representation of irregular target motion as defined by 4DCT generated MIP images. Since the spans of the target MIP images are smaller than the expected target motion, the ITV based on target MIP does not encompass the full target motion. Thus, even with 5mm margins added for PTV, isoline shifts become prominent for irregular target motions. The 5mm margin recommended by RTOG 0236 may not be adequate for targets moving irregularly with large amplitudes, and further investigation is needed to determine proper margin.

In this study, several important issues are raised. First, images obtained from 4DCT should be used with some caution, particularly when the target motion is irregular with large amplitude. Though 4DCT can provide important temporal and spatial information on moving targets, it still is limited by current technology. Our

study clearly demonstrates that 4DCT generated target MIP images may not adequately capture the entire target motion span, which can result in dosimetric inaccuracy in SBRT lung treatments. While other mechanisms exist for assessing range of motion, including fluoroscopy and 4DCT with amplitude binning, phase-binned 4DCT is the most widely used in clinical practice.[62, 74-76] Second, our study showed that the Patient_Small pattern, with a relatively small motion range, produced more accurate isoline matching. At our institution, we have observed that the motion range of tumors for many patients can be reduced to less than 0.5cm when abdominal compression is applied [77]. Our results imply that, for SBRT lung treatments, targeting is more accurate when abdominal compression is used to reduce motion, compared with even sophisticated free breathing approaches. Additionally, our results suggest that cautious approach to gated delivery is warranted [78-80], as dosimetric errors associated with MIP-based ITV definition could be greatly exacerbated in such an approach. Third, our study suggested the necessity for additional image guidance, such as the use of CBCT, to ensure accurate targeting with minimal shift. At our institution it is standard practice to obtain CBCT scans prior to SBRT lung procedures to verify that the motion range of target has not shifted from the PTV defined from the 4DCT. This method utilizing CBCT imaging may minimize clinical errors in targeting tumors.

3.5 Conclusion

We investigated the dosimetric accuracy of lung cancer treatment plan using AVG and MIP images in stereotactic body radiation therapy by a programmable phantom. The accuracy of 4DCT generated MIP images does not reflect the maximum motion range of phantom, as demonstrated by dosimetric shifts of 6.6 ± 1.6mm for cases of free breathing patients with irregular motion in the range of 20.8 ± 2.6mm. These shifts can be minimized with regular breathing, or through motion reduction with such techniques as abdominal compression and breath coaching. It is also necessary for additional image guidance like CBCT to guarantee the planed beams accurately cover the target prior to treatment. Therefore, caution should be taken when using 4DCT MIP images to treat the free breathing patient with large irregular lung motion presenting.

CHAPTER FOUR

CBCT AND 4DCBCT IMAGES STUDY

4.1 Introduction

Respiratory motion is recognized as one of major challenges in radiotherapy for lung cancer treatment. Movement of tumors and normal tissues during breathing may cause a huge uncertainty for patient setup and dose delivery.[81, 82] A large margin is added from CTV to PTV, assuring the planned dose delivery to the tumor. However, enlarged margins may significantly increase the toxicity. Cone beam computed tomography (CBCT) is used for patient setup in image guided radiotherapy (IGRT).[67] CBCT provides the volumetric patient's anatomy and has potential for adaptive correction between fractions.

Hugo *et. al.* reported that respiration pattern changes during radiotherapy for lung cancer and their results indicate that change as large as 7mm in relation to isocenter can occur.[74] Bissonnette *et al.* reported that using respiration-correlated CBCT quantifies inter-fraction and intra-fraction motion in lung SBRT.[83] The patients cases reported in this study were treated with abdominal compression for any patient for which the tumor excursion exceeded 10mm. However, some patients have to be treated with tumor excursion over 10mm, and these situations need more investigation. To correct the breathing effect, especially for large irregular breathing motions, the setup based on CBCT should be considered.

Wang *et. al.* [56]reported that CBCT volume images matched the ITV from 4DCT

for a moving phantom. The results of static target are within 1mm difference between CBCT and 4DCT images. The similar results for moving target are as large as 2mm in their study. However, the motions they used are only regular motions (sinusoid motion) with 5-20mm amplitude. Park *et. al.* [70] reported that the 4DCT captures the regular motions (5-10mm in amplitude) within 2-3mm difference. However, the difference can reach as much as 5-8mm for irregular motions. To evaluate the matching of CBCT images and the 4DCT images, we performed studies that intend to describe the accuracy of patient setups for treatment and ultimately improve the patient treatment procedure.

In our studies, we use moving phantom to quantify the image matching between 4DCT and CBCT scans. In our investigations we use the same irregular breathing patterns for 4DCT and CBCT scans. This approach has the advantage of eliminating additional complications arising from the change in the irregular breathing patterns during delivery relative to pattern registered at simulation and used for planning.

4.2 Material and methods

4.2.1 Lung phantom

The programmable motion platform used in this study, shown in Figure 4.1, has been presented in chapter three [84]. We use the same target as shown in chapter three. Three gafchromic films are inserted into the phantom to measure delivered dose. The phantom is tested with independent transducer system described in chapter two.

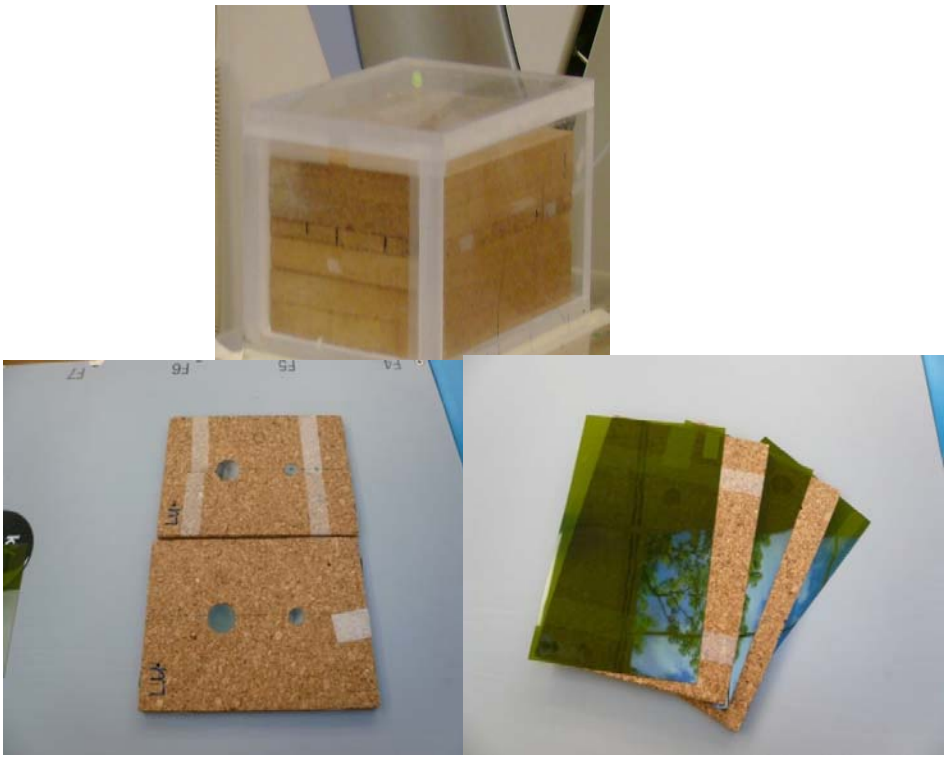

Figure 4.1 Lung phantoms with target 2.5cm diameter, gafchromic films inserted into each piece of corks.

4.2.2 Body frame

The phantom is positioned in an Elekta body frame to mimic the patient setup. The body frame provides three coordinators for moving phantom and assures the repeatability of phantom setup both in CT simulator and in treatment room. Three coordinates from body frame are used to line the phantom shown in figure 4.2.

Figure 4.2 The coordinators on body frame for phantom position alignment

4.2.3 Target motion

To investigate the dose distribution delivered to a moving target, the motion platform was programmed for eight separate motion profiles shown in table 4.1. These profiles are cataloged in our previous work[84]. We listed the expected MIP for each irregular breath patterns that have been characterized earlier in chapter three shown in table 4.1.

Breath patterns	Range (mm)	Irregularity	Expected MIP (mm)
1	17.1	6.42	42.1
2	7.3	5.58	32.3
3	8.2	2.7	33.2
4	23.2	1.56	48.2
5	21.4	4.14	46.4
6	5.7	1.87	30.7
7	12.1	1.43	37.1
8	10.0	3.64	35.0

Table 4.1 The characteristics of each breath patterns.

4.2.4 CBCT

All the 4DCT scans and patient treatment setup scans have been performed exactly as in chapter 3. To mimic the same clinical protocol, we use the same CBCT for phantom study as it is used for patient setup verification. We use Elekta XVI CBCT for position verification before each delivery. The lasers from linac were lined with the markers on the phantom in a static mode, and then shifted by the distance based on the location of target centroid determined from $4DCT_{MIP}$ images according to coordinates of the body frame. Phantom started then subsequently each one of programmed breathing motions with simultaneous 360 degree CBCT scan at median FOV protocol. With the volumetric images from CBCT, the shift was generated from

XVI software after matching between CBCT images and $4DCT_{average}$ images. There were two modes used for generating the shift: one was an auto mode and the other was a manual mode. For clinical treatments, manual mode is generally preferred. In this study, we used both modes and found less than 2mm difference in setup positioning between them.

4.2.5 4DCBCT

4DCBCT is reconstructed based on CBCT raw data. It provides target movement information at the format of ten phase's image sets, localizing the tumor with motions. Based on ten phases' images, $4DCBCT_{MIP}$ and $4DCBCT_{average}$ images have been generated and compared to $4DCT_{MIP}$ and $4DCT_{average}$ images appropriately.

After obtaining ten phase's images from XVI software, $4DCBCT_{MIP}$ and $4DCBCT_{average}$ images were generated by a Pinnacle treatment planning system 8.1y. There was no difference between 4DCT generated from Philips CT simulator and from Pinnacle g. Based on the reference (static marker) on phantom, we compared the true geometry of motion center to the 4DCBCT target center.

4.3 Results

4.3.1 CBCT of target centroid

The motion centroid was defined based on two methods: the use of coordinates from body frame as method one; the use of fixed markers on the moving frame as method two. The method one corresponds exactly to clinical protocol used in our institution. The method two has been used in this study because the images of

4DCBCT may capture only partial body frame while in each case it can easily capture the static markers on the phantom frame.

Based on the coordinate's reference from body frame, we explored the irregular breathing motion. In table 4.2, the shift between CBCT and geometry of tumor motion is in 3-5mm depending on the irregularity of large breathing patterns. However, the shift between CBCT and 4DCT is less than 2mm.

Breath patterns	Range	CBCT vs. Geometry	CBCT vs. $4DCT_{average}$
1	17.1 mm	5 mm	≤2 mm
2	20.3 mm	3 mm	≤2 mm
3	21.5 mm	2 mm	≤2 mm
4	23.2 mm	3 mm	≤2 mm
5	21.4 mm	1 mm	≤2 mm

Table 4.2 The shift between CBCT and geometry of tumor motion referenced by body frame.

The method two uses the static markers as a reference related to the target motion center/centroid. The static markers are around 2mm diameter and are located at the bottom of phantom. The markers related to target center were measured at the starting point in static mode. The distance of this measurement is recalculated based on the starting position and referred to the motion centroid from geometry breathing pattern. The shift between this recalculated distance to the measured distance from MIP images or CBCT images are presented in table 4.3. The comparison between the CBCT and true geometrical centroid shows the similar results to those obtained by the first method. The comparison between the 4DCT centroid data and true geometry derived data has been almost identical as presented in chapter 3.

Thus summing up, the CBCT image showed limited variation in centroid position relative to 4DCBCT. In previous results, we have used $4DCT_{average}$ images to compare with CBCT images. The comparison is based on the assumption that CBCT images are similar to the $4DCT_{average}$ images. However, this is not always true. To test this assumption, we need to compare the CBCT image not only with $4DCT_{average}$ images, but also with $4DCBCT_{average}$ images.

Breath patterns	Range (mm)	$4DCT_{average}$ vs. Geometry (mm)	CBCT vs. Geometry (mm)	$4DCT_{average}$ vs. CBCT (mm)
1	17.1	7.1	4.9	2.2
2	20.3	0.5	-1.2	1.7
3	7.3	1.8	3.9	-2.1
4	8.2	-1.9	0.6	-2.5
5	23.2	-7	-3.3	-3.7
6	21.4	-4.4	-1.1	-3.0
7	5.7	1.5	2.1	-0.7
8	12.1	-2.6	0.4	-3.0

Table 4.3 The shift between CBCT and geometry of tumor motion referenced by static marker.

4.3.2 4DCBCT of target centroid

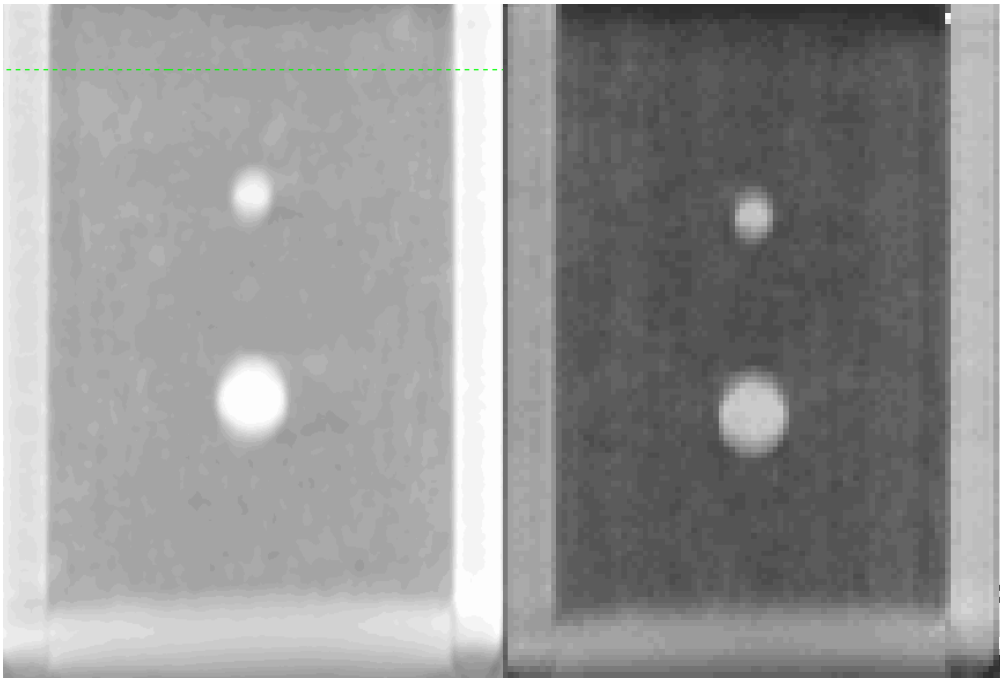

Figure 4.3 Comparison of CBCT (left) and $4DCBCT_{average}$ images (right)

In figure 4.3, an example of 2D image from CBCT and $4DCBCT_{average}$ is presented. We see that the image quality from CBCT is better than from 4DCBCT. However, we have found only slight difference in target shape and size between these two images. We need to point out the average image from 4DCT is slightly different from CBCT, but has similar shape as the average image from 4DCBCT. The $4DCBCT_{average}$ image with better quality will be a better choice for tumor position verification.

Table 4.4 listed the target centeroid positions of eight breathing patterns derived from $4DCT_{average}$ and from $4DCBCT_{average}$ images comparing with the true geometry centroid positions. Expect the breathing pattern 1 which has the highest irregularity, the difference of centroid location between the $4DCT_{average}$ and $4DCBCT_{average}$ images is less than 3 mm; the difference between the geometry and either one of these images is within 5mm. Due to the poor image quality of $4DCBCT_{average}$ images, the centroid position of small irregular breathing patterns is not as accurate as $4DCT_{average}$ images.

Breath patterns	Range (mm)	$4DCBCT_{average}$ vs. Geometry	$4DCT_{average}$ vs. Geometry
1	17.1	-5.9	7.1
2	20.3	-2.3	0.5
3	7.3	-4.8	1.8
4	8.2	-3.8	-1.9
5	23.2	-1.7	-7
6	21.4	-4.1	-4.4
7	5.7	-4.9	1.5
8	12.1	-2.5	-2.6

Table 4.4 Motion centroid of average image 4DCT / 4DCBCT vs. geometry motion center

4.3.3 4DCBCT of target size

The target size from $4DCT_{MIP}$ images for large irregular breathing patterns is underestimated as one of conclusions in chapter two. So we explore the target size from $4DCBCT_{MIP}$ and $4DCBCT_{average}$ images for comparison. For MIP images, $4DCBCT_{MIP}$ showed similar shape as $4DCT_{MIP}$. However, the image quality of $4DCBCT_{MIP}$ is low as is the image quality of $4DCBCT_{average}$ in figure 4.1. The $4DCBCT_{MIP}$ could improve the image quality and capture more accurate the target size.

Table 4.5 exhibits $4DCT_{MIP}$ and $4DCBCT_{MIP}$ images for eight irregular breathing patterns. The differences between sizes of target defined $4DCT_{mip}$ and $4DCBCT_{MIP}$ images are in eight cases smaller than differences between target sizes defined from expected MIP. Comparing to size of the expected MIP, the small irregular patterns (3, 4 and 7) showed less than 3mm difference for $4DCBCT_{MIP}$, but the large irregular patterns(1, 2, 5 and 6) showed 4-10 mm underestimations. The $4DCT_{MIP}$ results are similar as discussed in chapter two. The $4DCBCT_{MIP}$ images improve by 2-3mm the estimated of the expected MIP size in six cases, and 3-4 mm worse in the other two cases.

Breath patterns	Range (mm)	Expected MIP	$4DCT_{MIP}$	$4DCBCT_{MIP}$
1	17.1	42.1	35.8	38.5
2	20.3	45.3	40.9	40.2
3	7.3	32.3	30.3	31.2
4	8.2	33.2	31.8	31.1
5	23.2	48.2	38.3	38.8
6	21.4	46.4	39.9	43.3
7	5.7	30.7	29.9	26.0
8	12.1	37.1	35.7	31.9

Table 4.5 Target sizes from $4DCT_{MIP}$ and $4DCBCT_{MIP}$ images comparing with geometric MIP size.

In table 4.6, we presented the target size of $4DCT_{average}$ and $4DCBCT_{average}$ images in eight cases. The comparison of average images from 4DCT and 4DCBCT help us to explore the similarity between CBCT image and $4DCT_{average}$ image. It also helps us to evaluate the change tumor size during the whole treatment. As the $4DCBCT_{average}$ and $4DCT_{average}$ images theoretically provide similar target motion information, the size of these images should be less than 2mm. In eight cases, seven of them are less than 2.5mm. The last case is 4mm difference beyond we expect. The reason of more than 2mm difference is due to the poor images quality of $4DCBCT_{average}$.

Breath patterns	Range (mm)	$4DCT_{average}$	$4DCBCT_{average}$	Difference
1	17.1	35.28	37.08	-1.8
2	20.3	40.12	37.77	2.35
3	7.3	29.2	27.72	1.48
4	8.2	29.69	28.76	0.93
5	23.2	36.27	35.69	0.58
6	21.4	38.96	42.97	-4.01
7	5.7	28.32	25.99	2.33
8	12.1	32.58	31.53	1.05

Table 4.6 Target size from $4DCT_{average}$ and $4DCBCT_{average}$ images

4.3.4 Dose analysis

Dosimetry results for eight irregular breathing patterns show a clear shift in the measured isodose lines, revealing the discrepancy between the plan and the actual dose at delivery. The dosimetry results exhibit the similar geometrical shift of isodose lines as volumetric shift shown in chapter three. Below, we present one case exemplifying the detail of dose coverage over planned PTV.

In figure 4.4A, an example of isolines analysis for a large irregular breathing pattern (range over 23m) is presented. The mismatch between target outline and the 80% isodose lines have the similar shift as reported in chapter three. Since the prescription for this plan is 80% dose covering 95% PTV, we established an approximated 3D dose distribution based on dose measurement from the three films. The 3D dose distribution gave us an idea of how much volume is underdosed for the partial PTV. In the investigated case, the PTV size is 36.7cm^3, and around 20% of PTV is underdosed. In our analysis, 8% of PTV is underdosed less than 6 Gy; 7% of PTV is underdosed more than 6 Gy and less than 12 Gy; 3% of PTV is underdosed more than 12 Gy and less than 18 Gy; 2% of PTV is underdosed more than 18Gy.

In figure 4.4B, the total dose to PTV versus the tumor local control rate is presented from Timmerman *et.al.* The plot shows that less total dose to PTV decreases the local control rate. The local control rate will decrease by as much as 40% if the total dose covering PTV diminishes from 60 Gy to 40 Gy. Based on the above data, we may estimate that partial PTV underdosed as describe above for our

study may lead to the decrease of the local control rate by 36% if even small volume of PTV is underdosed by 18Gy.

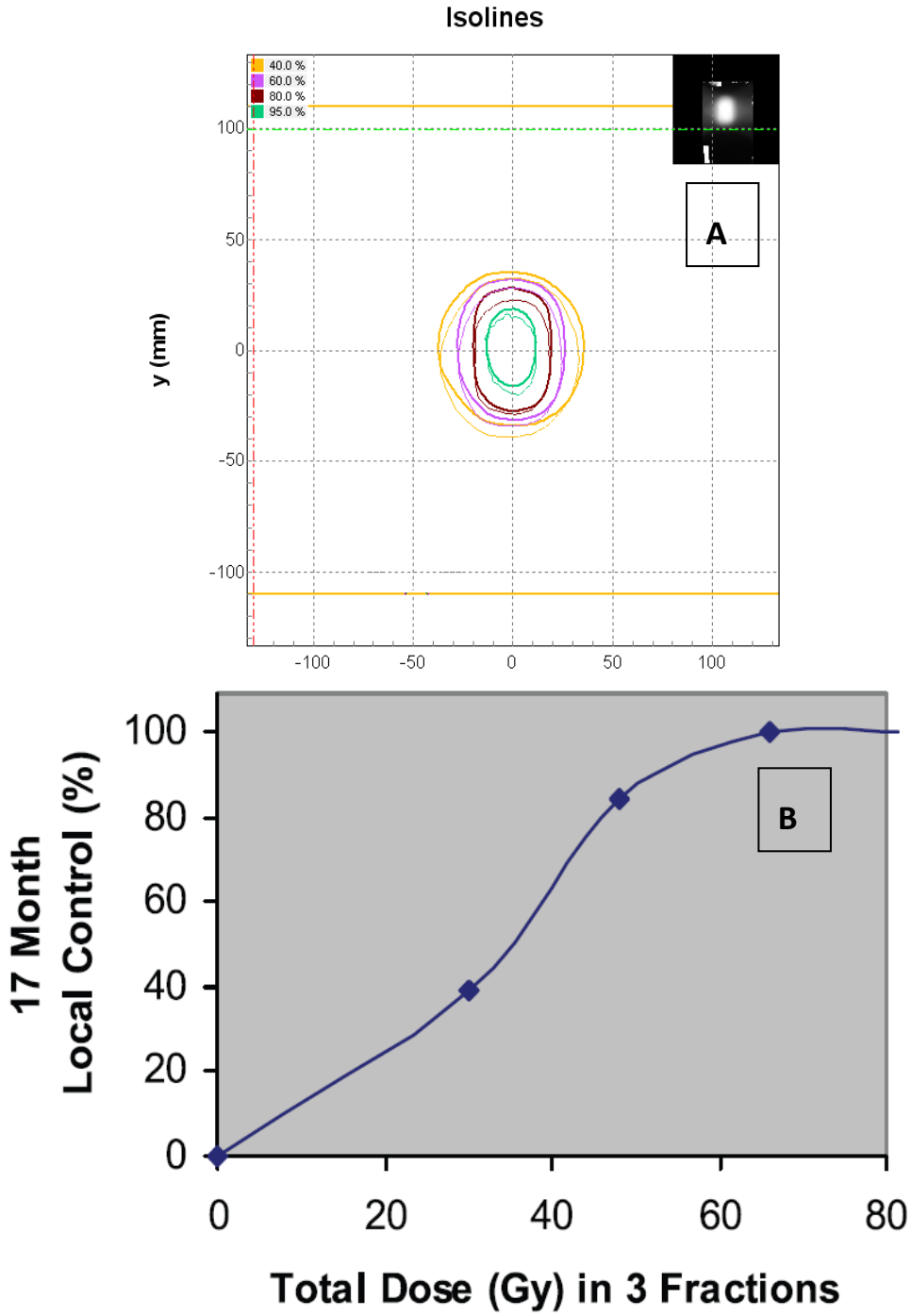

Figure 4.4 A: One irregular large breathing pattern (range is 23mm) dose isolines distribution: computed (thicker lines) vs. delivery (thinner lines). **B**: Total dose in 3 fractions for SBRT lung cancer vs. the local control rate.[85]

4.4 Discussion

In this study, we focused on CBCT for patient setup verification, especially in cases when irregular breathing patterns are involved. It is well known and documented that CBCT as a redundant verification system will provide the benefits for the patient treatment for static targets and static body anatomy. For example, Wang *et. al.* reported that for static and moving targets (with regular motion in less than 10mm motion range) the matching based on Varian OBI system is in the range of accuracy of 2mm. In this study, we repeated the regular motion as a reference on Elekta XVI system and found the same level of accuracy.

Following these results, we generalized the study in chapter two and three extending it to cases of irregular motion of target. In chapter two, the irregular breathing motions affect both MIP size and center position in $4DCT_{MIP}$ images, especially for large amplitude motions (over 20mm variation in rang of motion). In turn, we found that CBCT may capture wrong center position comparing to the true geometry and the error is worse in irregular free breathing with large motion range (over 20mm) occurs. The matching between CBCT and $4DCT_{average}$ images is based on the assumption that CBCT images are similar to the $4DCT_{average}$ images. In this study, we proved that the target shape and size in CBCT images is similar to shape and size as captured by $4DCT_{average}$ images. However, our results indicate that use of

$4DCBCT_{average}$ images with higher imager quality for patient setup may be advantageous for treatment. We also need to point out that both 4DCT and CBCT provide well coinciding determination of target centroid position (less than 3mm in difference). Interestingly, however, both these determinations do not reflect the true geometrical position of the target centroid as determined from target size and motion measurement.

To fully evaluate 4DCBCT images for patient setup, we compared $4DCBCT_{MIP}$ / $4DCBCT_{average}$ images with $4DCT_{MIP}$ / $4DCT_{average}$ images for irregular breathing patterns. The 4DCBCT with limited image quality provide similar target size and shape as 4DCT. However, the image quality of 4DCBCT is so poor due to the limit projections used in this study. The 4DCBCT can provide better image quality and more accurate target motion geometry if we got more projections and slowed the gantry speed.

In order to estimate the dose effect of irregular breathing patterns involved, we did dose measurement in phantom. Based on Timmerman's data in figure 4.4B, the local control rate may drop by 40% on the severe underdosed of the small (2% PTV volume) portion of the target. The use of CBCT showed no visible correction for this troubling result in case of large amplitude irregular free breathing patterns.

4.5 Conclusions

In this study, we successfully evaluated the CBCT and 4DCBCT images for patient setup and followed with a dosimetric study as irregular breathing pattern involved.

The CBCT cannot correct the shift from 4DCT and motion geometry. However, it shows less than 2mm centroid position and target size as $4DCT_{average}$ images.

In dosimetric measurement, we found 2% of PTV will be underdosed over 18 Gy, causing 38% local control rate dropping at the present of a large irregular breathing pattern (over 20mm). In this situation, we highly recommend breathing control for patient treatment.

CHAPTER FIVE

EXTENDED DISTANCE VIRTUAL ISOCENTER

5.1 Introduction

The results of our studies of accuracy of setups for SBRT treatments bases on 4D CT and CBCT reveal that for large range irregular motions of target in lung there exists a possibility of treatment under dose that can potentially lead to inadequate local tumor control.

The natural question is therefore how in clinical practice we can avoid these situations. Excluding the option of regularizing patient breathing through training (time consuming and uneconomical option for most clinics) we are left with two possibilities. The most obvious one is to increase the margins and the other one is to use abdominal compression that transforms any large range motion breathing pattern to small range motion breathing pattern, which removes the danger of inaccurate localization of lung tumor for SBRT.

The solution based on application of abdominal compression is simple and reliable but requires specialized body frame equipment. Thus if this type of equipment is not available the only choice in clinic may be just the enlargement of margins. It is obvious, in such a case, that danger of underdosing the target may be turned into danger of overdosing the healthy tissue. Thus it drives us to ask if there exists a method that may minimize this danger.

To discuss the issue in the proper perspective we have to notice first that the question can be divided into two queries. One is if the prescribed dose distribution

will cover larger volume if larger margins are assigned. The answer to this question is positive as long as irradiation of enlarged PTV is properly executed on the treatment machine. This means that the enlargement of margins to cover volume that otherwise may not be irradiated due to error in determination of target for planning and then the error in placement of target for treatment will eliminate the possibility of missing delivery of the dose prescribed to moving tissue of the target. This means also that some of the healthy tissue that does not constitute the target will be inevitably irradiated to high level of dose. In other words enlarging of margins will clearly enlarge the volume of tissue exposed to dose prescribed.

We should notice at this point, however, that not only healthy tissue exposed to prescribed dose may lead to toxicity but also healthy tissue exposed to large dose level that is below the level of prescribed dose. Let us recall that in SBRT treatments we try very much to minimize the volume healthy tissue exposed to large dose level that is below the level of prescribed dose. This we achieve by applying large number of beams intersecting in close vicinity of the target and by specific beam arrangement in space. The goal is to achieve as compact and symmetric dose around the target as possible to decrease the dose gradient descent away from target and thus decrease the volume of organ in which the target is embedded (lung) to decrease the toxicity in the organ.

As the quality of dose symmetry and compactness is to large degree dependent on techniques of irradiation we may hope that applying improved techniques we may

decrease the volume of healthy tissue exposed to large dose level that is below the level of prescribed dose, making just overall toxicity of treatment acceptable even in the case of enlarged margins that will inevitably lead to increase in the volume of healthy tissue exposed to prescribed dose. We easily notice at this point that technique of treatment that is capable to achieve this deed is the application of treatment of SBRT target in lung from extended SAD distance.

The reason for improvement of compactness of dose distribution when treating from extended distance is better possibility of avoiding collision between gantry and couch with the body on the larger separation of beam direction achievable under these conditions translates into smaller volume of intersection between beams outside of the target, that in turn minimizes the dose accumulation in the vicinity of the target contributing to better dose distribution compactness and faster gradient of dose away from the target. Resulting minimization of volume of lung tissue exposed to large dose will lead to the decreasing of treatment toxicity offsetting pat least partly the increased toxicity caused by the enlargement of volume of lung exposed to treatment dose as grounded in margin

The complete list of benefits of increasing the distance between the target and source are listed:

1. It is easier to avoid collisions between different parts of equipment as well as collisions and patient body. Various angles of beam impingement on target are used to attain highly conformal dose shaping around the target. Better

avoidance of collisions results in enlargement of the range of angles admissible for mutual positions of couch and gantry, making it possible to choose more pathways for photons moving from the source towards the target allowing more conduits for beams to better avoid irradiating organs at risk.

2. The other aspect of the increase of the distance between the source and the target is the decline of the effect of inverse square law on the dose variation between the target and dose at patient skin. The result is the decrease of the dose at skin for given dose prescribed for the beam at the target. This diminishing of the dose at skin provides clear advantage of lower toxicity for SBRT treatments [9].
3. The most valuable aspect of the extended distance between the source and target treatment in SBRT results from the enhanced compactness of the dose distribution realized when multiple beams from farther removed source from target are crossing at target producing more compact beams intersection volumes. The result is more compressed dose around the target and higher gradient of dose decrease away from target.

We aim in our investigations not only to demonstrate that treatment with extended distance between source and target has positive effect on shaping better dose distributions in SBRT but also describe the extended distance treatment technique that is practical and feasible to be applied for SBRT delivered with typically used in radiation treatment departments' linear accelerators. This new technique we will call

extended distance virtual isocenter (EDVI) technique.

5.2 Material and methods

5.2.1 Treatment plan

The phantom in this study only works in static mode. The detail description of phantom has presented in the chapter 2 and 3. We just focused on the treatment plans for EDVI technique.

To obtain data needed for our purpose we generate in sequence three SBRT plans. The first plan is a standard SAD 100cm plan. Ten non-coplanar beams are appropriately distributed in angular space shown in table 5.1. Beams are delineated to match the target outline in each beam's eye view and weighted to assure plan dosimetric criteria adopted in RTOG 0236. Dose calculations are performed with heterogeneity corrections utilizing collapsed cone algorithm.

The second plan is derived from the first plan by keeping gantry and couch angles unchanged relative to the first plan shown in table 5.1 while moving the center of the target for each beam along beam's central axis to increase the distance between the source and the target center from 100 cm to 120 cm. During this operation the beam's eye view (BEV) outline of the target and corresponding MLC leaf positions are appropriately scaled for each beam.

The prescription for the second plan is the same as that for the first plan assuring satisfaction of dosimetric criteria adopted in RTOG 0236. This prescription requires an increase in number of monitor units assigned per each beam in order to compensate

for extended treatment distance. Recalculation of monitor units is provided by the planning system and verified by independent calculations.

In laboratory (room) frame of reference the beam directions for the second plan are invariant with respect to the first plan while center of the target lies on the central axis of each beam and on the surface of the sphere of radius 20 cm. From the point of view of reference system with origin in the target center each beam of the second plan lies at surface of the sphere of radius 120 cm. The irradiation of the target seen from the point of view of target reference is therefore an isocentric irradiation at SAD distance equal to 120 cm. This justifies recognition of this technique as extended distance (virtual) isocentric treatment.

The third plan is a clinically beneficial modification of plan 2 that works as follows. The purpose of the modification is to separate beams in their angular degrees of freedom for SAD=120 cm more than it was achievable for a standard SAD=100 cm treatment technique. In Table 4.1, gantry and couch angles for the three plans are listed. BEV apertures are changed appropriately for the new source-to-target distance and new beam directions. Moreover beam weights re-optimized for new plan to achieve dose coverage of the target that is identical to dose prescribed for treatment plans one and two.

Beam number	100 SAD (first) Plan		120 SAD (second) Plan		120 SAD (third) Plan	
	Gantry	Couch	Gantry	Couch	Gantry	Couch
1	180	0	180	0	180	0
2	220	345	220	345	220	335
3	270	25	270	25	270	45
4	270	335	270	335	270	325
5	315	0	315	0	315	0
6	30	270	30	270	40	270
7	330	270	330	270	320	270
8	45	25	45	25	45	45
9	90	0	90	0	90	0
10	150	0	150	0	150	0

Table 5.1 Gantry and couch angels for each beam of 100 SAD plan, 120 SAD plan and new 120 SAD plan

5.2.2 Delivery and dose analysis

All three treatment plans are then exported from Pinnacle to MOSAIQ 1.6 (IMPAC Medical Systems, Inc., Sunnyvale, CA) and to the Elekta SynergyS (Elekta group, Stockholm Sweden) linear accelerators. Prior to phantom irradiation, all plans are checked to ensure collision avoidance. Moreover, we verify on the treatment machine that positioning of phantom target center at extended distance treatment for each beam is accurately placed at our pre-calculated coordinates of the couch that assure placing the target in actual isocenter (plans one and two) as well as virtual isocenter location for each beam for plan three.

Prior to irradiation, the beam isocenter is identified at the edge of each film using a permanent marker. This allows us to accurately align the beam isocenter from exposed film to the plan isocenter from the computed planar dose. Following irradiation, films are extracted from the phantom and are scanned using Epson

10000XL (Epson America Inc., Long Beach, CA USA) flatbed scanner together with Film QA (3cognition LLC, Wayne, NJ, USA) software for analysis. Scanned films are then compared with the computed planar dose images generated by Pinnacle planning system. Various dosimetric aspects of the computed and measured dose, including comparison of absolute dose and relative isodose lines, are evaluated.

5.2.3 Couch movement verification

To assure the successful delivery on patient, an independent couch movement verification system is required for extend SAD technique. We explore the two camera tracking system (Brainlab, Germany) for each couch movement in table 4.1. Each camera contains one optical system and one infrared system. It tracks the five markers on the phantom / patient with sample rate 15 per second. The software provides the couch position and angel on three dimension coordinators.

5.2.4 Characteristic dose analysis

We notice first that any compact SBRT dose distribution has to provide adequate coverage of the PTV and obligatory decrease of dose away from PTV towards healthy tissue. The verdict on the adequacy of PTV coverage will be completely satisfactory achieved from dose volume histograms (DVH). DVH will not be, however, a good measure for judging the gradient of dose decrease away from the target. In this case, the aim would be to see how tightly high dose is wrapping around the PTV without spilling far away from the target. To measure this type of behavior of the dose cloud we create first a sequence of histograms that quantify the relative change of dose

between close and detached regions in the vicinity of the target.

Therefore, after dose distribution is calculated by the treatment plan we group values of dose into histogram depending on the proximity of each point relative to the PTV. The convenient approach for building such histograms is to create first a sequence of shells that classify points outside of the target relative to their distance from the PTV. Each shell has its own dose distribution: values of dose in each shell vary between the smallest and largest found in the shell shown in figure 5.1. For histograms that are of interest it is constructive to get for each shell the average, max value, min value and standard deviation values of dose histograms.

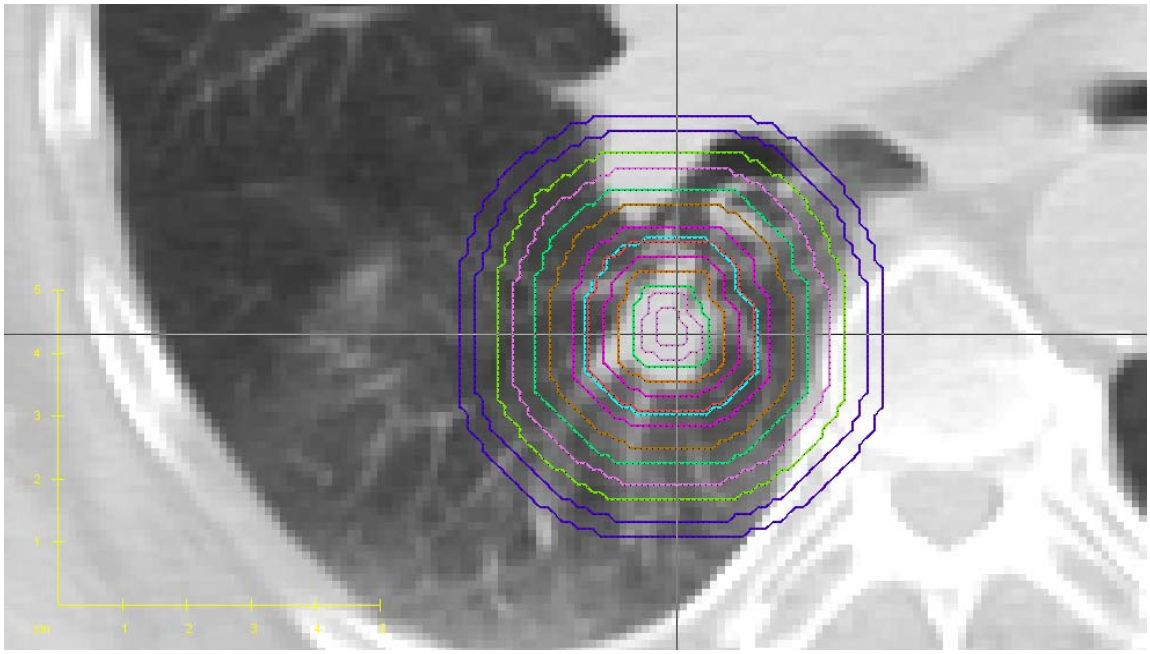

Figure 5.1 Shells based on the distance from PTV for dose distribution analysis.

5.2.5 Patient case analysis

There are three patient cases prepared for characteristic analysis method we

mentioned above. The patient cases are selected based on tumor size and location. The tumor location is critical for our analysis as we try to avoid more OARs in 120 cm SAD comparing the same case in 100cm SAD plan. The tumor size also decides the chance to avoid the OARs as larger tumor size may give less flexibility for beam arrangement. In some extreme cases, our analysis can show a huge improvement for some beam arrangement. However, we may gain minimum improvement in some cases due to the tumor size and location.

We verify the 120 SAD plans in patient data on linear accelerator to assure the achievability of delivery. To mimic the real treatment, the Brain lab camera tracking system provides the cough shift during our verification procedure.

5.3 Results

5.3.1 Dose analysis

As we expected the plan 1 and plan 2 has identical dose distribution which also reflected on film dose analysis. In figure 5.3, shows axial and coronal dose distributions in planes crossing the center of the phantom target for the three calculated plans. The plan 1 is a plan for SBRT treatment at SAD = 100 cm, plan 2 is the same plan (the same orientation of beams) as plan 1 but for SBRT treatment at EDVI = 120 cm and plan 3 is a modification of plan 2 (beam directions are optimized to use increased ability to avoid collision at extended distance between source and target) of original plan 1 for SBRT treatment at EDVI = 120 cm. With identical beam orientations, the dose distribution is essentially unchanged as the source to target

distance is increased from 100 to 120 cm (compare columns 1 and 2). The third column shows the enhanced with respect to SBRT criteria dose distribution resulting from the expanded set of beam orientations, re-optimized to take advantage of increased couch and gantry clearance. The modified plan (plan 3) shows visually more compact dose distribution. In order to rearrange the gantry angle and couch angle, we need physically verify the angles on line accelerator. We also consider the position of OAR during this rearrangement. Without this consideration, the dose on OAR will increase in some cases. It is not easy to use direct optimization by software, but manually optimization is easy achievable in this kind of situation.

Figure 5.2 shows a similar comparison of measured dose distributions superimposed on calculation. The left-hand distribution shows the 100 cm SAD plan (plan 1), the center distribution the 120 cm plan (plan 2) with a beam configuration identical to plan 1, and the right-hand distribution the 120 cm plan (plan 3) with the re-optimized beam configuration. In each case the calculated distribution is represented by the thick lines and the measures distribution by the thin lines. In each case there is excellent agreement between calculation and measurement. Again, the superiority of the dose distribution arising from the possibility of utilizing a larger space of beam angular separation when treating at extended distance between the source and the target.

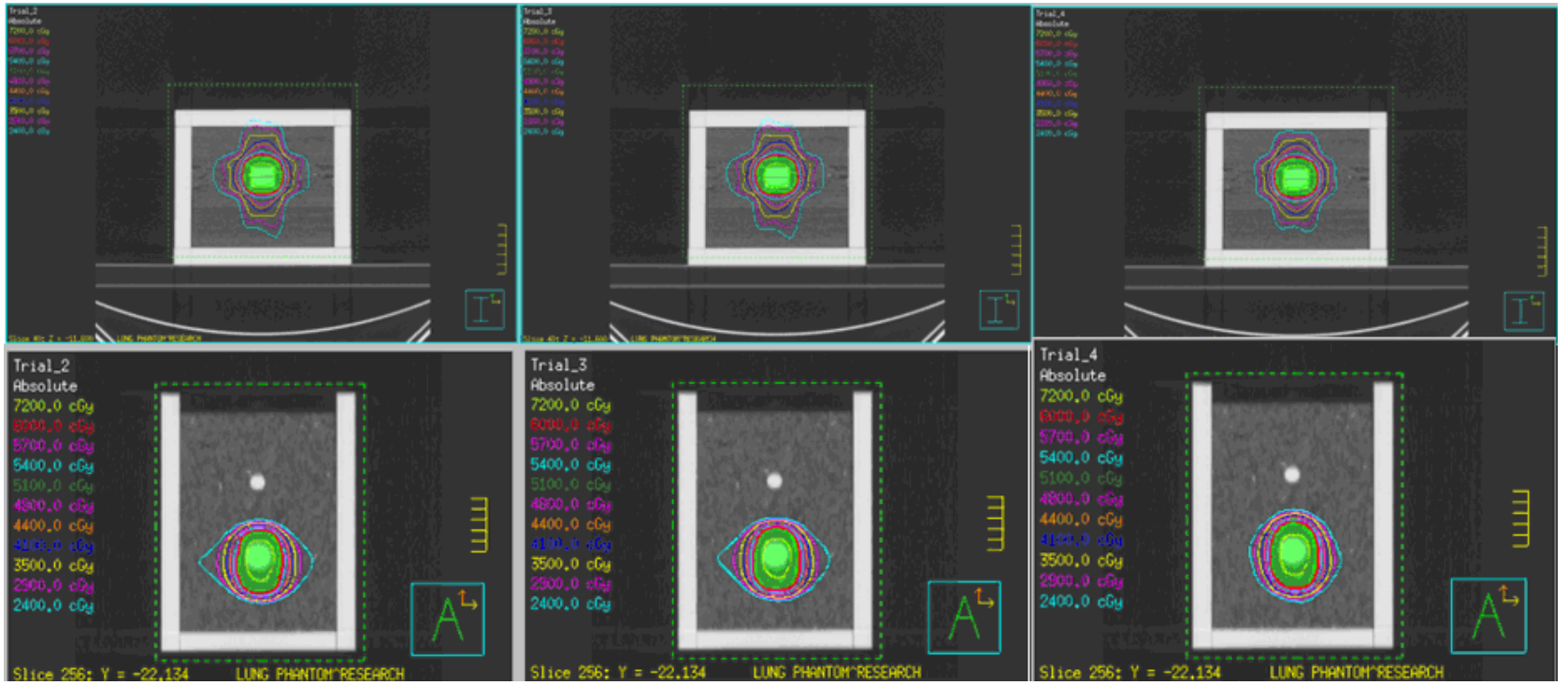

Figure 5.2 Axial and coronal dose distributions for a 100 SAD plan 1(left), a 120 SAD plan 2 (middle), which uses the same beam orientation as plan 1, and a 120 SAD plan 3 (right), which uses an expanded set of beam orientations. The additional conformity achieved by expanding the beam orientation space is evident in the higher conformity of plan 3.

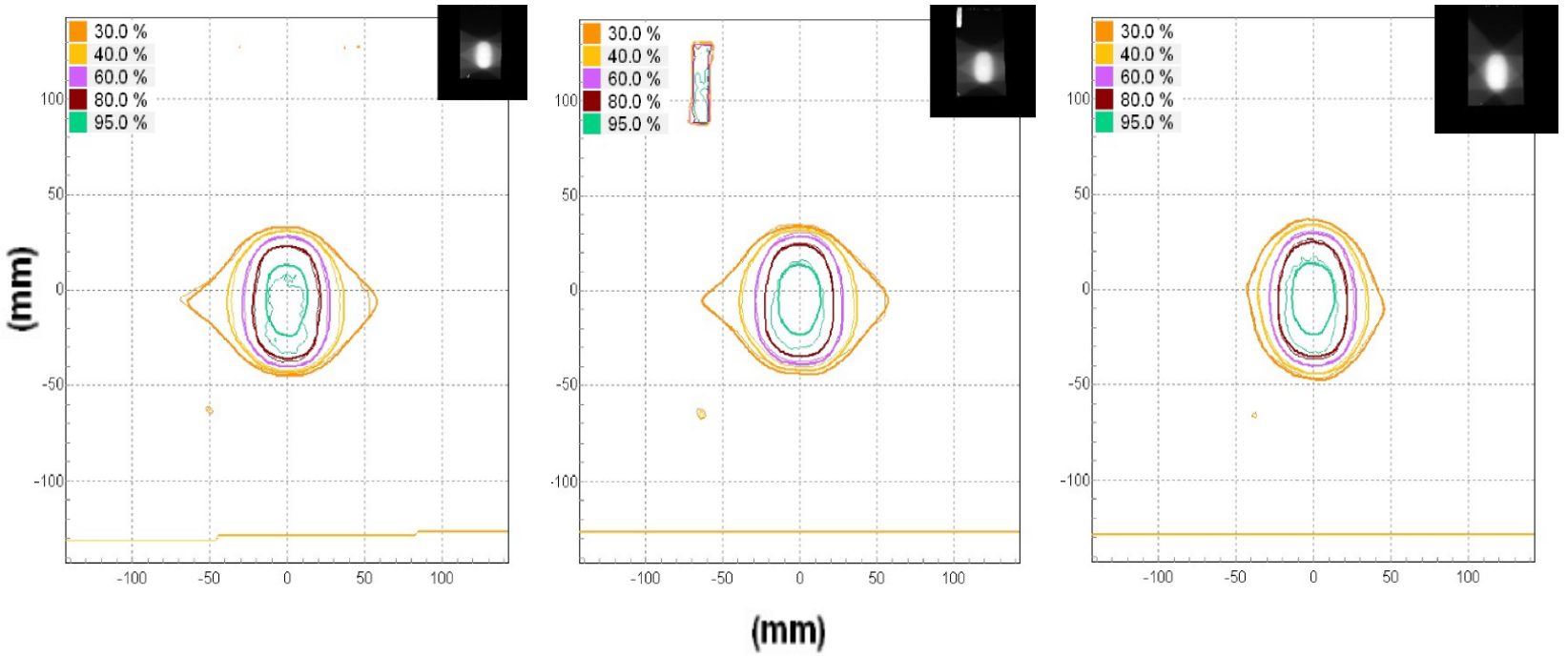

Figure 5.3 Film to calculated image matching for 100 SAD plan 1 (left), film to calculated image matching for 120 SAD plan 2 (middle) and film to calculated image matching for 120 SAD plan 3 (right)

Figure 5.3 shows a similar comparison of measured dose distributions superimposed on calculation. The left-hand distribution shows the 100 cm SAD plan (plan 1), the center distribution the 120 cm plan (plan 2) with a beam configuration identical to plan 1, and the right-hand distribution the 120 cm plan (plan 3) with the re-optimized beam configuration. In each case the calculated distribution is represented by the thick lines and the measures distribution by the thin lines. In each case there is excellent agreement between calculation and measurement. Again, the superiority of the dose distribution arising from the possibility of utilizing a larger space of beam angular separation when treating at extended distance between the source and the target.

5.3.2 DVH

Dose volume histogram (DVH) is one of basic analysis on these three plans. We presented the PTV coverage for three plans in figure 5.4. As no difference of PTV coverage, the dose on OARs plan 3 (extended distance method) is significant different on DVH comparison. However, the detail dose distribution around PTV in depth distance cannot be reflected in DVH.

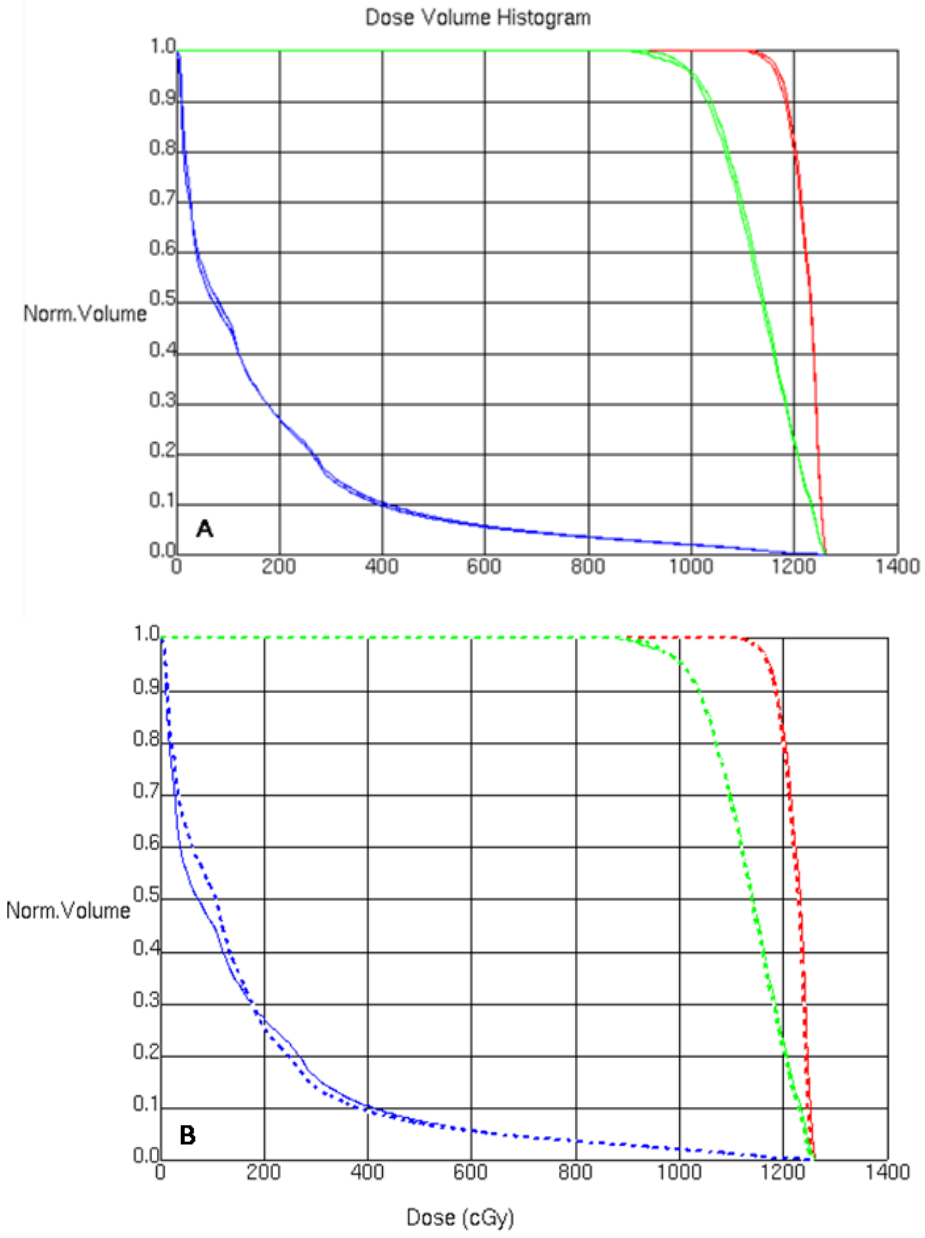

Figure 5.4 DVH: Green colors presents PTV, red color presents GTV and blue color presents total lung **A** Thicker lines present 100 SAD plans, the thinner lines present 120 SAD plans. **B** Thicker lines presents 100 SAD plans, the dash lines presents new 120 SAD plan

5.3.3 Statistical analysis

An example of shell method in figure 5.1 for plan 1 (100cm SAD) and plan 3

(120cm SAD) is presented in figure 5.5. The shell method provides how dose distribution dropping outside PTV. It will help us to understand the toxicity of health tissue outside PTV. In figure 5.6A, the outside max dose to the relative distance of PTV of plan 1 and plan 3 are compared. In plan 3, the max dose drop much faster after 1.5cm from PTV, which means the health tissue outside 1.5cm of PTV obtains lees dose than in plan 1. However, only max dose is not enough to measure the dose on the health tissue. The standard deviation (SD) of dose distribution can give clearer viewer on the behavior of dose distribution. In figure 5.6B, we presented the SD of plan 1 and plan 3 for comparison. The SD in plan 3 has 30-50% less than in plan 1. It means the dose distribution of plan 3 is always more compact from the edge of PTV to 4cm distance than plan 1. The more compact dose distribution benefits not only tiny amount but also a volumetric amount of health tissue around PTV.

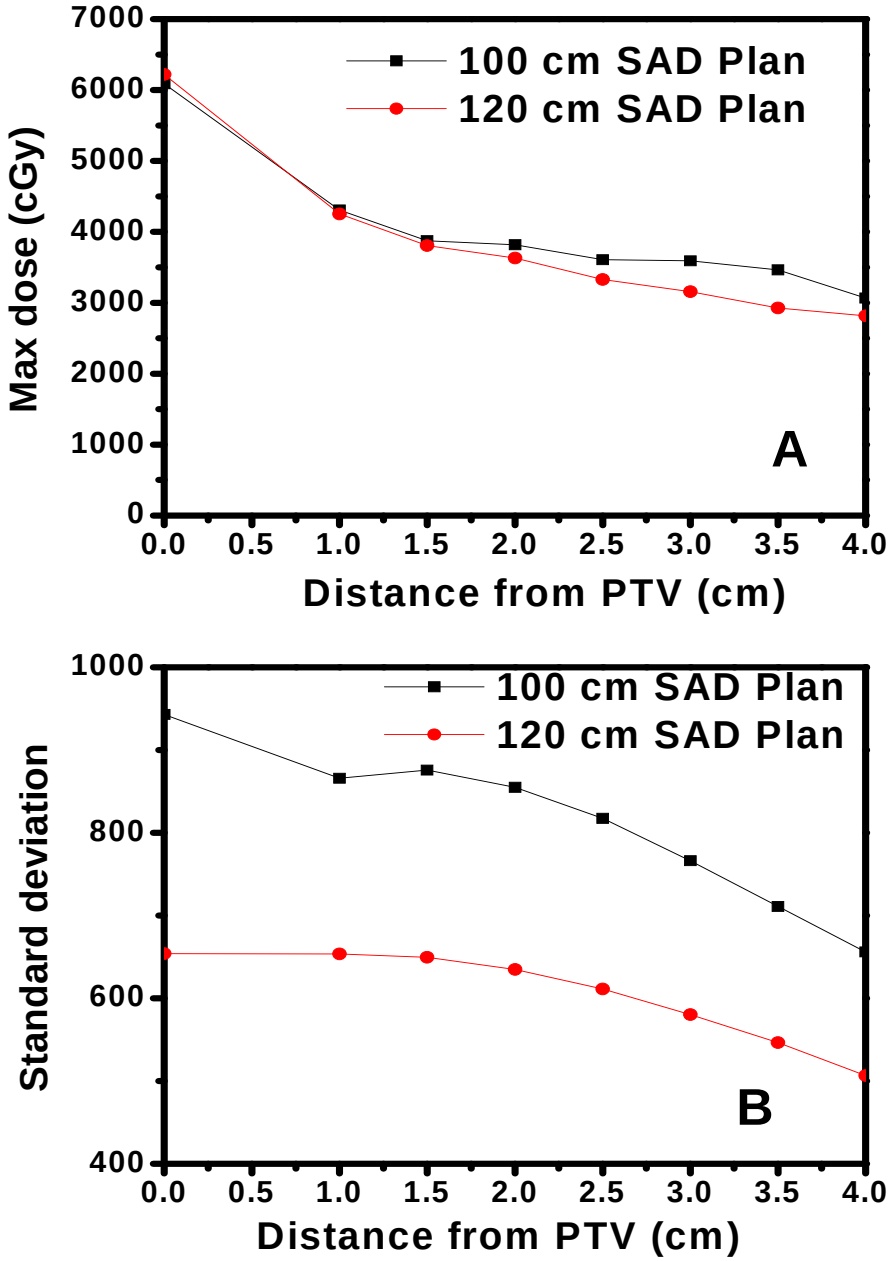

Figure 5.5 A: the max dose decreased on 100 SAD plan (black line) and 120 SAD plan (red line) **B:** the standard deviation on 100 SAD plan (black line) and 120 SAD plan (red line)

As the more compact dose distribution will benefit the health tissue around the PTV, the idea of EDVI will apply to the situation that requires larger margin around the tumor. The situation is related to the problem we mentioned in chapter 2 and 4. To

overcome the problem of 4DCT and CBCT, a larger margin is an alternator to treat patient safely. However, it will bring higher toxicity for health tissue. The EDVI method will benefit the patient treatment by fast dropping dose away from PTV.

5.3.4 Patient case analysis

We used one SBRT plan based on patient images to verify the improvement of our method. In figure 5.7, we listed the tumor position related to the esophagus from beam eye's view (BEV). From original plan in figure 5.6A, the beam cannot avoid the esophagus, otherwise the gantry and couch collision will happen. On the contrary, the beam can bypass the esophagus at EDVI plan which we do not need sacrifice the esophagus to avoid the collision. The EDVI plan exhibits better DVH for esophagus shown in figure 5.6B which will be benefits for patients.

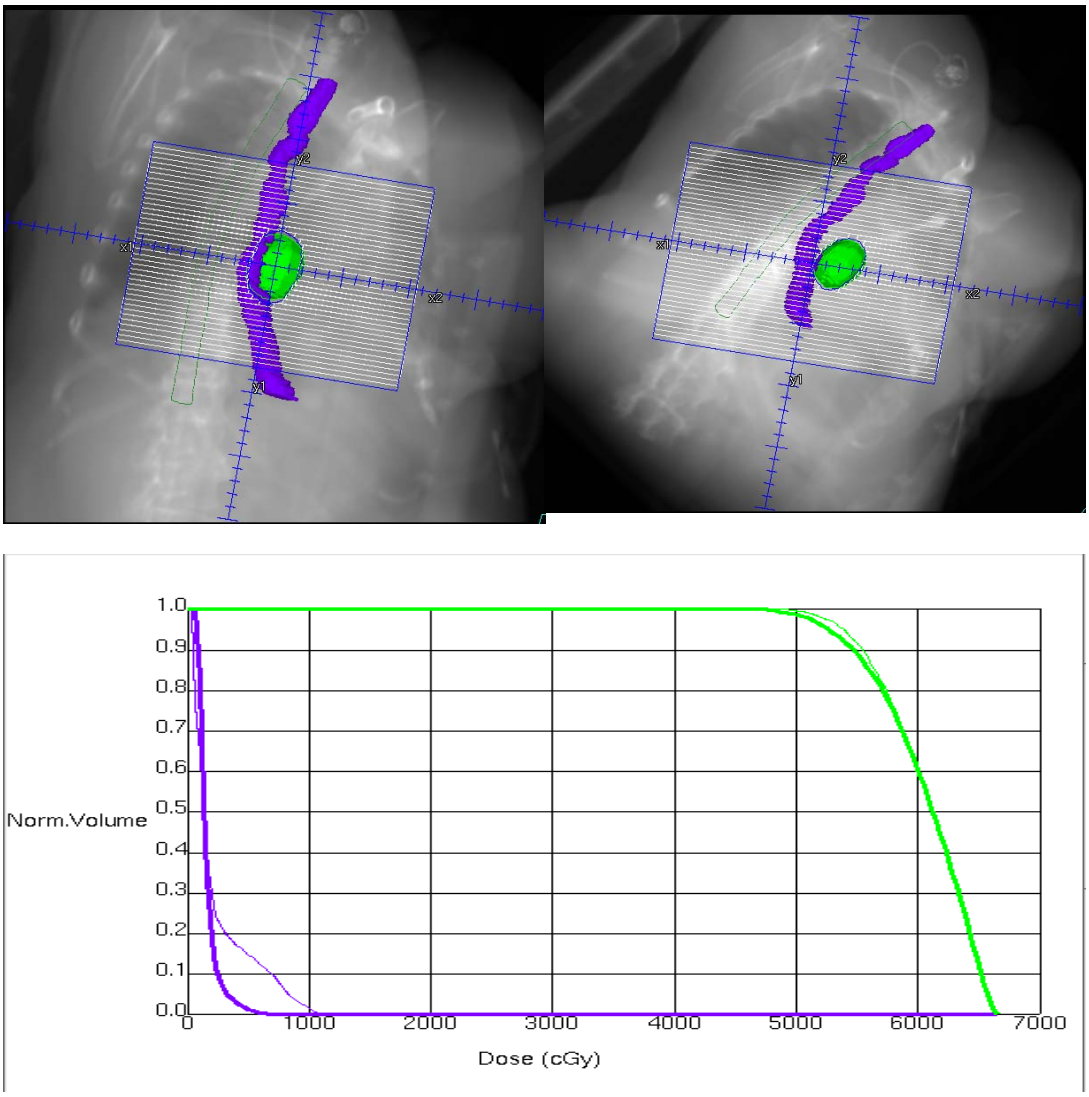

Figure 5.6 A The BEV that esophagus cannot be avoided at 100cm SAD plan (left), but can be avoided at 120cm SAD plans (right). **B** The DVH of dose on esophagus for 100cm SAD plan (thinner line) and 120cm SAD plan (thicker line)

5.4 Discussion

The main goal of EDVI is to provide a new treatment technique that is capable to remedy three weaknesses of dose distributions for standard distance SAD (100cm) SBRT therapies.

First disadvantage of standard distance SAD SBRT is potentially too large dose to patient skin. The reason for this concern of too large dose to D_{max} in SBRT is the fact

that even multiple beams used for SBRT irradiation may cause the dose at D_{max} especially when few beams are intersecting at surface, to reach 40 % to 50% of the dose prescribed to target. For hypofractionation this dose may cause extensive toxicity.[86] Decreasing dose to skin is thus an obliging characteristic of properly executed SBRT. A relatively simple remedy for this dosimetric disadvantage of standard SAD SBRT is the removal of the source from target's center. The dose decreases inside the body from D_{max} with increasing depth is governed by the attenuation and the inverse square law for divergent beams. The beam attenuation is a function of beam energy and is practically not dependent on the distance between the source and the surface of the body. In contrast, dependence of the relative change of fluence with distance is a clear function of beam divergence. As a result dose for points characterized by equal separation in the body leads to their decreased ratio as far as points close to surface and points inside the target are concerned when surface is removed further from the source. This is a simple consequence of the flattening of the function $1/r^2$ with r. The measure of dose improvement in this respect will thus require direct comparisons of dose at skin (practically, at dmax) for the same dose prescription for standard SAD distance (100 cm) SBRT and EDVI SBRT.

The second essential feature of quality of dose distribution for hypofractionated treatments is the containment of exposure for serially structured organs[85] . This attribute is the function of ability to avoid structures by beams directed towards target, or the ability to disperse beams over large space of angular directions. For the case of

irradiations by linear accelerators the space of available for treatment angular degrees of freedom is evidently related to the ability of the removal of the source away from patient body. The larger the distance between the target and the source means that the couch on which the body is supported is further away from the head of the accelerator and allows more freedom in setting mutual gantry and couch angles, facilitating better direct avoidance of serial structures by beams directed towards the target. The measure of dose improvement in this respect from standard SAD treatments to EDVI treatments will be best evaluated by standard DVH histograms.

The last and central characteristic of SBRT treatment, more indispensable than limitation of the dose to skin and serially structure sensitive organ, is the shape of beams around the target. The success of hypofractionated therapy (tumor ablation with none, or narrow toxicity) is critically dependent on the size of the volume of organ at in which the tumor is exposed to dose that is potentially harmful for tissues of this organ. Therefore, the important property of dose distribution outside of the target is uniform and tight clasp of high dose around the target. In other words, more uniform the embrace of target by dose cloud is and faster the gradient of dose decrease away from target boundary is achieved, the safer the ablation of tumor is anticipated and fewer complications are expected (quote). In RTOG 0236 at Chapter 1, the demand for suitable properties of dose distribution satisfying above described conditions have been expressed in the form of tables specifying coarse strictures for dose speed of decay away from target. However, for the purpose of more systematic

comparison of multiple dose distributions achievable under EDVI and standard SAD irradiations we need quantitatively more detailed measures of dose compactness. To this end we introduce dose distribution characteristics that measure dose gradient uniformity and dose gradient speed decrease away from the target. These characteristic quantities we call the maximum dose gradient (MDG), average dose gradient (ADG) and radial dose variability (RDV).

5.5 Conclusions

Investigations of this study demonstrate that utilization of extended distance source to virtual axis method enhances the capabilities of linear accelerators by allowing more angular separation between beams used for irradiation of patient body. In case of SBRT therapy, this capability leads to more compact dose distributions that allow decreasing volume of high dose exposure in sensitive organs (e.g. lung) and minimizing the treatment toxicity. Moreover, the technique allows to better spare organs at risk that may reside in the vicinity of the target and also makes possible to decrease the skin dose. Further, we demonstrate that the technique is easily implementable using existing commercial planning and delivery systems. Phantom measurements assure that EDVI treatment delivery can be accurate and that it truly provided improved dose distributions and excellent agreement between treatment planning calculations and actual dose at irradiated phantom.

CHAPTER SIX

SUMMARY, CONCLUSIONS AND FUTURE DIRECTIONS

The primary goal of this study is to evaluate the quality of lung treatments with radiation for patients that show the irregular breathing pattern and are treated with free breathing while their margin size and setup are based on recent technological innovations of 4DCT, CBCT and 4DCBCT.

Existing literature on the subject indicates that these tools allow precise patient positioning relative to beams and lead to accurate reproduction of treatment plan in the patient body during delivery. However, most studies so far has been performed on static or on moving targets that expose regular motion patterns. Being aware of the fact that binning of images that are used for the reconstruction in 4DCT and 4DCBCT is regularly distributed in time or in space while the moving of target may be substantially random in nature in spatiotemporal domain one may have doubts that reported results are also applicable to patients who have tendency to breathe irregularly. To test the hypothesis that 4DCT, CBCT and 4DCBC may not always lead to clinically adequate treatments we embarked on the following investigation. We have built for start the phantom capable to reproduce not only regular periodic motions but also irregular motions that repeat faithfully pattern of motions of targets in the lung for real patients.

Having these phantoms available we were able to determine very precisely the geometry of moving target in the phantom. Then using procedures that follow exactly

the pattern of target definition for treatment planning and delivery we verified how closely the image based determination of target size, including their motion, is coincident with our geometrical measurements. We have found that in large irregular motion cases considerable mismatch can occur between image derived and true data. Following on these results we measured for these cases the agreement between planned dose distribution and delivered dose distribution to moving target. This resulted in confirmation of the existence of discrepancy between computed in plan dose and dose delivered in reality to phantom. We estimated in some situations the discrepancy may lead to serious under-dosing of the target with clinical consequence of severely diminishing of tumor control.

To understand the impact on SBRT treatments of this condition we investigated the likelihood of patients falling into the category of expected under dose. Having not enough data from our institution I discussed the issue with researchers [87, 88]who analyzed hundreds of patients for the purpose of categorizing the characteristics of breathing motions in chest. Their results show that around 20 % of all free breathing, lung patients do fall into class of irregular breathing with large amplitude and thus can potentially be under-treated.

At this junction my research does not provide a solution for this problem as long as the pattern of target motion is irregular and has large range of displacement. As long as vendors do not provide better technological solutions the only remedies in clinic to avoid under-dosing in the case of lung therapy would be (1) the enlargement of

margins, (2) regularization of breathing pattern and (3) the use of breathing motion suppression (abdominal compression). We note that the first two solutions have considerable drawbacks as enlargement of margins may lead to increase of toxicity that is not well understood at present time for SBRT therapy, and as regularization of breathing is time consuming and inefficient solution that is not very likely to be embraced by routine clinical practice. We therefore recommend as best currently available technique for avoidance of this danger in SBRT lung the use of abdominal compression. The abdominal compression can be applied safely to great majority of patients exhibiting large motion range, does not require patient training and does not increase the treatment cycle. The decrease in range of motion achieved under abdominal compression reduces the error related to image based determination of true target position for planning and treatment to 2-3 mm that is in the range of positioning errors admissible at present for radiotherapy when image resolution inaccuracies and mechanical beam placement inaccuracies are combined.

In this study, I am conscious that my investigations opened the area of studies and have not closed them in any manner. I realize that the best solution to problems discovered and quantified in my study would be to improve geometrical accuracy of 4DCT, CBCT and 4DCBCT technologies. These solutions would require in my opinion much better algorithms on spatiotemporal correlation of images scored for moving anatomy (instead of separate binning for time and for space image coordination as it is done at present time). These solutions would demand more

sophisticated computational techniques and more advanced computer algorithms as well as massive amount of testing, both numerically and empirically in the phantom like and clinical settings. One may expect that lots of scientists, engineers, physicists and physicians will be occupied by these tasks, and I hope that I will be able to participate in this effort in future.

BIBLIOGRAPHY

1. Henson, C.F., et al., *Glycerol rhizotomy versus gamma knife radiosurgery for the treatment of trigeminal neuralgia: an analysis of patients treated at one institution.* Int J Radiat Oncol Biol Phys, 2005. **63**(1): p. 82-90.
2. Rosenthal, J.W., *Beta-radiation therapy of pterygium.* AMA Arch Ophthalmol, 1953. **49**(1): p. 17-23.
3. Berger, B., et al., *External beam radiotherapy as postoperative treatment of diffuse pigmented villonodular synovitis.* Int J Radiat Oncol Biol Phys, 2007. **67**(4): p. 1130-4.
4. Edsmyr, F., et al., *Radiation therapy in the treatment of keloids in East Africa.* Acta Radiol Ther Phys Biol, 1974. **13**(2): p. 102-6.
5. Strauss, J.B., et al., *Cost of radiotherapy versus NSAID administration for prevention of heterotopic ossification after total hip arthroplasty.* Int J Radiat Oncol Biol Phys, 2008. **71**(5): p. 1460-4.
6. Underwood, E.A., *Wilhelm Conrad Rontgen (1845-1923) and the Early Development of Radiology.* Proc R Soc Med, 1945. **38**(12): p. 697-706.
7. Curie, E., *Marie and Pierre Curie and the discovery of radium.* Br J Radiol, 1950. **23**(271): p. 409-12.
8. Purdy, J.A., et al., *Medical accelerator safety considerations: report of AAPM Radiation Therapy Committee Task Group No. 35.* Med Phys, 1993. **20**(4): p. 1261-75.
9. Beckmann, E.C., *CT scanning the early days.* Br J Radiol, 2006. **79**(937): p. 5-8.
10. Suit, H., *The Gray Lecture 2001: coming technical advances in radiation oncology.* Int J Radiat Oncol Biol Phys, 2002. **53**(4): p. 798-809.
11. Schad, L.R., et al., *Three dimensional image correlation of CT, MR, and PET studies in radiotherapy treatment planning of brain tumors.* J Comput Assist Tomogr, 1987. **11**(6): p. 948-54.
12. Hansen, E.K., et al., *Image-guided radiotherapy using megavoltage cone-beam computed tomography for treatment of paraspinous tumors in the presence of orthopedic hardware.* Int J Radiat Oncol Biol Phys, 2006. **66**(2): p. 323-6.
13. Xing, L., et al., *Overview of image-guided radiation therapy.* Med Dosim, 2006. **31**(2): p. 91-112.
14. Meeks, S.L., et al., *Performance characterization of megavoltage computed tomography imaging on a helical tomotherapy unit.* Med Phys, 2005. **32**(8): p. 2673-81.
15. Ward, J.F., *Mechanisms of DNA repair and their potential modification for radiotherapy.* Int J Radiat Oncol Biol Phys, 1986. **12**(7): p. 1027-32.
16. Moulder, J.E. and S. Rockwell, *Hypoxic fractions of solid tumors: experimental techniques, methods of analysis, and a survey of existing data.*

Int J Radiat Oncol Biol Phys, 1984. **10**(5): p. 695-712.
17. Wiltshire, C.R., et al., *Clinical studies with misonidazole.* Br J Cancer Suppl, 1978. **3**: p. 286-9.
18. Stone, H.B. and H.R. Withers, *Metronidazole: effect on radiosensitivity of tumor and normal tissues in mice.* J Natl Cancer Inst, 1975. **55**(5): p. 1189-94.
19. Brown, J.M., *Hypoxic cytotoxic agents: a new approach to cancer chemotherapy.* Drug Resist Updat, 2000. **3**(1): p. 7-13.
20. Le, Q.T., et al., *Phase I study of tirapazamine plus cisplatin/etoposide and concurrent thoracic radiotherapy in limited-stage small cell lung cancer (S0004): a Southwest Oncology Group study.* Clin Cancer Res, 2004. **10**(16): p. 5418-24.
21. Masunaga, S., et al., *Influence of manipulating hypoxia in solid tumors on the radiation dose-rate effect in vivo, with reference to that in the quiescent cell population.* Jpn J Radiol, 2010. **28**(2): p. 132-42.
22. Baker, D., et al., *The influence of warfarin of levamisole on the incidence of metastases following local irradiation of a solid tumor.* Cancer, 1982. **49**(3): p. 427-33.
23. Looney, W.B., et al., *Solid tumor models for the assessment of different treatment modalities. XII. Combined chemotherapy-radiotherapy: variation of time interval between time of administration of 5-fluorouracil and radiation and its effect on the control of tumor growth.* Cancer, 1979. **44**(2): p. 437-45.
24. Looney, W.B., H.A. Hopkins, and M.S. MacLeod, *Solid tumor models for the assessment of different treatment modalities: VIII. The scheduling of treatment for a chemotherapeutically resistant experimental solid tumor.* Cancer, 1979. **43**(4): p. 1201-10.
25. Allard, A., et al., *Role of Radiation Dose in the Risk of Secondary Leukemia After a Solid Tumor in Childhood Treated Between 1980 and 1999.* Int J Radiat Oncol Biol Phys, 2010.
26. Wolbarst, A.B., L.M. Chin, and G.K. Svensson, *Optimization of radiation therapy: integral-response of a model biological system.* Int J Radiat Oncol Biol Phys, 1982. **8**(10): p. 1761-9.
27. Jemal, A., et al., *Cancer statistics, 2009.* CA Cancer J Clin, 2009. **59**(4): p. 225-49.
28. Timmerman, R., et al., *Stereotactic body radiation therapy for inoperable early stage lung cancer.* JAMA, 2010. **303**(11): p. 1070-6.
29. Timmerman, R., et al., *Extracranial stereotactic radioablation: results of a phase I study in medically inoperable stage I non-small cell lung cancer.* Chest, 2003. **124**(5): p. 1946-55.
30. Ernster, V.L., *Female lung cancer.* Annu Rev Public Health, 1996. **17**: p. 97-114.
31. Pearson, F.G., *Lung cancer. The past twenty-five years.* Chest, 1986. **89**(4 Suppl): p. 200S-205S.

32. Fingerhut, A.G., F.K. Chin, and E.H. Shultz, *Radical radiation therapy for cancer of the lung.* Chest, 1971. **60**(3): p. 244-5.
33. Reed, R.C., G.S. Lowery, and D.G. Nordstrom, *Single high dose-large field irradiation for palliation of advanced malignancies.* Int J Radiat Oncol Biol Phys, 1988. **15**(5): p. 1243-6.
34. Coutard, H., *The Results and Methods of Treatment of Cancer by Radiation.* Ann Surg, 1937. **106**(4): p. 584-98.
35. Baclesse, F. and A. Ennuyer J Radiol Electrol Arch Electr Medicale, 1947. **28**(5-6): p. 235-7.
36. Terahara, A., *[Gamma knife].* Gan To Kagaku Ryoho, 1993. **20**(14): p. 2133-42.
37. Hamilton, A.J., et al., *LINAC-based spinal stereotactic radiosurgery.* Stereotact Funct Neurosurg, 1996. **66**(1-3): p. 1-9.
38. Hamilton, A.J., et al., *Preliminary clinical experience with linear accelerator-based spinal stereotactic radiosurgery.* Neurosurgery, 1995. **36**(2): p. 311-9.
39. Lax, I., et al., *Stereotactic radiotherapy of malignancies in the abdomen. Methodological aspects.* Acta Oncol, 1994. **33**(6): p. 677-83.
40. Blomgren, H., et al., *Stereotactic high dose fraction radiation therapy of extracranial tumors using an accelerator. Clinical experience of the first thirty-one patients.* Acta Oncol, 1995. **34**(6): p. 861-70.
41. Shirato, H., et al., *Physical aspects of a real-time tumor-tracking system for gated radiotherapy.* Int J Radiat Oncol Biol Phys, 2000. **48**(4): p. 1187-95.
42. Herfarth, K.K., et al., *Stereotactic single-dose radiation therapy of liver tumors: results of a phase I/II trial.* J Clin Oncol, 2001. **19**(1): p. 164-70.
43. Wulf, J., et al., *Stereotactic radiotherapy of targets in the lung and liver.* Strahlenther Onkol, 2001. **177**(12): p. 645-55.
44. Nagata, Y., et al., *Clinical outcomes of 3D conformal hypofractionated single high-dose radiotherapy for one or two lung tumors using a stereotactic body frame.* Int J Radiat Oncol Biol Phys, 2002. **52**(4): p. 1041-6.
45. Timmerman, R.D. and B.D. Kavanagh, *Stereotactic body radiation therapy.* Curr Probl Cancer, 2005. **29**(3): p. 120-57.
46. Mayer, R., et al., *Two-dimensional film dosimetry application in heterogeneous materials exposed to megavoltage photon beams.* Med Phys, 1997. **24**(3): p. 455-60.
47. Papiez, L., et al., *Extracranial stereotactic radioablation: physical principles.* Acta Oncol, 2003. **42**(8): p. 882-94.
48. Xi, M., et al., *Defining internal target volume (ITV) for hepatocellular carcinoma using four-dimensional CT.* Radiother Oncol, 2007. **84**(3): p. 272-8.
49. Keall, P.J., et al., *Acquiring 4D thoracic CT scans using a multislice helical method.* Phys Med Biol, 2004. **49**(10): p. 2053-67.
50. Fitzpatrick, M.J., et al., *Displacement-based binning of time-dependent*

computed tomography image data sets. Med Phys, 2006. **33**(1): p. 235-46.
51. Rietzel, E., T. Pan, and G.T. Chen, *Four-dimensional computed tomography: image formation and clinical protocol.* Med Phys, 2005. **32**(4): p. 874-89.
52. Mutaf, Y.D., J.A. Antolak, and D.H. Brinkmann, *The impact of temporal inaccuracies on 4DCT image quality.* Med Phys, 2007. **34**(5): p. 1615-22.
53. Pan, T., X. Sun, and D. Luo, *Improvement of the cine-CT based 4D-CT imaging.* Med Phys, 2007. **34**(11): p. 4499-503.
54. Jaffray, D.A. and J.H. Siewerdsen, *Cone-beam computed tomography with a flat-panel imager: initial performance characterization.* Med Phys, 2000. **27**(6): p. 1311-23.
55. Jaffray, D.A., et al., *Flat-panel cone-beam computed tomography for image-guided radiation therapy.* Int J Radiat Oncol Biol Phys, 2002. **53**(5): p. 1337-49.
56. Wang, Z., et al., *Cone-beam CT localization of internal target volumes for stereotactic body radiotherapy of lung lesions.* Int J Radiat Oncol Biol Phys, 2007. **69**(5): p. 1618-24.
57. Letourneau, D., et al., *Cone-beam-CT guided radiation therapy: technical implementation.* Radiother Oncol, 2005. **75**(3): p. 279-86.
58. Timmerman, R.D., *Surgery versus stereotactic body radiation therapy for early-stage lung cancer: who's down for the count?* J Clin Oncol, 2010. **28**(6): p. 907-9.
59. Underberg, R.W., et al., *Use of maximum intensity projections (MIP) for target volume generation in 4DCT scans for lung cancer.* Int J Radiat Oncol Biol Phys, 2005. **63**(1): p. 253-60.
60. Bradley, J.D., et al., *Comparison of helical, maximum intensity projection (MIP), and averaged intensity (AI) 4D CT imaging for stereotactic body radiation therapy (SBRT) planning in lung cancer.* Radiother Oncol, 2006. **81**(3): p. 264-8.
61. Cai, J., et al., *Estimation of error in maximal intensity projection-based internal target volume of lung tumors: a simulation and comparison study using dynamic magnetic resonance imaging.* Int J Radiat Oncol Biol Phys, 2007. **69**(3): p. 895-902.
62. Rietzel, E., et al., *Design of 4D treatment planning target volumes.* Int J Radiat Oncol Biol Phys, 2006. **66**(1): p. 287-95.
63. Simon, L., et al., *Initial evaluation of a four-dimensional computed tomography system using a programmable motor.* J Appl Clin Med Phys, 2006. **7**(4): p. 50-65.
64. Shimizu, S., et al., *Impact of respiratory movement on the computed tomographic images of small lung tumors in three-dimensional (3D) radiotherapy.* Int J Radiat Oncol Biol Phys, 2000. **46**(5): p. 1127-33.
65. Wink, N.M., M.F. McNitt-Gray, and T.D. Solberg, *Optimization of multi-slice helical respiration-correlated CT: the effects of table speed and rotation time.*

Phys Med Biol, 2005. **50**(23): p. 5717-29.
66. Smeenk, C., S. Gaede, and J.J. Battista, *Delineation of moving targets with slow MVCT scans: implications for adaptive non-gated lung tomotherapy.* Phys Med Biol, 2007. **52**(4): p. 1119-34.
67. Sonke, J.J., et al., *Respiratory correlated cone beam CT.* Med Phys, 2005. **32**(4): p. 1176-86.
68. van der Voort van Zyp, N.C., et al., *Stereotactic radiotherapy with real-time tumor tracking for non-small cell lung cancer: clinical outcome.* Radiother Oncol, 2009. **91**(3): p. 296-300.
69. Guckenberger, M., et al., *Four-dimensional treatment planning for stereotactic body radiotherapy.* Int J Radiat Oncol Biol Phys, 2007. **69**(1): p. 276-85.
70. Park, K., et al., *Do maximum intensity projection images truly capture tumor motion?* Int J Radiat Oncol Biol Phys, 2009. **73**(2): p. 618-25.
71. Admiraal, M.A., D. Schuring, and C.W. Hurkmans, *Dose calculations accounting for breathing motion in stereotactic lung radiotherapy based on 4D-CT and the internal target volume.* Radiother Oncol, 2008. **86**(1): p. 55-60.
72. Low, D.A., et al., *A technique for the quantitative evaluation of dose distributions.* Med Phys, 1998. **25**(5): p. 656-61.
73. Xiao, Y., et al., *Dosimetric evaluation of heterogeneity corrections for RTOG 0236: stereotactic body radiotherapy of inoperable stage I-II non-small-cell lung cancer.* Int J Radiat Oncol Biol Phys, 2009. **73**(4): p. 1235-42.
74. Hugo, G., et al., *Changes in the respiratory pattern during radiotherapy for cancer in the lung.* Radiother Oncol, 2006. **78**(3): p. 326-31.
75. Abdelnour, A.F., et al., *Phase and amplitude binning for 4D-CT imaging.* Phys Med Biol, 2007. **52**(12): p. 3515-29.
76. Heinzerling, J.H., et al., *Four-dimensional computed tomography scan analysis of tumor and organ motion at varying levels of abdominal compression during stereotactic treatment of lung and liver.* Int J Radiat Oncol Biol Phys, 2008. **70**(5): p. 1571-8.
77. Wu, J., et al., *An evaluation of planning techniques for stereotactic body radiation therapy in lung tumors.* Radiother Oncol, 2008. **87**(1): p. 35-43.
78. Hughes, S., et al., *Assessment of two novel ventilatory surrogates for use in the delivery of gated/tracked radiotherapy for non-small cell lung cancer.* Radiother Oncol, 2009. **91**(3): p. 336-41.
79. Wang, L., et al., *Dosimetric comparison of stereotactic body radiotherapy using 4D CT and multiphase CT images for treatment planning of lung cancer: evaluation of the impact on daily dose coverage.* Radiother Oncol, 2009. **91**(3): p. 314-24.
80. Kontrisova, K., et al., *Dosimetric comparison of stereotactic body radiotherapy in different respiration conditions: a modeling study.* Radiother Oncol, 2006. **81**(1): p. 97-104.
81. Bortfeld, T., S.B. Jiang, and E. Rietzel, *Effects of motion on the total dose*

distribution. Semin Radiat Oncol, 2004. **14**(1): p. 41-51.
82. Sixel, K.E., et al., *Digital fluoroscopy to quantify lung tumor motion: potential for patient-specific planning target volumes.* Int J Radiat Oncol Biol Phys, 2003. **57**(3): p. 717-23.
83. Bissonnette, J.P., et al., *Quantifying interfraction and intrafraction tumor motion in lung stereotactic body radiotherapy using respiration-correlated cone beam computed tomography.* Int J Radiat Oncol Biol Phys, 2009. **75**(3): p. 688-95.
84. Huang, L., et al., *A study on the dosimetric accuracy of treatment planning for stereotactic body radiation therapy of lung cancer using average and maximum intensity projection images.* Radiother Oncol, 2010. **96**(1): p. 48-54.
85. Timmerman, R.D., C. Park, and B.D. Kavanagh, *The North American experience with stereotactic body radiation therapy in non-small cell lung cancer.* J Thorac Oncol, 2007. **2**(7 Suppl 3): p. S101-12.
86. Hoppe, B.S., et al., *Acute skin toxicity following stereotactic body radiation therapy for stage I non-small-cell lung cancer: who's at risk?* Int J Radiat Oncol Biol Phys, 2008. **72**(5): p. 1283-6.
87. Brandner, E.D., et al., *Abdominal organ motion measured using 4D CT.* Int J Radiat Oncol Biol Phys, 2006. **65**(2): p. 554-60.
88. Brandner, E.D., et al., *Localizing moving targets and organs using motion-managed CTs.* Med Dosim, 2006. **31**(2): p. 134-40.

LIST OF ABBREVIATIONS

4DCT – Four Dimensional Computed Tomography

4D-CBCT – Four Dimensional Cone Beam Computed Tomography

AP – Anterior posterior

BEV – Beam's Eye View

BPM – Breathing per Minute

CBCT – Cone Beam Computed Tomography

CFRT – Conventionally Fractionated Radiation Therapy

CTV – Clinical Target Volume

DVH – Dose Volume Histogram

EDVI – Extended Distance Virtual Isocenter

EPID – Electronic Portal Imaging Device

FOV – Field of View

GTV – Gross Tumor Volume

IGRT – Image-Guided Radiation Therapy

IMRT – Intensity Modulated Radiation Therapy

ITA – Internal Target Area

ITV – Internal Target Volume

KV – Kilo-Voltage

MIP – Maximum Intensity Projection

MINIP – Minimum Intensity Projection

MRI – Magnetic Resonance Image

NSCLC – Non Small Cell Lung Carcinoma

PTV – Planning Target Volume

QA – Quality Assurance

ROI – Region of Interest

RPM – Respiratory Position Monitor

RTOG – Radiation Therapy Oncology Group

SAD – Source Axial Distance

SBRT – Stereotactic Body Radiation Therapy

SCLC – Small Cell Lung Carcinoma

SD – Standard Deviation

SRS – Stereotactic Radio Surgery

SSD – Source Surface Distance

XVI – X-ray Volume Image